A petrographic-coded model – Derivation of relationships between thermal and other physical rock properties

Ausgeführt zum Zweck der Erlangung des akademischen Grades eines Doktors der montanistischen Wissenschaften

vorgelegt von

Dipl.-Ing. Nina Maria Gegenhuber Bakk.techn.

am Lehrstuhl für Angewandte Geophysik

Montanuniversität Leoben

Leoben, Juli 2011

I declare in lieu of oath, that I wrote this thesis and performed the associated research myself, using only literature cited in this volume.

Dipl.-Ing. Nina Maria Gegenhuber

Leoben, am 7.Juli 2011

Acknowledgment

First of all, I want to say thank you to my supervisor, Hon.Prof.Dr.rer.nat.habil. Jürgen Schön, for all his ideas for this work during the years, for his patience, for explaining things in such understanding way, for many times of reading the manuscript and so many other things. Additionally I have to say thank you for all the emotional support and the private talks.

My gratefulness is directed to Priv.Doz. Dr. Roman Leonhardt, for two years of supporting this work and teaching me a lot of important things for doing good research.

I would like to thank Dipl.-Ing. Claudia Steiner-Luckabauer for supporting me as friend and colleague, for all the talks, new ideas, other ways in thinking and for listening so many times.

I am thankful to all stuff members of the Chair of Geophysics (especially Franz Pusterwallner) and Joanneum Research for supporting me in different ways.

I want to express my gratitude to those who directly or indirectly helped to finish this work.

Last but not least I want to thank my family for all the support during the years. To keep me grounded and to give me the strength to finish this thesis. I want to thank my friends, who give me the emotional support and to distract me in a positive way whenever I needed a break.

Alles Wissen und alles Vermehren unseres Wissens endet nicht mit einem Schlusspunkt, sondern mit einem Fragezeichen.

(Hermann Hesse)

Abstract

Thermal conductivity is one of the key properties of geothermal and other geological and geophysical applications. Due to difficult measurements of thermal conductivity in boreholes, in most cases only laboratory data are available. Therefore the knowledge of correlations between thermal conductivity and other petrophysical properties (compressional wave velocity, density, electrical resistivity), which are measurable in a well, could deliver it indirectly.

The analysis of experimental data clearly indicates that correlations between thermal conductivity and parameters like compressional wave velocity or density are very complex with partially opposite directions of influences from the controlling parameters. Three main influences could be detected

- mineral composition or rock type
- pore- or fracture volume fraction (porosity)
- pore- or fracture geometry.

In order to implement these influences a modular concept of model architecture has been developed. It comprises two main steps and is focussed mainly on the relationship between thermal conductivity and compressional wave velocity:

Step 1: Modelling of mineral composition – this controls the petrographic code or rock type

Step 2: Modelling or implementation of fractures, pores etc. with two model types (inclusion model, defect model).

For implementation of fractures, pores etc., two models have been designed. The first one is an inclusion model and the second one a simpler defect model. Both can demonstrate the two main influencing factors on derived correlations: mineral composition and fractures/pores. These models have furthermore been applied on different rock types (metamorphic/magmatic rocks, sandstone, carbonates). The result is “a petrographic-coded thermal parameter estimation”. The application of correlations to measured logs results in a “thermal conductivity log”.

The correlation between thermal conductivity and density seems relatively simple, but has a principal problem: Thermal conductivity is strongly controlled by pore and fracture shape, and by porosity – but, density is controlled only by porosity. Thus, density cannot cover the influence of internal rock geometry. -As a test also electrical resistivity was considered for carbonates. Compared with thermal conductivity the electrical resistivity cannot cover and express a variation of mineral composition. Therefore it works only within one exactly defined rock type (in this case carbonates).

Specific models for the calculation of the anisotropy of thermal conductivity and an improved method to determine heat production from integral gamma ray logs have been developed. In the additional section the calculation of thermal heat production from rocks was evaluated and a new equation - implementing also a petrographic-coded concept - could be derived and tested.

Zusammenfassung

Wärmeleitfähigkeit ist eine der Haupteigenschaften von geothermischen und anderen geologischen und geophysikalischen Anwendungen. Da sich das Messen der Wärmeleitfähigkeit im Bohrloch schwierig gestaltet, sind meist nur Laborwerte vorhanden. Daher könnte die Kenntnis von einer Korrelation zwischen Wärmeleitfähigkeit und anderen petrophysikalischen Eigenschaften (Kompressionswellengeschwindigkeit, Widerstand, Dichte), die im Bohrloch messbar sind, diese indirekt liefern.

Die Analyse von experimentellen Daten zeigen klar, dass diese Korrelationen zwischen Wärmeleitfähigkeit und Kompressionswellengeschwindigkeit oder Dichte sehr komplex sind und durch die kontrollierenden Parameter zum Teil gegensätzliche Effekte hervorgerufen werden. Drei Haupteinflüsse wurden erkannt:

- Mineralzusammensetzung oder Gesteinstyp
- Poren oder Bruch - Volumen
- Poren oder Bruch-Geometrie

Um diese Einflüsse wiederzugeben wurde ein modulares Konzept für ein Model entwickelt. Dieses umfasst zwei Schritte und ist auf den Zusammenhang zwischen Wärmeleitfähigkeit und Kompressionswellengeschwindigkeit fokussiert.

Schritt 1: Modellieren der Mineralzusammensetzung - kontrolliert den Gesteinstyp

Schritt 2: Modellieren oder Einfügen der Brüche und Poren mit zwei Modelltypen.

Um die Poren, Brüche,… zu modellieren wurden zwei Modelle entwickelt. Das erste ist ein Inklusion-Model und das zweite ein einfacheres „Defekt-Model“. Beide können die zwei Haupteinflussfaktoren auf die Korrelationen wiedergeben: Mineralzusammensetzung und Brüche/Poren. Diese Modelle wurden weiters auf unterschiedliche Gesteinstypen (magmatische/metamorphe Gesteine, Sandstein, Karbonate) angewandt. Das Ergebnis ist eine „petrographisch kodierte thermische Parameter Abschätzung“. Die Anwendung der Korrelationen auf Bohrlochmessungen resultiert in einem „Wärmeleitfähigkeitslog“.

Die Korrelation zwischen Wärmeleitfähigkeit und Dichte scheint relativ simpel, aber hat ein grundsätzliches Problem: Wärmeleitfähigkeit hängt stark von Poren und Bruch-Formen und von der Porosität ab. Dichte hingegen ist nur von der Porosität abhängig. Daher kann die Dichte nicht den Einfluss der internen Gesteinsgeometrie wiedergeben. Zusätzlich wurde der elektrische Widerstand für Karbonate betrachtet. Verglichen mit der Wärmeleitfähigkeit kann der Widerstand nicht den Einfluss der komplexen Mineralzusammensetzung widerspiegeln. Daher funktioniert diese Korrelation nur bei einem vorgegebenen Gesteinstypen (hier: Karbonate).

Spezifische Modelle für die Berechnung der Anisotropie der Wärmeleitfähigkeit und eine verbesserte Methode zur Bestimmung der Wärmeproduktion des integralen Gammalogs wurden entwickelt. In einem zusätzlichen Kapitel wurde die Berechnung der radiogenen Wärmeproduktion bewertet und eine neue Gleichung – ebenfalls mit dem „petrographisch kodierten Konzept“- entwickelt und getestet.

Index

1. Introduction

Geothermal investigations are of increasing importance with respect to tectonic processes, renewable energy resources, engineering projects- like deep tunnels, and the protection of the Earth's natural environment. Finally, paleothermal processes are components of the generation of oil and gas. The thermal regime of the Earth is influenced by a complex interaction of heat generation, internal heat flow, convection, and tectonic processes.

Heat flow and temperature distribution in the zones of interest for geothermal energy resources and engineering applications are controlled by the heat sources and the processes of heat flow. Sources of the internal heat of the Earth are:

- heat production and flow from the Earth's interior (originated by gravitational contraction) and
- heat production by radioactive decay of instable isotopes (Potassium, Uranium and Thorium) in the rocks.

External sources (radiation from the sun) are only relevant for the uppermost region and surface temperature distribution.

Therefore the geothermal field in general is connected with the geologic-tectonic position of the region and some specific geologic-petrophysical key properties which contribute to the energy and control the heat flow and distribution under a more local aspect. Such key properties are:

- local radiogenic heat production from the formations/rocks, that are present,
- thermal conductivity and heat capacity of the formation/rock,
- properties controlling convective heat (and fluid) transport, particularly permeability and heat exchange properties of fractured and/or porous rocks.

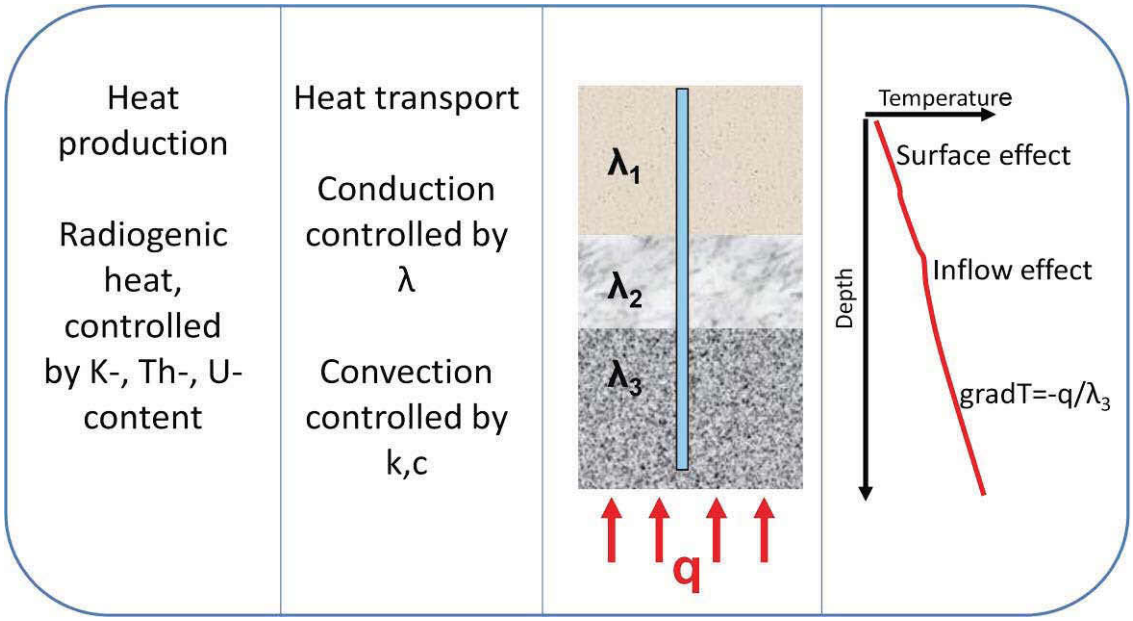

Figure 1-1: Illustrates the different components controlling a temperature log in a well (λ...thermal conductivity, c...heat capacity, k...permeability, q...heat flow)

As a contribution to geoscientific aspects of geothermal processes and resources the investigations of this study are directed at a complex understanding of the first two (thermal) properties and processes and is focused on

- development of an experimental laboratory method in order to determine and study the complex behaviour and correlation between thermal properties and properties measured by geophysical field and/or borehole techniques,
- development of a model concept as physical fundament of correlation of the various parameters and extraction of equations for practical parameter estimation,
- development and application of a methodical concept for the determination of key properties from conventional geophysical field data (well log measurements) and for up-scaling.

1.1. Thermophysical properties – State of the art

Geothermal studies, research and applications are of growing interest and presence in the literature, on conferences and are subject of international, national and industrial projects. Two topics are of particular relevance and subject of a brief state of the art analysis:

- experimental basis of thermal key property-measurements,
- methodical concepts and models for a complex analysis and practical application of thermophysical rock properties.

International the experimental technique of laboratory measurements is determined by the standard of leading research institutes (ETH Zuerich, GFZ Potsdam, RWTH Aachen, MIT/USA et al.) and the core laboratories of the oil industry. Thermal key properties can be measured with only some types of instruments. Thermal conductivity is determined by the transition measurement (needle probe), the stationary "divided-bar" technique or a newer optical scanning method (Popov et al, 1999).

Pore space properties, which control convective processes like porosity and permeability, are measured with instruments developed mainly for the oil industry (for example Tiab & Donaldson, 2004). In most cases instruments are computer controlled and allow a statistical data management.

For the methodical concepts different "rock models" and empirical equations are published.

There are two groups:

- The first group are generally theories describing effective physical properties of a composite material (layer models, bound theories) and inclusion effects (a systematic description is given by Berryman (1995)).
- The second group refers to models for specific rock types (for example clastic sediments). In most cases the investigations are connected with results of experimental measurements (e.g. Buntebarth, 1980; Schoen, 1996). Data allow the validation and calibration of model derived equations and the derivation of trends and empirical equations.

There are some fundamental papers about the radiogenic heat production in general (Rybach, 1976) and papers in connection with the thermal conductivity related to different parts of the world (e.g. Abbady et al, 2006; Chiozzi et al, 2002; Norden & Foerster, 2006). Relationships to other petrophysical parameters – particularly density and seismic properties - are empirical. Most papers deal with the relationship of thermal conductivity or heat capacity with temperature and pressure, like Abdulgatov (2006), Abdulgatova (2009), Birch & Clark (1940), Gunn et al (2005), Mottaghy & Vosteen, (2008) or Seipold (1990, 1998), just to mention a few. Hartmann et al (2005) discussed equations for correlations of the aspect ratio, compressional wave velocity, density and porosity versus thermal conductivity.

Summarizing there is no general model concept for a practical application upon the main rock types and for a derivation of thermal properties from other geophysical parameters. That's the point, where this thesis picks up at. Many ideas and conclusions have been developed during discussions with my supervisor J.H. Schoen.

1.2. Target of my work

The thesis covers a complex investigation of experimental methods and the development of model-based and empirical algorithms for a parameter estimate from geologic input and geophysical data (Figure 1-2). It is aimed at the following target components:

- Complex method for laboratory determination of key properties (thermal conductivity, heat capacity, porosity) and properties for expected correlations (elastic wave velocities, specific electrical resistivity, density).

- Analysis and correlation of laboratory data connected with the development and application of model concepts. The models will be developed as a modular concept which allows an adaption/modification for various rock types (e.g. dense rock, porous rock, fractured rock). With respect to the real rock texture a model will be designed for tensorial thermal properties (anisotropy).

- Methods for an estimation of thermal properties from geophysical field data and a petrographic classification. This component represents the step from the laboratory scale and technique to field scale and methods. Based on the laboratory data and model algorithms the derivation is directed at:

    - thermal conductivity for example from acoustic/seismic, electric and other data with a geological input (rock type)

    - radiogenic heat production from conventional integral gamma logs with a geological input (rock type)

Thus, the basic concept is the combination of petrographic type (mineral composition) and textural-structural effects (fractures, cracks) in a two-step methodology referred to as “petrographic-coded thermal parameter estimation”.

This should allow the derivation of thermal properties from geological and geophysical field data. Laboratory measurements are assigned the function of calibration and verification.

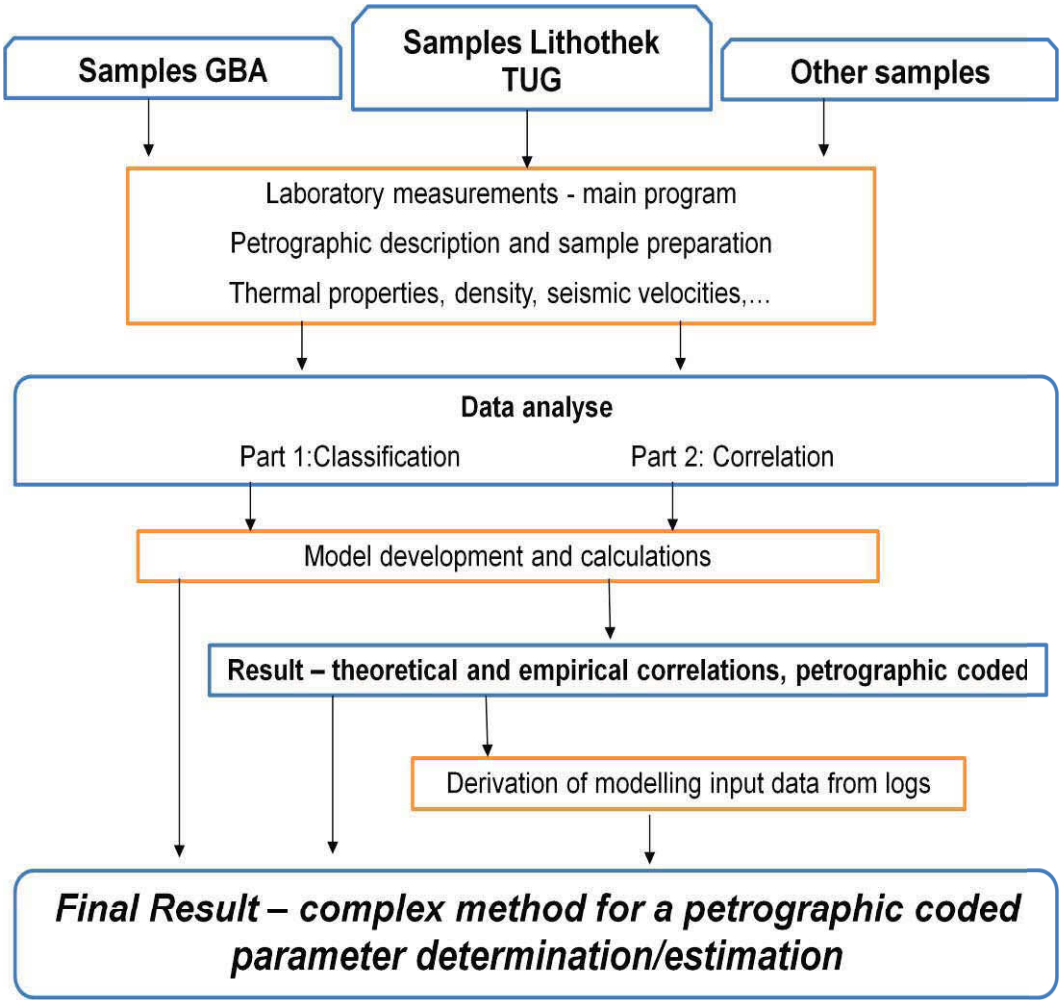

Figure 1-2: Flowchart for the working schedule of this thesis, experimental input comes from data measured at samples described in Chapter 2.1.

2. Data source and sample description

In order to derive relationships and correlations for different rock types for different geological units of Austria the sample selection was directed at:

- Sedimentary rocks (clastic sediments as well as carbonate sediments)
- Magmatic and metamorphic rocks (like granite, gneiss and basalt).

Samples have been selected especially from the "Lithothek", samples from the projects "THERMALP" and "THERMTEC", the "Stainzer Plattengneis" and granites from upper and lower Austria and basalts from Kloech, Styria. Some cretaceous sandstone samples are from Saxonia/Germany.

Additionally logs from the Geological Survey of Austria and Joanneum Research are used for derivation of correlations.

A description of individual samples and results of all measurements are given in Appendix A2.

2.1. Samples

2.1.1. Regional overview

Figure 2-1 shows the local position of the samples related to the geological units.

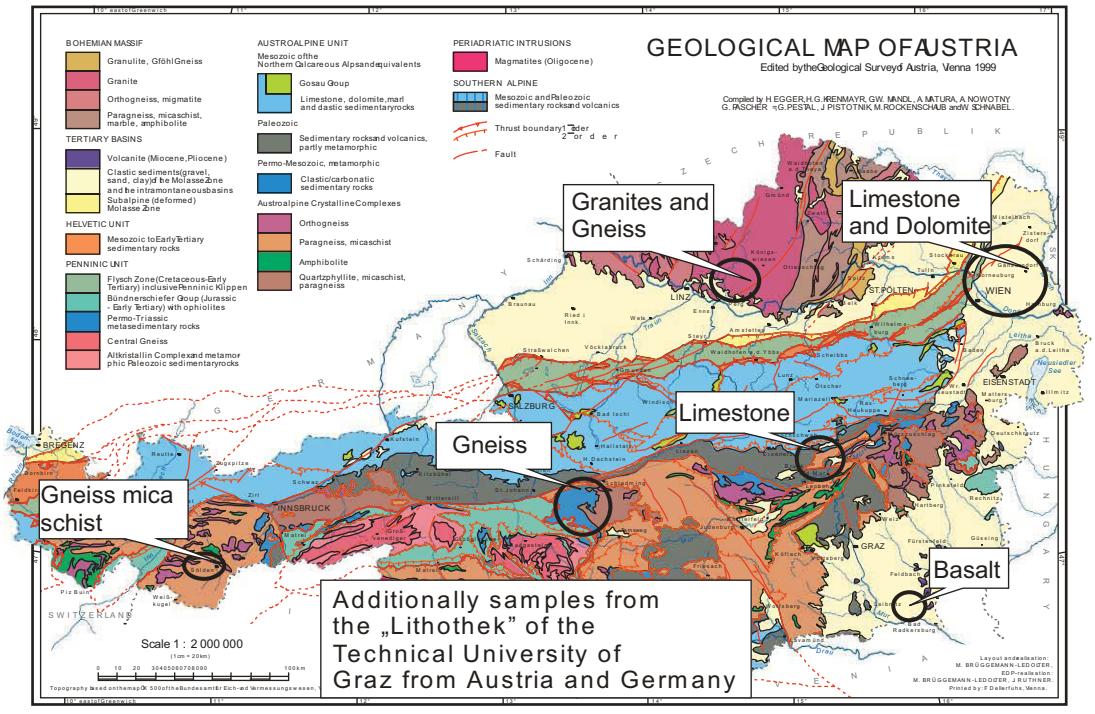

Figure 2-1: Overview of the sampling areas from Austria

Additionally Table 2-1 gives an overview of the investigated samples with respect to the lithology.

Lithology	Number of Samples	Remarks
Granite	10	Lithothek, Upper and Lower Austria
Gneiss	10	Lithothek, Cores
Sandstone	9	Lithothek, Pirna (D)
Dolomite	17	Vienna Basin
Limestone	25	Vienna Basin, Northern Calcareous Alps
Basalt/Diorite/Gabbro	12	Lithothek, Kloech (A)
Others	6	Cores

Table 2-1: Investigated samples

The following sections give a short description of the material and the sources.

2.1.2. Samples from the "Lithothek"

The "Lithothek" at the Technical University of Graz is one of the largest collections of rocks in Austria. There are hundreds of different rocks, from sedimentary and igneous to metamorphic ones from all over the world. All specimens are cut in the form of a slab (30x20x3cm) and are polished. Zirkl E.J. published in 1987 a small book about this "Lithothek".

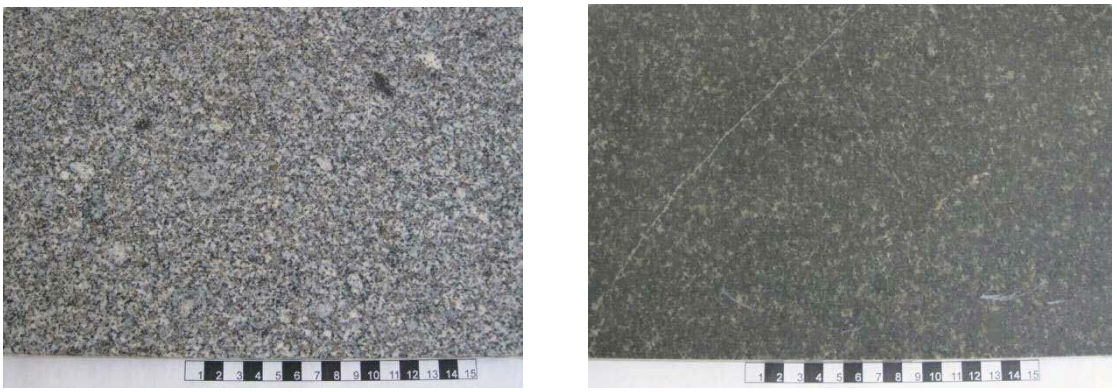

Figure 2-2: Two selected samples from the Lithothek: Granite (left) and Gabbro (right)

4 to 5 samples from each type of rock (granites, sandstones, basalts, diorites, carbonates) are used for the first systematic measurements of physical properties. Figure 2-2 shows two examples of the selected samples. Because of their polished surface the results from the thermal conductivity measurements were really good and there was no sample preparation necessary before measuring.

The shape of the samples and conservation limited the type of possible measurements. There was no feasibility to get the resistivity or the porosity, because saturated samples would be needed and we were not allowed to saturate them.

The results of these measurements form the basis for the model calculations, especially for the correlation between compressional wave velocity and thermal conductivity.

2.1.3. Samples from the projects "THERMALP" and "THERMTEC"

These both projects are funded by the "Oesterreichische Akademie der Wissenschaften" and are realized by the Geological Survey of Austria (GBA). The measurements are used to calibrate their geological and thermal models.

The samples for the "THERMALP" project from the Vienna Basin (from boreholes) are basically limestone and dolomite (two examples are shown in Figure 2-3). The Vienna basin is a 200km long and 50km wide rhombus between the Alps and the Carpathians. The Danube separates the basin into a Northern and a Southern part. It is composed of a fault and slap system.

Figure 2-3: Limestone (left) and dolomite (right) from the Vienna Basin

The samples for the "THERMTEC" project are mainly from the area around the Tauern window, from the new "Tauern-tunnel" and also from the tungsten mine next to Mittersill/Austria. The samples are gneiss, anhydrites and granites. They were taken during field trips from the GBA. The measured properties (if possible due to the state of the sample) are: thermal conductivity, density, specific electrical resistivity, porosity, heat capacity, compressional wave velocity and radiogenic heat production. All these data are included in a database and are used for different correlations.

The samples are cut and polished to get a plane surface for the thermal conductivity measurements. After these measurements, 1-inch cores are drilled out of the samples. These cores are used to determine the other petrophysical properties, like density, compressional wave velocity and specific electrical resistivity.

2.1.4. "Stainzer Plattengneis"

The selected rock sample is an anisotropic gneiss ("Stainzer Plattengneis") from the Koralpe/Austria (Figure 2-4). It consists of about 50 per cent of quartz, 45 per cent of feldspar and the rest is mica, garnet, tourmaline and disthene.

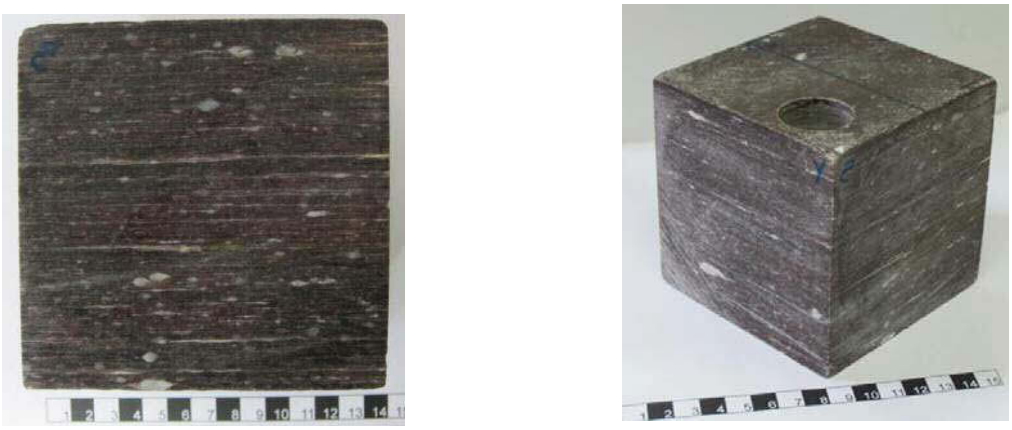

Figure 2-4: "Stainzer Plattengneis"

For experimental investigations a sample is cut in form of a cube (10cm x 10cm x 10 cm). The cube edges are normal and perpendicular to the visible schistosity. Before measuring, the planes have to be polished because even small roughness causes errors particularly for thermal conductivity measurements. The anisotropy of the thermal conductivity in three directions is measured. Results are then used for calculating and modelling the anisotropy (Chapter 10). It is a prime example of an anisotropic rock. Additionally the compressional wave velocity in three directions is measured. Measuring methods are described in Chapter 3.

2.1.5. Other sample sources

To obtain more data for the correlation between compressional wave velocity and thermal conductivity, further granites and basalts were taken. The granites are from upper and lower Austria. These differ in grain size and density. The basalt is from Kloech in Styria. Limestone is collected in the Northern Calcareous Alps and the Greywacke Zone. Additionally two Cretaceous sandstone samples from Pirna in Germany are measured.

2.2. Cores from logged wells

Cores from boreholes, where logs were available, are selected. These are used as reference for the calculations of the thermal conductivity from logs (Chapter 12).

For the comparison and the calculations of the thermal conductivity out of logs, acoustic, resistivity, gamma, density and neutron logs are needed. For this purpose, logs from different parts of Austria (from the Geological Survey of Austria and Joanneum Research) are used. Additionally the heat production is calculated with an improved equation from gamma logs (Chapter 11).

Key logs are:

- Gamma log (integral and spectral measurement)
- Acoustic log/Sonic log
- Density log

Table 2-2 gives an overview of the available logs. For the investigations the logs (and core material) from the following wells are used:

Austria: Example 1 – well with crystalline rock profile

Example 2 – well with carbonate rock profile

Example 3 – well with carbonate rock profile

Germany: KTB Windischeschenbach–Research well with alternate gneiss and metabasite

Well/Location	Depth interval	Used logs	Remarks
Example 1/A	0-1000 m	GR, Sonic, Dens	additionally cores
Example 2/A	2960-3080 m	GR, Sonic, Dens, PEF	additionally cores
Example 3/A	130-2400 m	Sonic, Dens, GR	
KTB(Kontinentale Tiefborung, Oberpfalz, D)	0-4000 m	Dens, Sonic, SpectralGR, GR	core data

Table 2-2: Selected boreholes with depth interval and used logs (GR – Gamma log, SpectralGR – spectral gamma log, Sonic – Sonic/Acoustic log, Dens – Gamma-Gamma-Density log, PEF – Gamma-Gamma-Photoelectric cross section log)

3. Experimental determination of physical key properties

3.1. Overview

Key properties of the investigations are

a.) The petrographic characteristic of the individual samples (rock type, mineral composition, geological position)
b.) Physical parameters from laboratory measurements
- Thermal conductivity
- Specific heat capacity
- Elastic wave velocity (Compressional wave velocity)
- Specific electrical resistivity
- Density and porosity

Measurements are realized depending on the sample conditions. The different measuring methods need specific sample preparation. Figure 3-1 shows a flowchart of the experimental sample investigations.

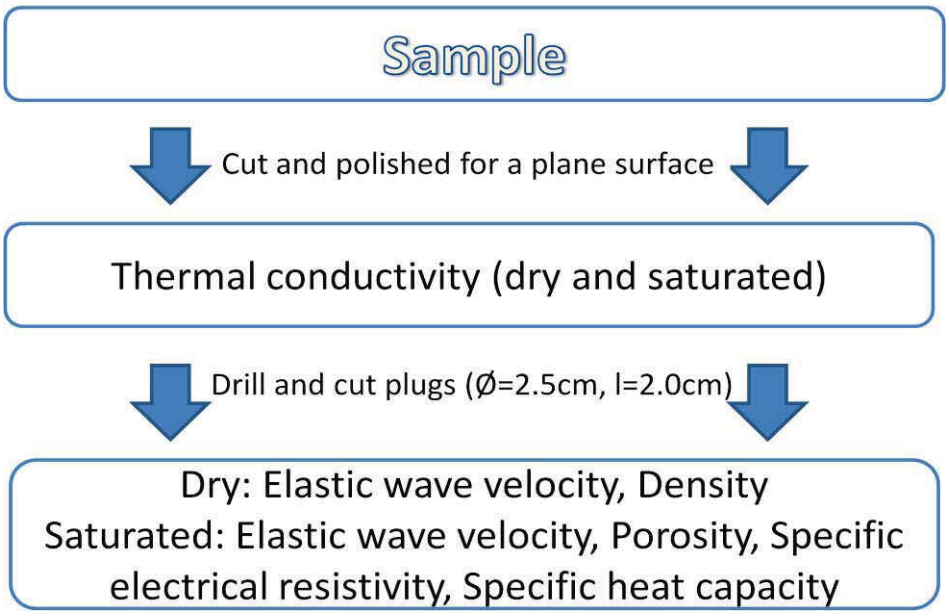

Figure 3-1: Flowchart providing an overview of the measurements

In the following sections the physical parameters and the laboratory techniques are described. Additionally some notes regarding known correlations are made.

3.2. Thermal conductivity

3.2.1. Overview

Thermal conductivity λ is the ability of a rock to transport energy in terms of heat. The SI unit is $Wm^{-1}K^{-1}$.

Thermal conductivity is one of the key parameters for geothermal studies: it connects thermal heat flow and temperature gradient via Fourier's law:

$$q = -\lambda * gradT \quad (3\text{-}1)$$

where q is the heat flow density [Wm^{-2}], λ is the thermal conductivity [$Wm^{-1}K^{-1}$] and $gradT$ [Km^{-1}] is the temperature gradient. Thermal conductivity is a tensor and characterized by a directional dependence in anisotropic rocks (Schoen, 1996).

"Thermal conductivity can be divided into lattice conductivity and radiative conductivity. Lattice conductivity (or phonon conductivity) is produced by the diffusion of thermal vibration in a crystalline lattice, while radiative conductivity is produced by infrared electromagnetic waves. Because of the multi-mineral composition of rocks, heating causes micro-fracturing due the different thermal expansion of mineral grains. Therefore, heating of rocks alters their properties. The temperature dependence of the ETC (effective thermal conductivity) of rocks strongly depends on the conductivity of its skeleton solid mineral from which it is formed."(Abdulagatova, 2009)

Thermal conductivity is influenced by mineralogical composition (particularly fractional content of quartz), porosity, fracturing, pore fluid, distribution, orientation, size and shape of the components and temperature and pressure. These are all factors that can explain why thermal conductivity varies within the same rock type (Schoen, 1996).

Table A1 (Appendix) gives thermal conductivities for rock forming minerals and pore fluids and explains the following tendencies:

- Increase of thermal conductivity with quartz content
- Decrease of thermal conductivity with porosity and fracturing
- Increase of thermal conductivity with water content

A tendency within igneous rocks is that the thermal conductivity increases from acid to ultrabasic rocks. Sedimentary rocks show an increase from

clay -> sandstone -> limestone and dolomites -> rock salts.

Generally it can be stated, that thermal conductivity decreases with increasing temperature, if material is dominant crystalline, and increases if the solid material is amorphous (except obsidian or glass). The reason for the decrease is the phonon scattering effect (Mottaghy &Vosteen, 2008).

Thermal conductivity increases with increasing pressure because of the crack and fracture closing and the increase of contact conductance. This trend depends on the mineral composition, porosity, density and rocks nature (Abdulagatov et al, 2006).

3.2.2. Measuring method

There are three different methods to determine thermal conductivity in the laboratory:

- static, divided-bar or steady-state method
- dynamic, transient or non-steady state method
- newer optical scanning method (Popov et al, 1999).

For our thermal conductivity measurements the thermal conductivity meter TK04 (from TeKa, Berlin), which is a non-steady state (transient) method (Figure 3-2) was used.

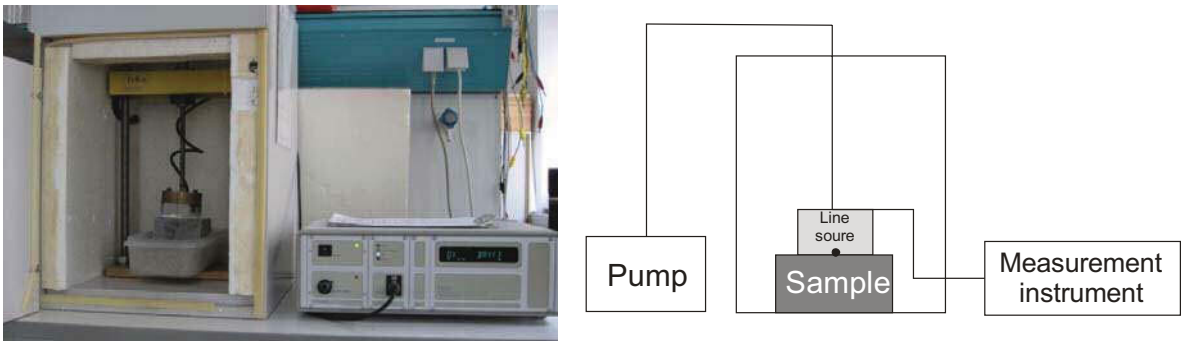

Figure 3-2: Tk04 Thermal conductivity meter from TeKa, Berlin (left: insulating chamber with half-space line)

The half-space line-source (HLQ) is a needle encased in a cylinder. The needle acts as heat source of defined energy. A temperature sensor in the middle of the needle measures the temperature as a function of time. Needle and cylinder are pressed onto the sample. Heat flow is mainly radial from the needle axis. Thus this method determines the thermal conductivity value perpendicular to the line source.

With a probe plane of 10x10cm and a needle length of 7cm (Plexiglass cylinder: diameter: 9cm), boundary effects are negligible (Erbas, 2001). The HLQ and the sample get fixed by a contact pressure of 15bars. In order to establish an optimal heat flow between probe and sample a contact agent (here: “Nivea” cream) is applied. The samples are stored in the laboratory to obtain thermal equilibrium with measurement conditions.

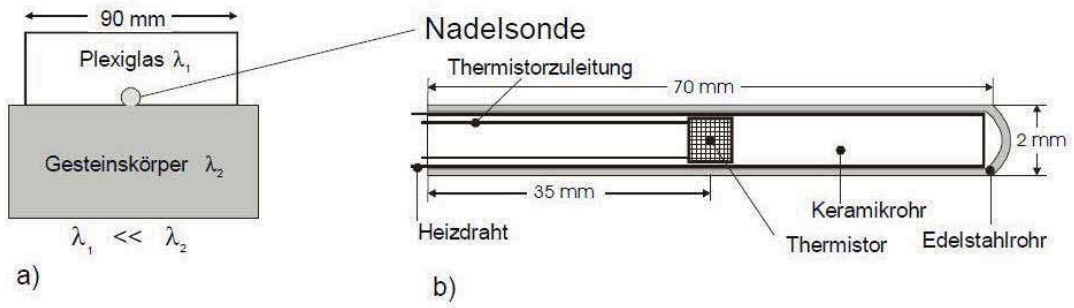

Figure 3-3: Design of the half-space line source (Erbas, 2001)

During analysis the line-source is heated by a defined heating power (here: 3Wm^{-1}) and the temperature is measured as a function of time at the midpoint of the needle with a thermistor (Figure 3-3). The heating period is 80 seconds and a maximum of 99 repeats can be taken. The resulting heating/cooling cycle is recorded and analysed. Thermal conductivity is calculated directly from the heating curve (Davis et al, 2007). For each measurement the needle was rotated clock-wise in 45° steps. In this way an anisotropic effect would have been recognized.

The reproducibility is ±1.5% in relation to conductivity λ. For this study at least two measurement sets, each five single repeated values are made. A weighted average is calculated and the standard deviation which is between 0.01 and 0.2Wm^{-1}K^{-1} is determined. For routinely checking the system, a Macor standard is measured. Macor has a well-defined low thermal conductivity of 1.46Wm^{-1}K^{-1}.

Erbas (2001) described a new method to determine the thermal conductivity out of the heating cycle. This Special Approximation Method (SAM) is directly used by the instrument's program and works with an approximation of the heating curve. The appropriateness is checked after certain intervals with mathematical and physical criteria. A quality parameter (LET) is calculated for each interval. The maximal LET value gives the best estimation for the real thermal conductivity.

In order to identify and quantify the effect of anisotropy, the orientation of the HQL probe relative to the samples coordinate system is changed with regard to possibly present cleavage planes (Chapter 10).

3.3. Specific heat capacity

3.3.1. Overview

"Specific heat capacity is defined as the amount of heat required to change a unit mass of a substance by one degree in temperature. " (Gunn et al, 2005)

The SI unit is $Jkg^{-1}K^{-1}$. It is described as the heat input [J] divided by the product of mass [kg] and temperature increase [K]. When a material with a certain temperature is in contact with a material with higher temperature, an energy flow, in form of heat, will get from the warmer material to the cooler one (Gong, 2005). It is a scalar property. With increasing temperature, specific heat capacity increases (Vosteen & Schellschmidt, 2003).

Table A1 (Appendix) gives specific heat capacity for rock forming minerals and pore fluids and explains the following tendencies:

- Increase of heat capacity with water content.
- Increase of heat capacity with temperature.

3.3.2. Measuring method

The used instrument is a "self-made" liquid calorimeter (Figure 3-4).

Figure 3-4: Liquid calorimeter for determining specific heat capacity

The sample gets heated up in a boiling water bath. After half an hour, the sample is put into a Dewar vessel with a well-defined amount of distilled cold water (200ml). The temperature is permanently measured in the boiling water bath and the Dewar vessel. A magnetic stirrer constantly moves to get a temperature equalisation in the Dewar vessel. When the heated sample is put into the Dewar vessel, the sample emits heat to the water. The temperature of the water increases and is permanently measured.

The Dewar vessel is weighted with and without the water, to get the mass of it. Before and after each measurement cycle, aluminium, steel and brass standard are measured, in order to control and determine the heat capacity of the calorimeter. With the temperature increase, the mass of the sample (m_{sample}), the mass of the water (m_{water}), the heat capacity of the water (c_{water}) and the heat capacity of the calorimeter ($c_{calorimeter}$ = 43.4 [JK^{-1}]), the specific heat capacity (c_{sample}) can be calculated with the equation:

$$c_{\mathrm{sample}} = \frac{(c_{\mathrm{calorimeter}} + c_{\mathrm{water}} * m_{\mathrm{water}}) * (T_{\mathrm{m}} - T_1)}{m_{\mathrm{sample}} * (T_2 - T_{\mathrm{m}})} \quad (3\text{-}2)$$

T_1 is the temperature of the water in the Dewar vessel before the heated sample is put into it

T_2 is the temperature of the hot water

T_m is the temperature of the water in the Dewar vessel after the heated sample is put into it.

3.4. Compressional wave velocity

3.4.1. Overview

In isotropic elastic material two wave types can be observed:

- compressional wave with the velocity v_p
- shear wave with velocity v_s.

$$v_{\mathrm{p}} = \sqrt{\frac{M}{d}} = \sqrt{\frac{E}{d} * \frac{1-\nu}{(1+\nu)*(1-2*\nu)}} = \sqrt{\frac{\lambda+2*\mu}{d}} = \sqrt{\frac{k+\left(\frac{4}{3}\right)*\mu}{d}} \quad (3\text{-}3)$$

$$v_{\mathrm{s}} = \sqrt{\frac{\mu}{d}} = \sqrt{\frac{E}{d} * \frac{1}{2*(1+\nu)}} \quad (3\text{-}4)$$

where d is the bulk density.

Velocities are connected with the elastic moduli and density:

- Young's modulus *E,* defined as ratio of stress to strain in an uniaxial stress state,
- compressional wave modulus *M*, defined as ratio of stress to strain in an uniaxial strain state,
- bulk compressional modulus k , defined as ratio of hydrostatic stress to volumetric strain,
- shear modulus μ , defined as ratio of shear stress to shear strain,
- Poisson's ratio ν , defined as the (negative) ratio of lateral strain to axial strain in an uniaxial stress state.

Wave velocity is controlled by the elastic properties of the rock forming minerals, their fractional volume, their contact, cementation or bonding properties, porosity, saturation, pressure and temperature and pore filling.

In magmatic and metamorphic rocks it is mainly influenced by effects of cracks, fractures and pores, their anisotropy, temperature and pressure. For sedimentary rocks, porosity and matrix are the important factors. In an anisotropic material a directional dependence can be indicated.

With increasing pressure and closure of the cracks, fractures and pores, the velocity increases. With increasing temperature velocity decreases because of the change of the elastic properties of the rock forming minerals, the change of the pore filling and changes in contact conditions of the grains (Schoen, 1996).

Seismic velocities are sensitive to fluids exhibiting strong influence on compressional wave velocity and a low influence on shear wave velocity (Mavko et al, 1998).

3.4.2. Measuring method

For this study only compressional wave velocities as first arrivals are measured.

The compressional wave velocity was determined with an ultrasonic device (Figure 3-5) at core samples (diameter= 1inch). The sample gets fixed between a transmitter and receiver with a contact agent (ultrasonic gel) and a pressure of 5bar. Both transducers are piezoceramic systems (Type: S12 HB0.8-3 vertical probe, Karl Deutsch, Germany) designed for compressional wave measurement.

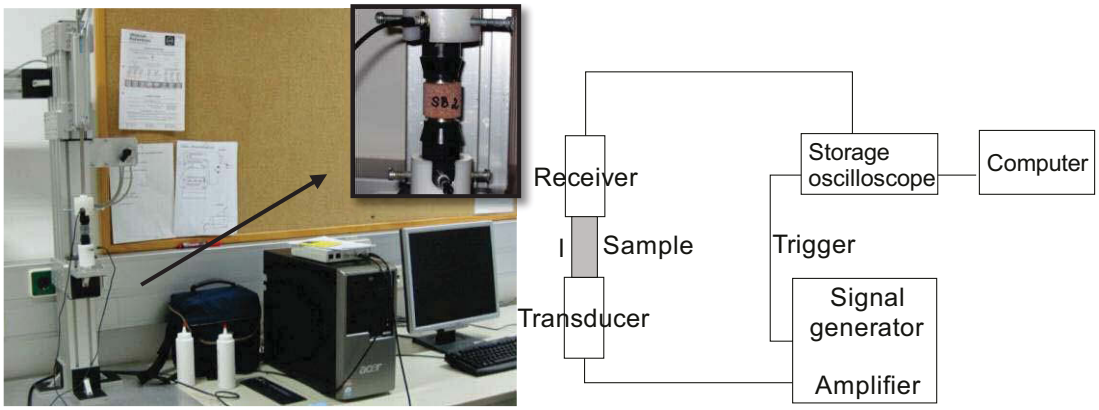

Figure 3-5: Ultrasonic device (left: transducers with sample in between, right: computer and storage oscilloscope)

A Dirac impulse is sent to the transducer and results in a mechanical pulse transmitting the sample. The arriving signal is visualized on the computer screen with a storage oscilloscope. A self-written program picks the first arrival and calculates the velocity from the digitally stored signal. At the start of each new measurement cycle, the dead time (delay time between electrical impulse and mechanical pulse) is determined. So all measurements are dead time corrected.

The reproducibility is about 1% of the compressional wave velocity.

3.5. Electrical properties

3.5.1. Overview

The SI unit for the specific electrical resistivity ρ is Ohmm. The inverse of specific electrical resistivity is the conductivity in Sm^{-1}.

Materials are divided into conductors, semiconductors and isolators (non-conductors). Most rock forming minerals, oil and gas are non-conductors in contrast to aqueous solutions, which are conductors. Their conductivity is dependent on the concentration of ions, the charge number of the ions and temperature (Schoen, 1996).

The specific electrical resistivity of a rock mainly depends on the water content in connected pores or fractures and on the specific resistivity of this water. The correlation between water saturation, porosity, water resistivity and rock resistivity is described by Archie's equations (Archie, 1942). The equations are not valid if other conductive components, like clay, ore or graphite are present.

For magmatic and metamorphic rocks the range of specific electrical resistivity is between 10^3 and 10^5Ohmm, depending on fracturing and water saturation. Sedimentary rocks show resistivity's - depending on porosity and fluid saturation - between 10^1 and 10^4Ohmm. Clays have low values between 3 and 20Ohmm.

Clay alteration, dissolution, faulting, salt water intrusion, shearing and weathering decrease resistivity. In contrast indurations, carbonate precipitation and silification increase resistivity (Schoen, 1996).

Specific electrical resistivity is measured at low frequencies. With increasing frequency in addition to the real component an imaginary component occurs and resistivity becomes a complex property with frequency dependence. Frequency dependent behaviour of electrical resistivity is subject of SIP (Spectral induced polarization) measurements. The complex character of conduction delivers information about interface properties in addition to Archie's relationships (Boerner, 2006).

3.5.2. Measuring method

Electrical properties of rock samples are measured only at low frequencies (real component of resistivity).

Following Archie's equation the electrical measurements are aimed at two parts:

- specific resistivity of the water
- specific resistivity of the saturated rock sample.

Temperature and conductivity of the water are measured with a conductivity meter (Type: LF 325 from WTW, Germany). For the measurements on saturated samples a 4-point-light instrument (LGM Lippmann) and a 4-electrode cell (Figure 3-6) were used.

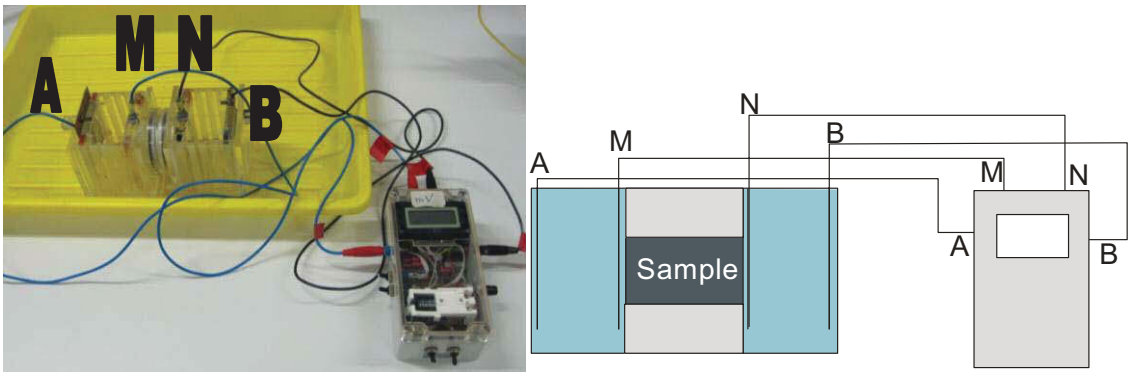

Figure 3-6: 4-point-light instrument for resistivity measurements; left: the cell where the sample is positioned in the middle between M and N electrodes. Right: measuring instrument

The cylindrical 1- inch cores get wrapped with Teflon tape so that no parallel bypass current can flow outside the sample. Platinum electrodes A, B (Figure 3-6) send an alternating current into the cell; the voltage is measured as potential difference between the two electrodes M, N at the faces of the sample.

With the following equation the specific electrical resistivity is calculated:

$$\rho = k * R \quad (3\text{-}5)$$

$$R = U/I \quad (3\text{-}6)$$

where *k* is the geometric factor [m], *ρ* is the specific resistivity[Ωm], *R* is the resistivity [Ω], *I* is the current and *U* is the voltage.

For a cylindrical sample the geometric factor *k* is given as ratio of the cross section of the sample and the distance between voltage electrodes M and N (equals the length of the cylindrical sample).

Only saturated samples with porosity can be measured, otherwise there is no conductive material.

3.6. Density and porosity

3.6.1. Overview density

Density [gcm^{-3} or kgm^{-3}] is the ratio of mass *m* [g or kg] and the volume *V* [cm^3 or m^3]:

$$d = m/V \quad (3\text{-}7)$$

Because the symbol *ρ* is used for the specific electrical resistivity, *d* represents the density in this work.

For a rock being a heterogeneous material, different densities must be distinguished:

- bulk density: mean density of a rock including pores
- density of an individual rock component
- grain density: Mean density of mineral grains without pores
- density of the pore fluid

Table A1 (Appendix) shows densities for rock-forming minerals and fluids.

For igneous rocks there is the tendency of an increase of density from acid to basic rocks. Metamorphic rocks are mainly influenced by composition and density of the initial rock material, the degree of metamorphism, thermodynamic conditions and processes (Schoen, 1996). Density of sedimentary rocks is controlled by matrix density (grain density), porosity and fluid density.

3.6.2. Overview porosity

In the engineering classification porosity is divided into total and effective porosity. The total porosity is the whole pore space with all connected and isolated pores. Effective porosity is referred to all connected pores (Tiab & Donaldson, 2004).

3.6.3. Measuring Method

Grain density is measured with a helium-pycnometer (Figure 3-7). The basic idea for these calculations of the instrument is the ideal gas equation particularly for grain volume determination. Measurement gives directly the grain density and the volume of the sample.

Figure 3-7: Helium pycnometer for grain density determination

The bulk density is calculated with the volume (length and diameter measured with calliper rule) and the mass of the sample.

Effective porosity is determined by measurement of pore volume as difference of mass of water-saturated sample and mass of the dry sample. Sample volume can be measured using Archimedes' principle. Additionally the total porosity with the grain density can be calculated.

4. Results of the measurements – an overview

All measured data are compiled in the Appendix A2. This chapter gives an overview of these results as cross plots and histograms. The histograms give a first impression of the range and distribution of the measured parameters.

4.1. Histograms

a.) Granite and Gneiss with lower and higher content of quartz

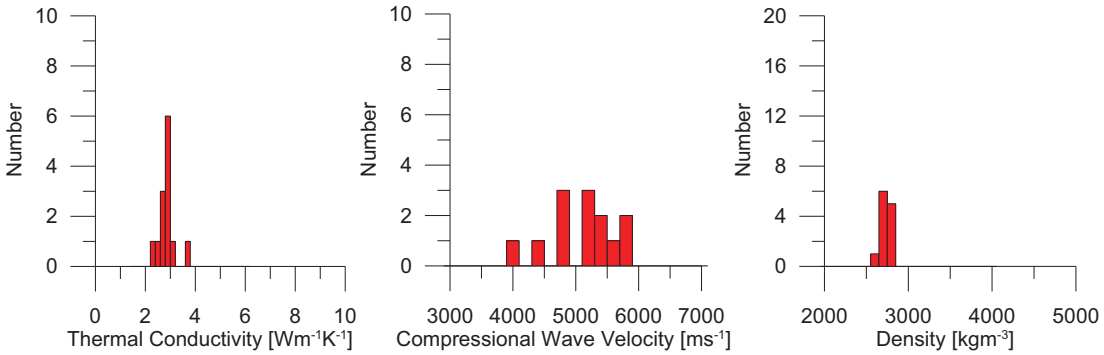

Figure 4-1: Histograms for Granite and Gneiss with lower content of quartz

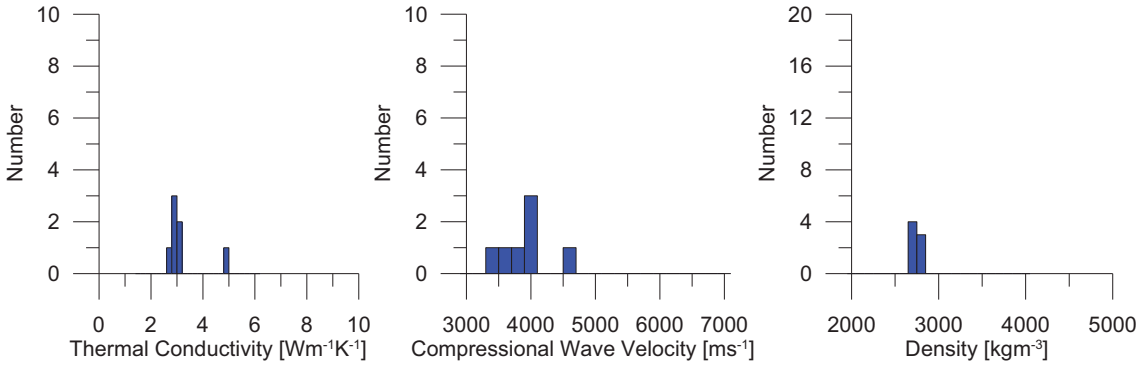

Figure 4-2: Histograms for Granite and Gneiss with higher content of quartz

b.) Basalt/Diorite/Gabbro

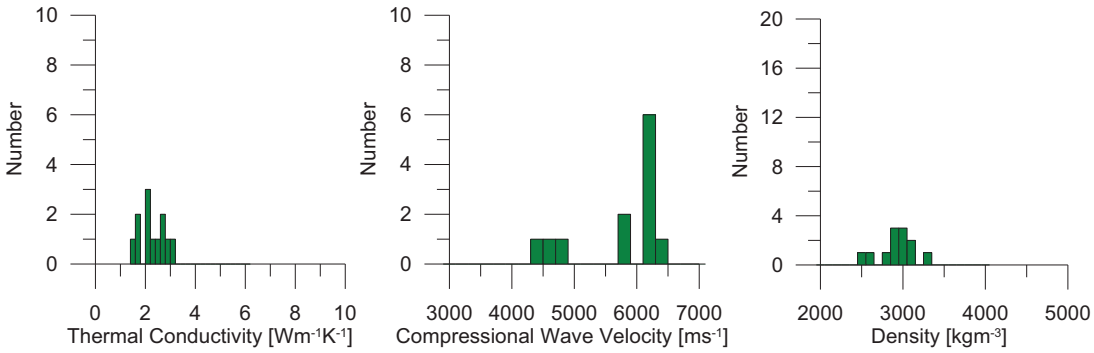

Figure 4-3: Histograms for Basalt/Diorite/Gabbro

c.) Sandstone

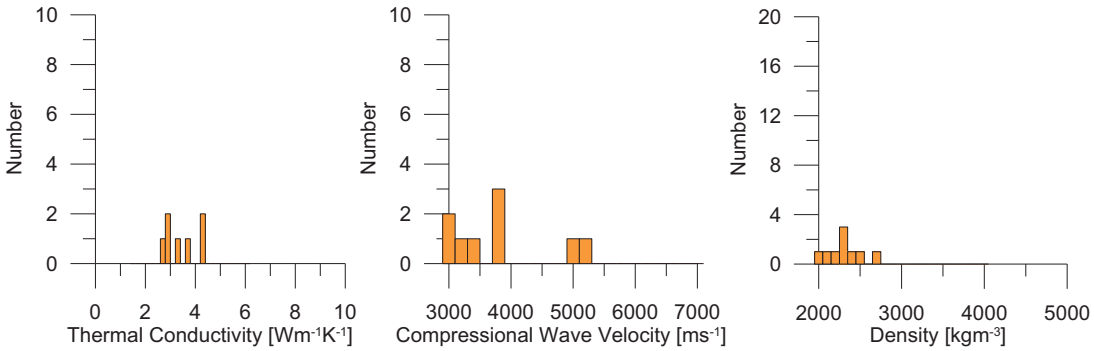

Figure 4-4: Histograms for Sandstone

d.) Gneiss-mica schist

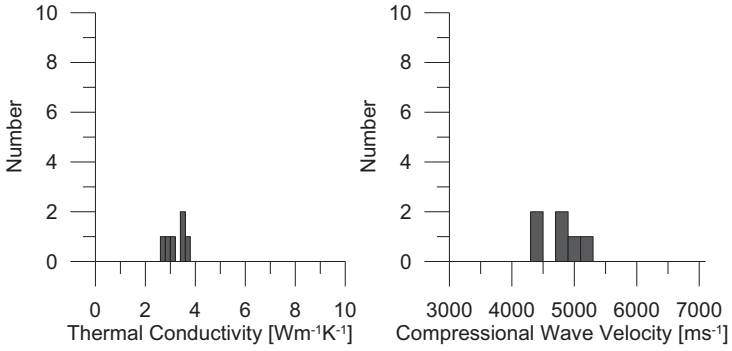

Figure 4-5: Histograms for Gneiss-mica schist

e.) Carbonate (Dolomite and Limestone)

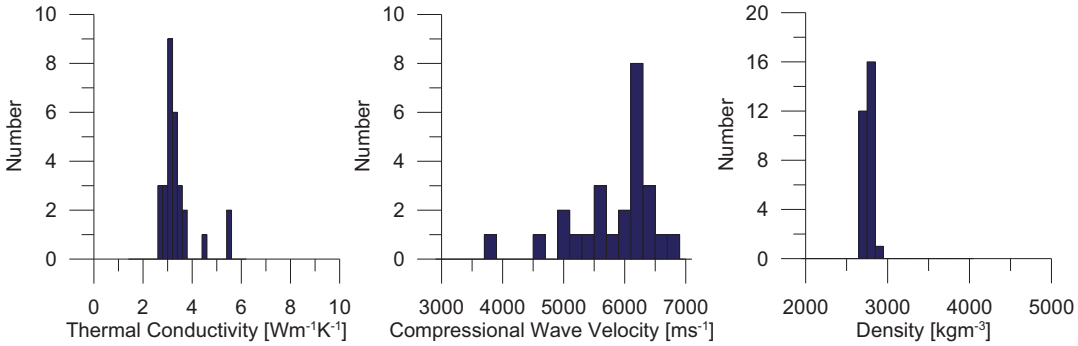

Figure 4-6: Histograms for Limestone

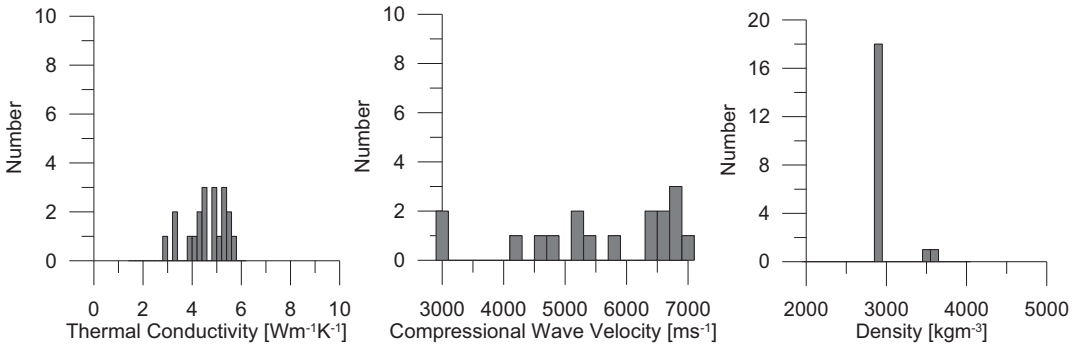

Figure 4-7: Histograms for Dolomite

4.2. Cross plots

Cross plots represent the experimental basis for the following comparison with model calculations and for interpretation. In this chapter the following cross plots are presented for the three main rock types:

- thermal conductivity versus compressional wave velocity,
- thermal conductivity versus density and
- thermal conductivity versus specific electrical resistivity (only for carbonates).

A cross plot density versus specific heat capacity is shown and discussed in Chapter 9.

According to the basic concept of “petrographic-coded thermal parameter estimation” the data sets are classified with respect to the rock type. Rock types are granites and gneiss with higher and lower content of quartz, gneiss-mica schist and basalt/diorite

and gabbro. Sandstone is plotted here in the same plots as the magmatic and metamorphic samples. For further correlations these are separated.

For carbonates with their diversity in mineral composition and pore types separate plots are created if all data are considered. Considering the different rock types shows empirically that there is a tendency of correlation between the two properties (thermal conductivity increases if compressional wave velocity increases). Therefore for the following investigations such cross plots are “petrographic-coded”.

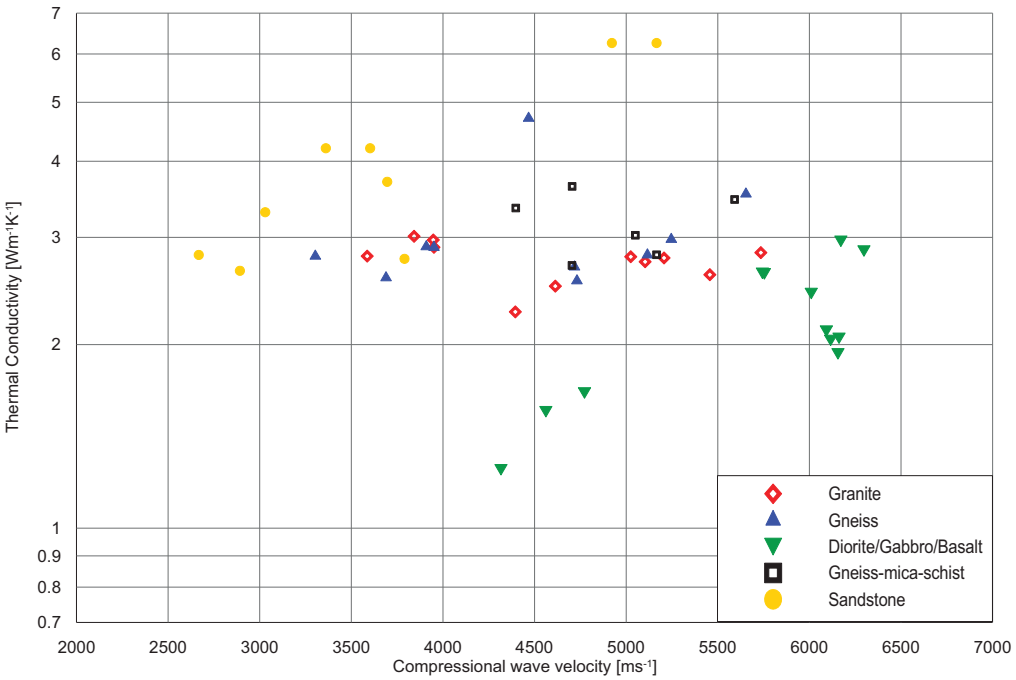

Figure 4-8: Thermal conductivity versus compressional wave velocity for different rock types (dry)

Figure 4-8 is one of the most important plots. It shows the measured data of thermal conductivity versus compressional wave velocity for different rock types under dry conditions. These values form the basis for the correlations and the model calculations (defect and inclusion model).

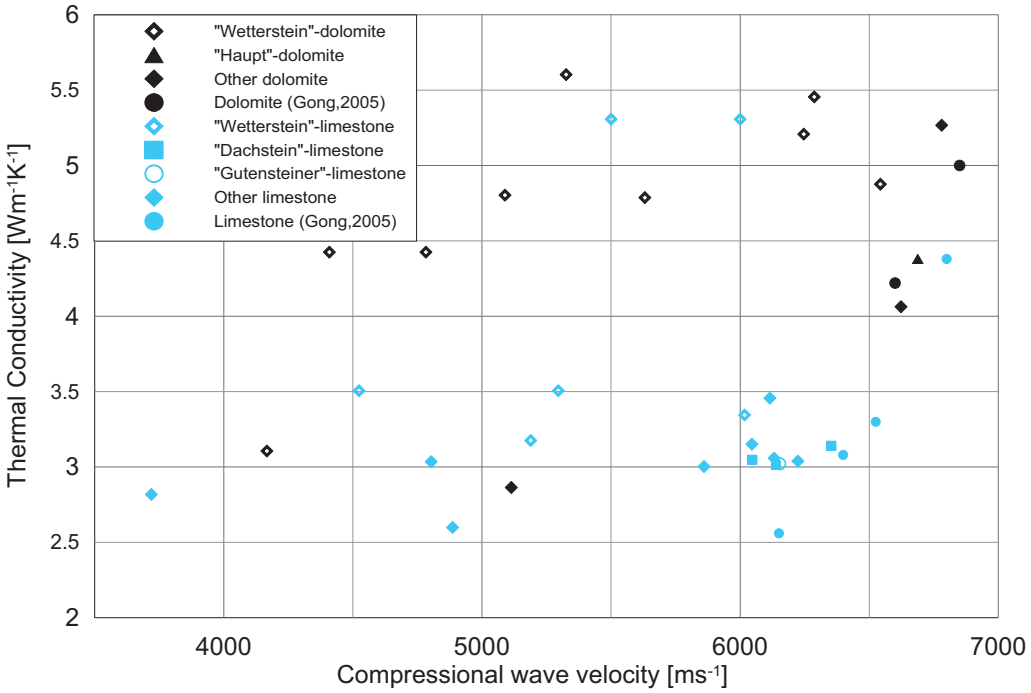

Figure 4-9: Thermal conductivity versus compressional wave velocity for carbonates (dry)

Thermal conductivity versus compressional wave velocity for dolomite and limestone is displayed in Figure 4-9. Data are again from dry samples.

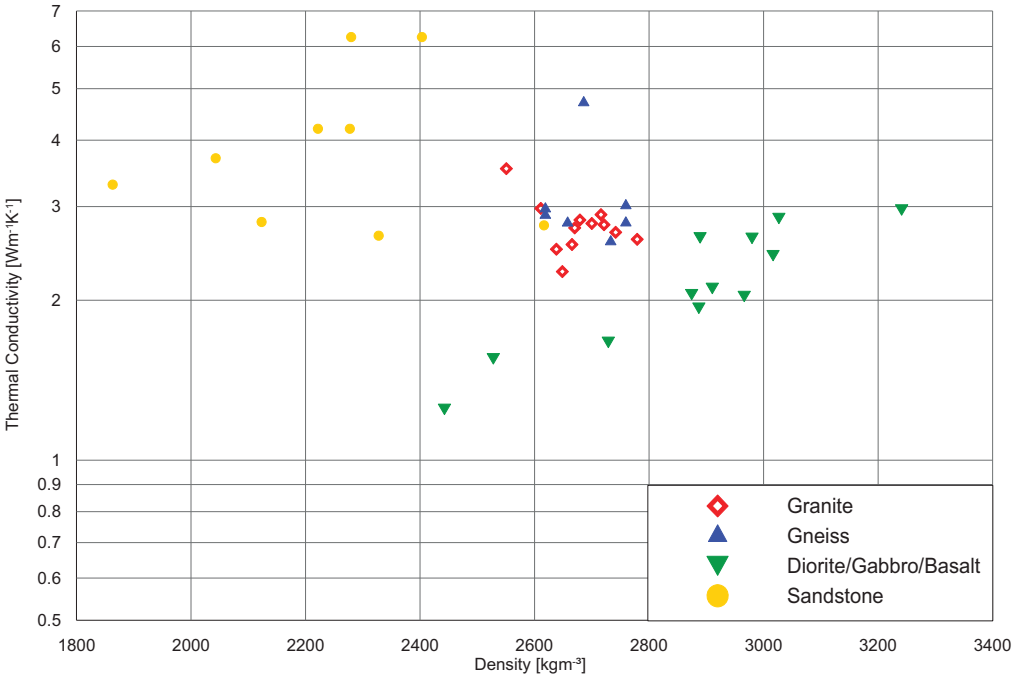

Figure 4-10: Thermal conductivity versus density for different rock types (dry)

Figure 4-10 presents the measured data for thermal conductivity and density for different rock types and Figure 4-11 for carbonates. Here the trend gets visible that with increasing thermal conductivity density increases.

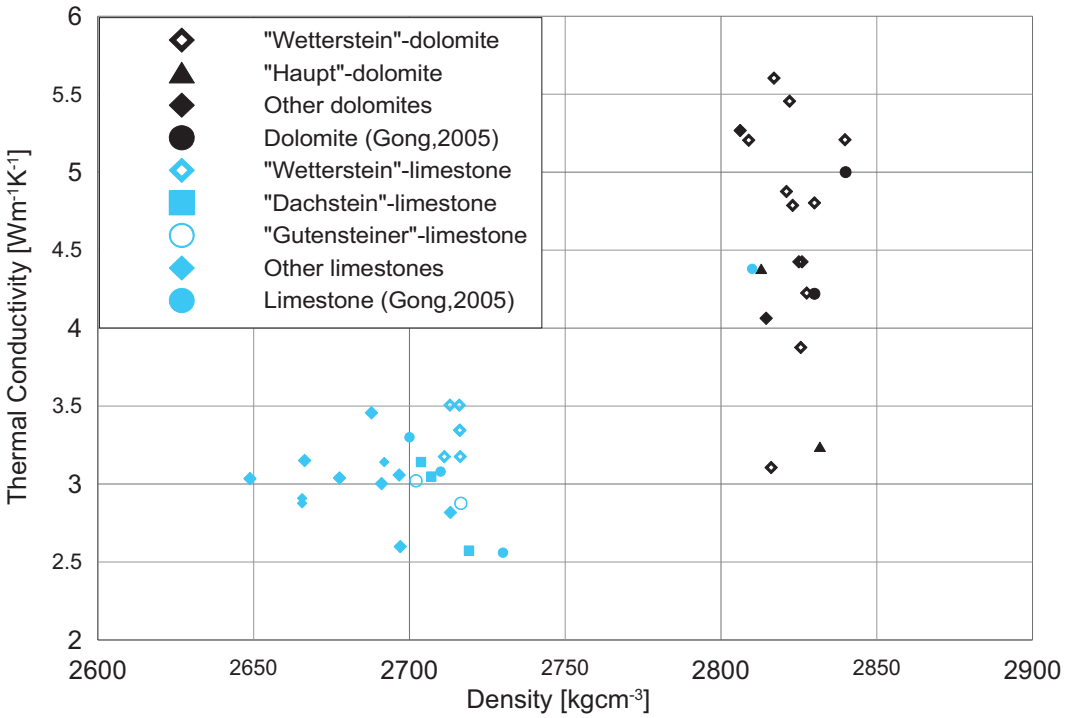

Figure 4-11: Thermal conductivity versus density for carbonates (dry)

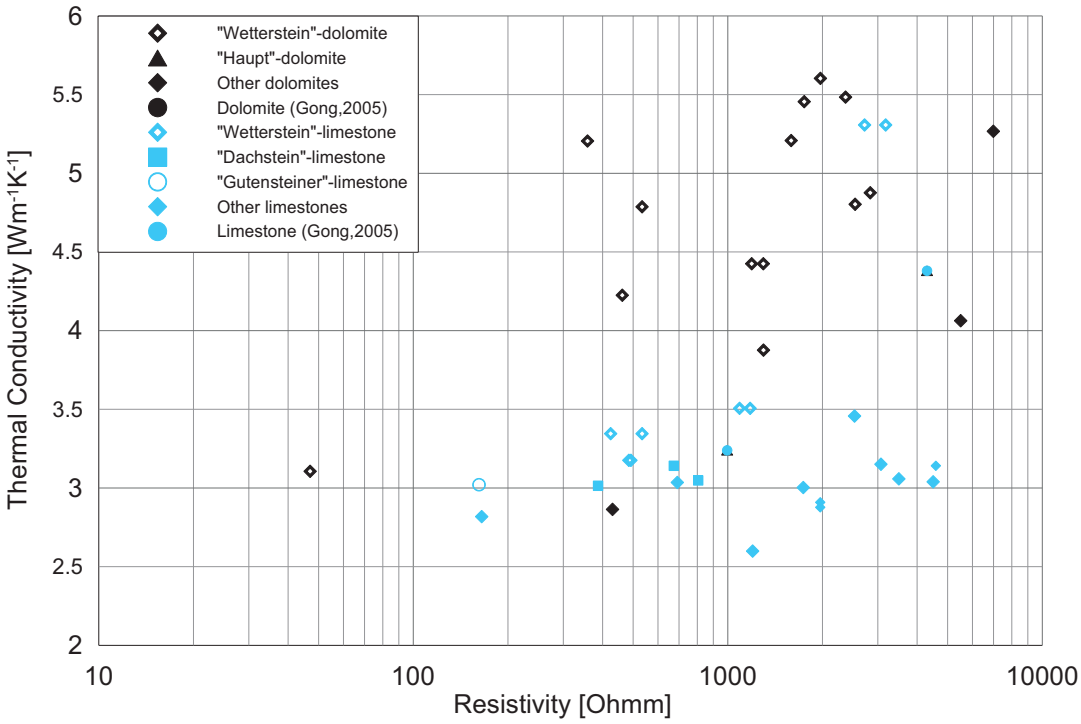

Figure 4-12: Thermal conductivity versus specific electrical resistivity for carbonates

Thermal conductivity versus specific electrical resistivity is displayed for carbonates (Figure 4-12), because porosity for magmatic rocks is small and resistivity was not measurable. Dolomites show a little bit higher thermal conductivity than the limestone. This is the effect of mineral thermal conductivity. Both-dolomite and limestone- show the trend, that with increase of thermal conductivity, electrical resistivity increases; this reflects the combined effect of porosity and mineral composition in case of carbonates.

Cross plots show:

- In some cases a tendency of a correlation.
- A different position of such tendencies in the plot indicating a strong influence of rock type.
- A wide scatter of data points; this expresses the effect of a variety of parameters (mineral composition, fracturing, etc.).

Therefore any model design must implement at least the following influences:

- mineral composition and mineral properties (petrographic-coded)
- porosity, fracturing and other “defects”
- parameters describing the geometry of pores, fractures,...- and mineral aggregates

5. Model calculations

In petrophysics models are developed and applied in order to:

- understand and explain the dominant dependencies on various influences
- derive relationships between different properties
- establish fundamentals for a combined interpretation of petrophysical data.

Models implement a simplification mainly of the internal geometry (structure, texture) of rocks. Therefore a classification in some basic types follows the type of geometrical idealization. There are four basic types that are relevant for the following investigations (Figure 5-1): The first types of models are simple sheet or layer models. The foundation was laid by Voigt (1910) and Reuss (1927). These models deliver the upper and the lower bound of a property for a given mineral composition (mineral properties and volume fraction). It is not an approximation for fractures and cracks because their effect is not represented with these models. Additionally there are bound-models that give narrower bounds for compound media, for example Hashin & Shtrikman (1963).

More complex models are linked “matrix and fluid components” models. Members of this group are in case of elastic properties the theory of Gassmann (1951), Biot (1956) and Geertsma & Smith (1961). Special types - preferred for fractured rocks - are inclusion models as for example from Eshelby (1957), Toksoez et al (1976) or Budiansky & O’Connell (1976). These models are generally applicable and directed at elastic, thermal and electrical properties. Here a broad range of possibilities with the shape of inclusions and the pore properties are available.

A simplification of such model types for fractured rocks is the “defect model”.

Sphere models defined for example by Gassmann (1951), Hara (1935) and White (1983) are preferred for elastic properties. These models are relevant for granular materials (unconsolidated rocks) and describe the nonlinear pressure influence, but fail for porosity description.

Pore channel models consider only “pore controlled properties” like permeability and electrical conductivity in clean rocks.

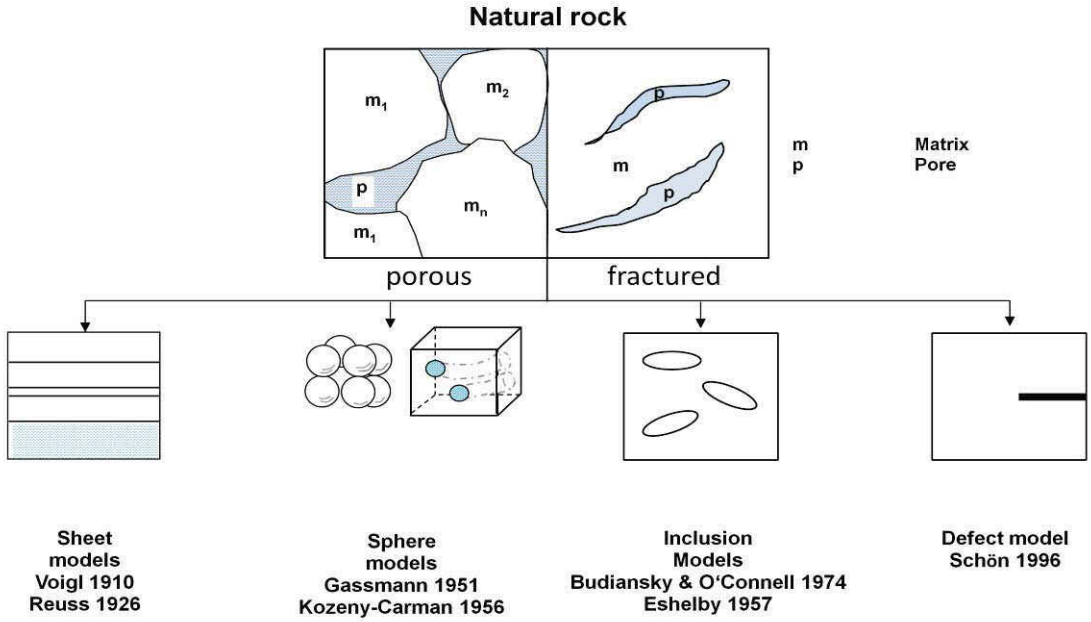

Figure 5-1: Classification of main model types (modified, Schoen, 1996)

For the interpretation of the experimental data measured on igneous rocks (dense and fractured) and sedimentary consolidated rocks (sandstones, carbonates) three model types are selected:

- layered models for the host material calculations and
- inclusion models for implementation of pores and fractures.
- Additionally a specific simplified "defect model" was applied.

Carbonates are discussed separately in Chapter 8, because of their special character and behaviour.

The model types are combined in the concept of petrographic-coded thermal parameter estimation.

5.1. The concept of petrographic coded thermal parameter estimation

Main motivation of the study is the derivation of relationships between thermal conductivity and other properties which can be measured using geophysical methods.

Experimental investigations show that thermal conductivity is controlled mainly by mineral composition, porosity and/or fracturing. For the magnitude of thermal conductivity the solid mineral components are dominant (particularly quartz with highest thermal conductivity).

Among the “geophysical” properties seismic velocity shows some similarities: Seismic velocity is also controlled mainly by mineral composition, porosity and/or fracturing. For the magnitude of elastic wave velocities also solid mineral components are dominant.

Density is also controlled by mineral composition, but pores and fractures are only of influence as a volume effect (thus, fractures with low volume have a very small effect upon density).

Electrical rock conductivity is primarily controlled by porosity and fracturing, by water saturation and water conductivity – mineral properties as insulators are without contribution to electrical rock conductivity.

This consideration shows that for a direct correlation thermal conductivity and seismic velocity probably provide the strongest correlation. The following tendencies control the character of the expected relationships (Schoen, 2011):

- velocity decreases with increasing fracturing or porosity and increases from acid/felsic (granite) to basic/mafic (basalt) types,
- thermal conductivity decreases with increasing fracturing or porosity but decreases from acid/felsic (granite, high quartz content) to basic/mafic (basalt) types.

The expected correlations are complicated because the two influences act in an opposite direction; this leads to a scatter as a result of variation in fracturing and in mineral composition and confirms the need of a petrographic-coded model.

As conclusion a model concept (Figure 5-2) is used for the following derivations. It consists of two steps

Step 1: Modelling of solid matrix properties of the host material

Step 2: Implementation of pores and fractures using different models.

Depending on which relationships should be shown, fundamental requirements for the models are:

- They should contain the mineral composition with their properties, as one of the most important factors for rocks.
- Other necessary influencing factors are the cracks, fractures and pores as well as their fluid content, the geometry (shape) and the internal structure (connectivity and orientation).
- Especially for anisotropic rocks the geometry and internal structure is important (Schoen, 1996).

But, for all models the same important fact is valid: They are all idealized. So they will always be just an approximation to experimental data.

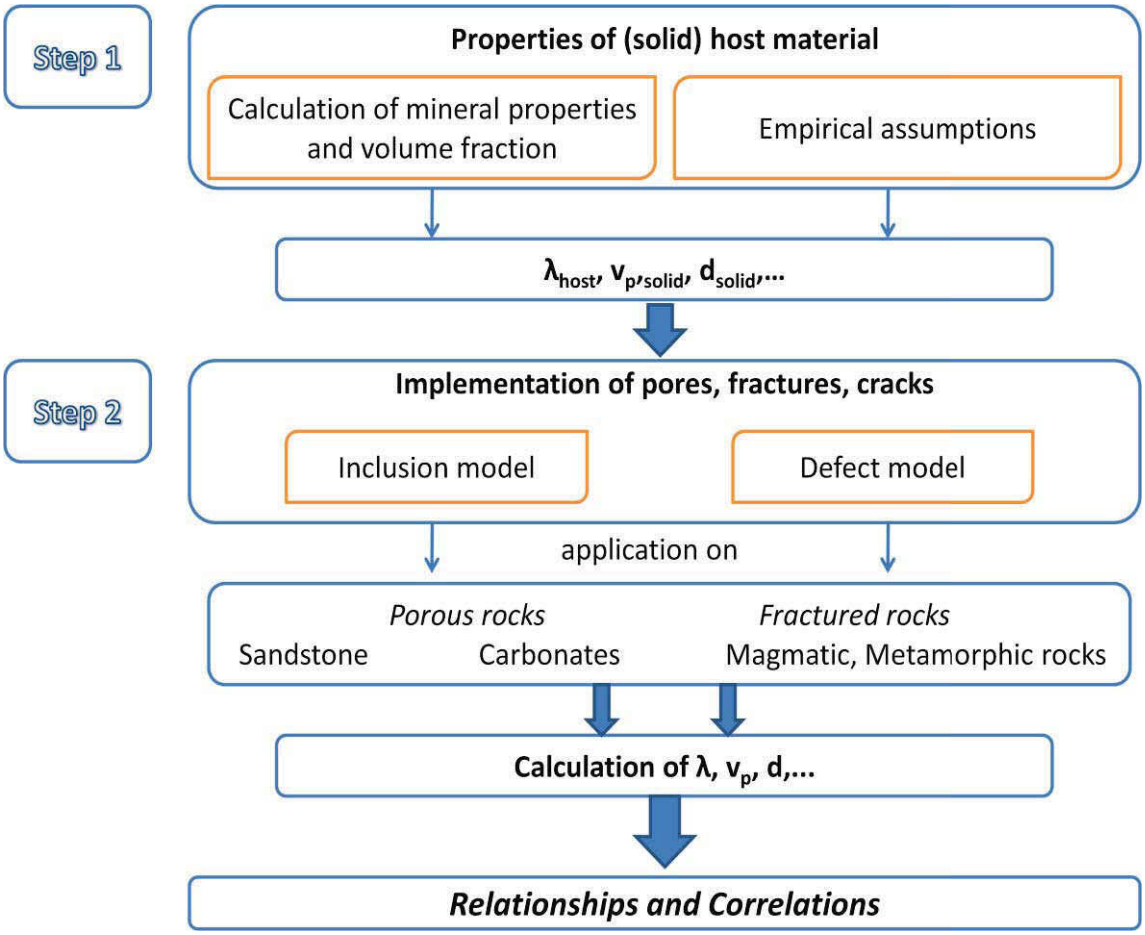

Figure 5-2: Schematic flowchart for the model calculations

5.2. Strategic concept for derivation of model-based relationships between thermal conductivity and geophysical parameters

Following the concept above (Figure 5-2) two steps must be realized:

Step 1:

In this step for example the composition of clastic sediment matrix (quartz, clay), carbonate (dolomite, calcite) and magmatic/metamorphic rocks (quartz, feldspar, mica etc.) is used in order to calculate the properties of the solid part (matrix) of the rock.

Different “mixing rules” are available for these calculations. They are based on Voigt-Reuss- or Hashin- bounds and any averaging (Hill average, geometric mean).

As input are necessary: mineral composition (volume fractions) and mineral properties (elastic and thermal properties). There are different ways to design the mineral composition:

- assumption of typical values for fractional composition of different rocks
- petrographic analysis
- volumetric interpretation of well log data (for example carbonate rocks: calcite and dolomite content).

The result of this first step represents the final parameters in case of a dense, non-fractured rock. For fractured or porous rocks this step delivers the properties of the solid rock compound (host material, matrix).

In some cases - particularly if mineral composition is not available - these “host properties” can be assumed empirically. They represent the properties of a completely dense, non-fractured material.

Step 2:

In step 2 all fluid components are introduced into the model - representing pores, fractures and all other “defects” within the solid host material.

Inclusion models are applied here. These models offer the possibility to consider the volume (porosity) and the shape of the inclusion (as a textural-structural property). Thus, the effect of pores and fractures is not reduced on a volumetric effect of the fluid (porosity). If inclusions have an orientation, modelling of anisotropy is possible (Chapter 10).

In addition to the inclusion concepts of Budiansky and O`Connell (1976) and Clausius-Mossotti (Chapter 5.4.1) a simplified “defect model” (Chapter 5.4.2) is applied (Schoen, 1996).

5.3. Modelling of mineral composition effects (Step 1)

The two most important approaches for models with the mineral content are the “series model” of Reuss (1927) and the “parallel model” of Voigt (1910). Using the idea of a layered or sheet idealization for rocks, these two models occur (Figure 5-3). Each sheet represents one mineral with its properties and the relative thickness of the sheet is proportional to the volume fraction of the mineral.

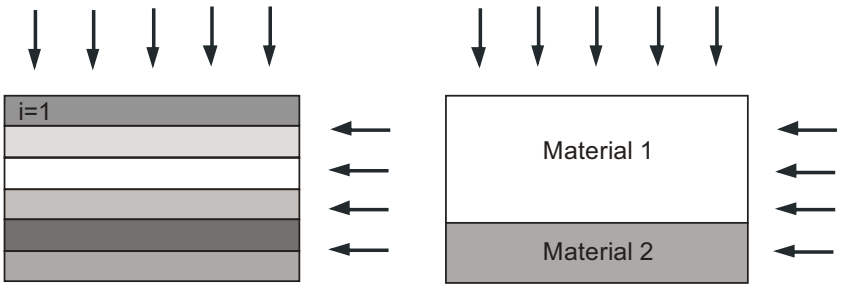

Figure 5-3: Idea of the sheet models with two (right) or more (left) components

As mentioned before, the two models give the lower (Reuss, 1927) and the upper (Voigt, 1910) bound and the "real" values (measured values) lie in between these.

The "parallel" model assumes the heat flow or wave propagation parallel to the boundaries between the components. The "series" model assumes the heat flow or wave propagation perpendicular to the boundaries between components.

This results in the following two equations for examples for the thermal conductivity:

$$\lambda_{//} = \sum_{i=1}^{n} V_i \cdot \lambda_{i_i} \qquad (5\text{-}1) \qquad\qquad \lambda_{\perp} = \left[\sum_{i=1}^{n} V_i \cdot \lambda_i^{-1} \right]^{-1} \qquad (5\text{-}2)$$

where n are the components, V_i is the volume fraction of each component i and λ_i the thermal conductivity of the component i. In the same kind elastic properties (compressional and shear modulus) can be calculated.

Different combinations of these two models were developed as for example "Hills-mean", which is the arithmetic mean of the two extreme values, or the geometric mean. Krischer & Esdorn (1956) applied a kind of "weighted" average for thermal conductivity of both models - the weighting factor shows a correlation with the strength of contacts between solid components.

Table 5-1 shows results of a forward calculation of elastic properties and thermal conductivity for two rocks of different mineral composition and the mean input values for some rock forming minerals. The density results as weighted arithmetic mean (Voigt equation).

Minerale	d	λ	k	G	Volume	Volume
	[gcm^{-3}]	[Wm^{-1}K^{-1}]	[GPa]	[GPa]	(Granite)	(Basalt)
Quartz	2.65	5.50	38.00	44.00	0.50	0.00
Olivine (forsterite)	3.20	4.10	130.00	80.00	0.00	0.15
Pyroxene	3.29	4.63	102.60	60.35	0.00	0.35
Hornblende	3.12	2.81	87.00	43.00	0.00	0.00
Feldspar (mean)	2.62	2.00	37.50	15.00	0.00	0.00
Feldsp.- Orthoclase	2.57	2.20	45.00	20.00	0.25	0.00
Feldsp.-Plagi. albite	2.63	2.30	60.00	24.00	0.15	0.50
Mica-muscovite	2.79	2.28	52.00	32.00	0.05	0.00
Mica-biotite	3.05	2.00	51.00	25.00	0.05	0.00

Property (Granite)	Voigt	Reuss	Hill mean
Compressional modulus k [GPa]	44.4	43.2	43.8
Shear modulus μ [GPa]	33.5	29.7	31.6
Density d [gcm^{-3}]	2.7		
Compressional wave velocity [ms^{-1}]	5790.9	5584.8	5688.8
Thermal conductivity [$Wm^{-1}K^{-1}$]	3.9	3.2	3.5

Property (Basalt)	Voigt	Reuss	Hill mean
Compressional modulus k [GPa]	85.4	77.5	81.5
Shear modulus μ [GPa]	45.1	35.1	40.1
Density d [gcm^{-3}]	3.0		
Compressional wave velocity [ms^{-1}]	7041.5	6506.6	6779.3
Thermal conductivity [$Wm^{-1}K^{-1}$]	3.4	3.0	3.2

Table 5-1: density *d*, compressional modulus *k*, shear modulus μ, thermal conductivity λ - mean values for rock forming minerals (upper part of the table) and the calculated Voigt-Reuss bounds and Hill mean for an acid (granite) and a basic (basalt) rock type (lower part of the table)

A more complex approach is the theory of Hashin & Shtrikman (1963), which results in narrower boundaries compared with Voigt- and Reuss- bounds.

As noted before, another method to estimate the starting values for the solid host material (formed by mineral composition) of the models is the direct input of mean values for the composite material (Schoen, 1996). This is easier because no calculation has to be done before. I used this empirical assumption for the model calculations.

5.4. Modelling of pore and fracture effects (Step 2)

With this step in the solid host material pores and fractures are implemented. Two model types were selected, an inclusion and a defect model. Either can give the main influences: the mineral composition and the cracks/fractures. Using nearly the same input values for both models, make them more comparable.

5.4.1. Inclusion model – dry rock

The idea behind inclusion models is a homogeneous solid material with isolated pores or cracks (Figure 5-4). The pores and cracks are modelled mostly as ellipsoidal inclusions described by the aspect ratio (Figure 5-5). The geometry of the inclusion can be varied by its size and aspect ratio. Size, aspect ratio and concentration (number) of inclusions give the porosity.

The properties of solid host material can be varied depending on the material composition (mineral content). Berryman (1995) described various models for rock properties for example the dielectric properties and elastic constants. Earlier models were presented for example by Clausius-Mossotti (in Mavko et al (1998)) and Eshelby (1957).

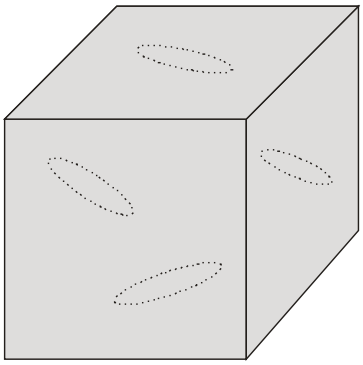

Figure 5-4: Illustration of an inclusion model

Budiansky & O'Connell (1976) derived with a self-consistent algorithm an equation for the elastic properties assuming a penny-shaped cracked medium, which form the basis for the calculations of the inclusion model. Compressional modulus k_{sc} and shear modulus μ_{sc} result as:

$$k_{SC} = k_S * \left[1 - \frac{16}{9} * \frac{1-\nu_{SC}{}^2}{1-2*\nu_{SC}} * \varepsilon\right] \quad (5\text{-}3)$$

$$\mu_{SC} = \mu_S * \left[1 - \frac{32}{45} * \frac{(1-\nu_{SC})*(5-\nu_{SC})}{2-\nu_{SC}} * \varepsilon\right] \quad (5\text{-}4)$$

where k_s and μ_s are the compressional and shear modulus of host material are.

ε is a "crack density parameter"

$$\varepsilon = \frac{N}{V}\alpha^3 \quad (5\text{-}5)$$

defined as the number of cracks per unit volume times the crack radius cubed, k_s is the compression modulus for the solid material and μ_s is the shear modulus for the solid material (Mavko et al, 1998).

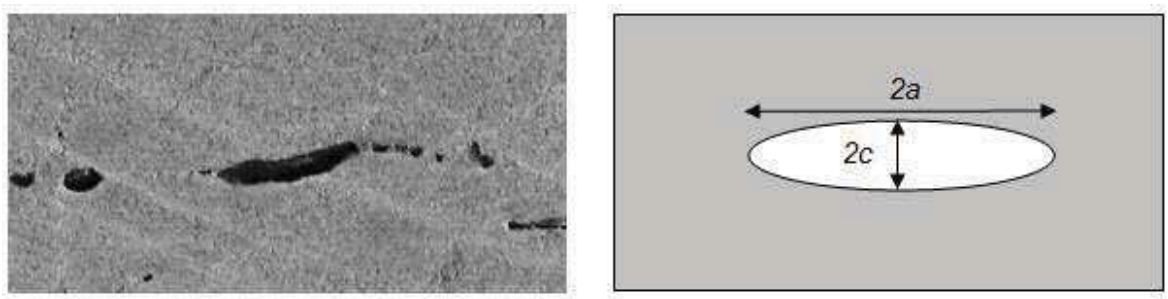

Figure 5-5: Illustration of the aspect ratio with an example in a rock (Schoen, 2011)

The crack porosity is $$\phi = \frac{4*\pi}{3} * \alpha * \varepsilon \quad (5\text{-}6)$$

where α is the aspect ratio *(α=a/c).*

The effective Poisson's ratio is:

$$\nu_{\mathrm{SC}} \approx \nu_{\mathrm{S}} * \left[1 - \frac{16}{9} * \varepsilon\right] \quad (5\text{-}7)$$

where v_s is the Poisson's ratio of the solid material.

The calculation is simplified by the nearly linear dependence of v_{SC} on ε (5-7) (Mavko et al, 1998).

The equations (5-3), (5-4), (5-5) and (5-6) present some remarkable characteristics:

- in equation (5-3) the second term in brackets describes the effect of inclusions on the elastic moduli of the rock
- this effect of the elastic moduli is controlled only by Poisson's ratio of the host material v_s and the "crack density parameter" ε
- equation (5-6) shows after rearrangement that the crack density parameter represents a combination of porosity ϕ and aspect ratio α

This explains the strong effect of aspect ratio on elastic properties and shows additionally that inclusion is controlled by the ϕ/α ratio. Thus, high porosity and high aspect ratio can have the same effect as low porosity and low aspect ratio. Porosity alone is not sufficient to describe thermal and elastic (or more general-tensorial) properties of a rock.

In addition, density *d* is needed for the calculation of the compressional wave velocity

v_p: $$d = (1 - \phi) * d_{\mathrm{s}} + \phi * d_{\mathrm{air}} \quad (5\text{-}8)$$

which results in:

$$v_{\mathrm{p}} = \left(\frac{k_{\mathrm{sc}} + \frac{4}{3} * \mu_{\mathrm{sc}}}{d}\right)^{1/2} \quad (5\text{-}9)$$

d_s is the density of the solid material, ϕ is the porosity and d_{air} is the density of the air (assuming dry rocks). Density depends only on densities of components (fluid, solid) and porosity – there is no influence of pore or fracture geometry.

For the calculations of thermal conductivity equations of Clausius-Mossotti (see Berrymann, 1995) can be used for the inclusion model:

$$\lambda_{\mathrm{CM}} = \lambda_{\mathrm{S}} * \frac{1-2*\phi*R^{\mathrm{mi}}*(\lambda_{\mathrm{S}}-\lambda_{\mathrm{i}})}{1+\phi*R^{\mathrm{mi}}*(\lambda_{\mathrm{S}}-\lambda_{\mathrm{i}})} \quad (5\text{-}10)$$

where

$$R^{\mathrm{mi}} = \frac{1}{9} * \left(\frac{1}{L_{\mathrm{a,b,c}}*\lambda_{\mathrm{i}}+(1-L_{\mathrm{a,b,c}})*\lambda_{\mathrm{s}}}\right) \quad (5\text{-}11)$$

λ_i is the thermal conductivity of the inclusion

λ_s is the thermal conductivity of the solid mineral composition

R^{mi} is a function (5-11) of the depolarization exponents L_a, L_b, L_c where the subscript a, b, c refer to the axis direction of the ellipsoid. Depolarization exponents are related to the aspect ratio (Berryman, 1995) where $L_a+L_b+L_c=1$. There are also values and approximations for some extreme shapes:

sphere: $L_a = L_b = L_c = 1/3$

needle: $L_c = 0$ (along needle long axis), $L_a = L_b = 1/2$ (along needle short axes)

disk: $L_c = 1$ (along short axis), $L_a = L_b = 0$ (along long axes).

Sen (1981) recommends the following approximation for plate-like objects ($a = b >> c$)

$$L_{\mathrm{c}} = 1 - \frac{\pi}{2} * \frac{c}{a} = 1 - \frac{\pi}{2} * \alpha \quad (5\text{-}12)$$

where $\alpha = \frac{c}{a}$ is the aspect ratio.

This can be applied for an estimate of L_c. In a second step, the results are

$$L_{\mathrm{a}} = L_{\mathrm{b}} = \frac{1-L_{\mathrm{c}}}{2} = \frac{\pi}{4} * \alpha \quad (5\text{-}13)$$

Table 5-2 gives an overview of some different aspect ratios and the resulting depolarization exponents.

$\alpha = c/a$	$L_a = L_b$	L_c
0.1	0.0785	0.8429
0.05	0.0393	0.9215
0.02	0.0157	0.9686
0.01	0.0079	0.9843
0.005	0.0039	0.9921
0.002	0.0016	0.9969
0.001	0.0008	0.9984

Table 5-2: Aspect ratios and resulting depolarization factor

Furthermore thermal conductivity equations show that the effect of an inclusion is controlled by both geometrical parameters - inclusion porosity ϕ and aspect ratio α via depolarization factors.

Figure 5-6 shows results of forward-calculated relationships between compressional wave velocity and thermal conductivity. The two curve sets represent different rock types (petrographic code) expressed in terms of the solid (host material) properties:

Rock A (represents for example granite):

λ_s = 3.5 WmK^{-1} λ_f = 0.025 WmK^{-1} k_s = 44 GPa μ_s = 31 GPa d_s = 2.66 gcm^{-3};

with a resulting host velocity $v_{p,s}$ = 5675 ms^{-1}

Rock B (represents for example basalt):

λ_s = 3.2 WmK^{-1} λ_f = 0.025 WmK^{-1} k_s = 80 GPa μ_s = 45 GPa d_s = 3.00 gcm^{-3};

with a resulting host velocity $v_{p,s}$ = 6831 ms^{-1}

Three different aspect ratios are used for both rock types (type A and B):

$\alpha = 0.20$: L_a = 0.157 L_c = 0.686 and $R_{mi,granite} = 0.175$ $R_{mi,basalt} = 0.191$

$\alpha = 0.10$: L_a = 0.079 L_c = 0.843 and $R_{mi,granite} = 0.264$ $R_{mi,basalt} = 0.287$

$\alpha = 0.05$: L_a = 0.039 L_c = 0.921 and $R_{mi,granite} = 0.439$ $R_{mi,basalt} = 0.477$

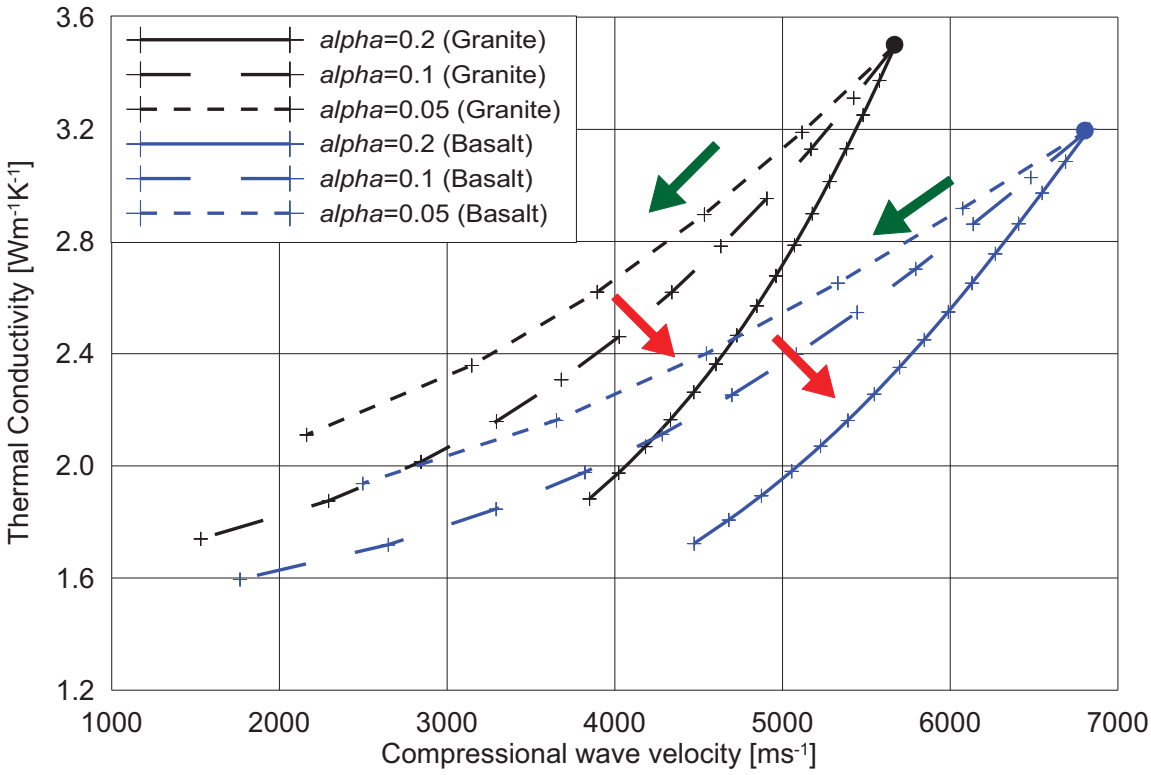

Figure 5-6: Result of forward-calculated relationships between compressional wave velocity and thermal conductivity. Rock A: λ_s = 3.5 WmK^{-1} λ_f = 0.025 WmK^{-1} k_s = 44 GPa μ_s = 31 GPa d_s = 2.66 gcm^{-3} ; $v_{p,s}$ = 5675 ms^{-1}; Rock B: λ_s = 3.2 WmK^{-1} λ_f = 0.025 WmK^{-1} k_s = 80 GPa μ_s = 45 GPa d_s = 3.00 gcm^{-3} ; $v_{p,s}$ = 6831 ms^{-1}; aspect ratios α = 0.20 , 0.10 and 0.05; The crosses along the curves are 0.02 (2 %) steps of porosity increase.

The dots at the beginning demonstrate the “host material point” in the cross plot. The green arrows indicate the effect of increasing porosity and the red arrows show the effect of decreasing aspect ratio.

Rock type A represents an acid rock (granite) whereas B stands for a basic rock (basalt). The plot shows the strong influence of aspect ratio on the position of the curve. With decreasing aspect ratio the effect on both properties increases – for low aspect ratio small porosity change has a dramatic effect upon both parameters.

5.4.2. Defect model – dry rock

The second approach is the defect model (Figure 5-7). The defect parameter in a solid matrix is characterized by its relative length D (Schoen, 1996).

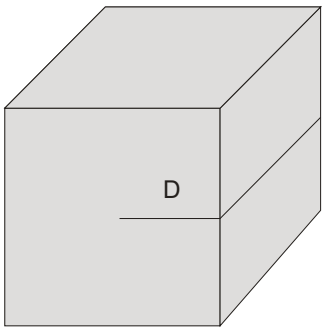

Figure 5-7: Illustration of the defect model

As a first approximation and using only linear terms the decrease of properties caused by defects (fractures, cracks) in a dry rock can be described as follows

$$k_{rock} = k_{solid}(1 - D) \tag{5-14}$$

$$\mu_{rock} = \mu_{solid}(1 - D) \tag{5-15}$$

$$v_{p,rock} = v_{p,solid}\sqrt{1 - D} \tag{5-16}$$

$$\lambda_{rock} = \lambda_{solid}(1 - D) \tag{5-17}$$

k_{solid}, μ_{solid}, $v_{p,solid}$ and λ_{solid} are the values of the solid compressional modulus, shear modulus, compressional wave velocity and thermal conductivity, respectively of the solid matrix block. For the relationship between thermal conductivity and elastic wave velocity the simple equation results in

$$\lambda_{\mathrm{rock}} = v^2{}_{\mathrm{p,rock}} * \left(\frac{\lambda_{\mathrm{solid}}}{v^2{}_{\mathrm{p,solid}}}\right) = v^2{}_{\mathrm{p,rock}} * A_{\mathrm{solid}} \tag{5-18}$$

The equation reflects the correlation between thermal rock conductivity and the square of elastic wave velocity as result of the defect influence. The rock type ("petrographic code") is expressed as the parameter A_{solid} (solid matrix value), which is controlled only by mineral composition and properties (same position as host material in case of inclusion models).

A solid matrix value needs to be determined or defined for the calculations of the defect model, using the equations (5-14 - 5-17). Almost the same input values as for the inclusion model are used. Figure 5-8 shows a forward calculation for two types of rock: an acid one (granite) and a basic one (basalt). Input values are the before calculated data from Table 5-1. Defect parameters increase in steps of 0.1.

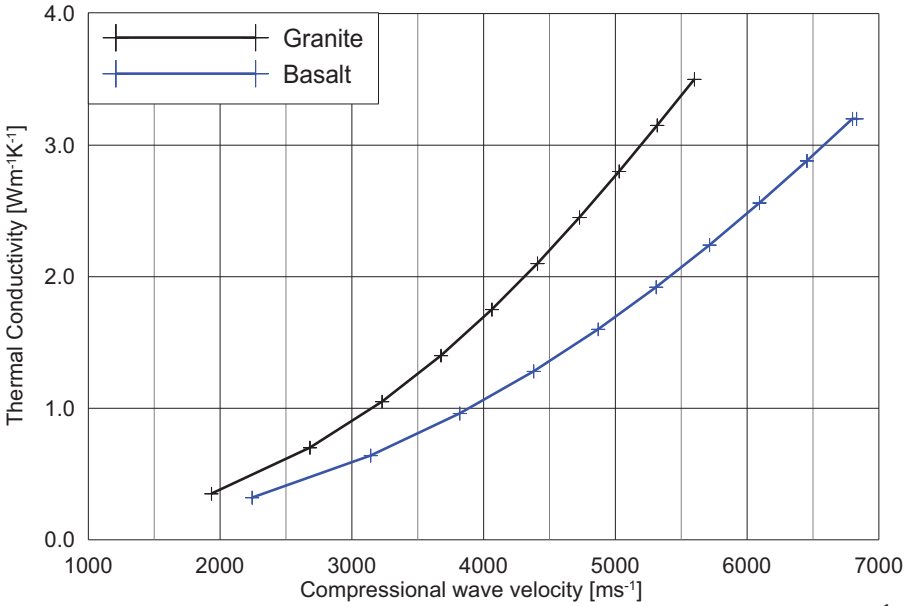

Figure 5-8: Defect model calculations for an acid (granite, λ_{solid}= 3.51 $Wm^{-1}K^{-1}$, $v_{p,solid}$=5688 ms^{-1}, A_{solid}=1.09E-7 $Ws^2m^{-3}K^{-1}$)and a basic (basalt, λ_{solid}= 3.21 $Wm^{-1}K^{-1}$, $v_{p,solid}$=6779 ms^{-1}, A_{solid}=0.70E-7 $Ws^2m^{-3}K^{-1}$) rock type

A comparison of the defect and the inclusion model shows, that the defect model cannot express different shapes (aspect ratio). The defect model lies between the curves of the inclusion model with α=0.2 and α=0.1. The interpretation of the experimental data using the defect model is more comfortable in a logarithmic scale (Figure 5-9). The result is a straight line for the model calculations.

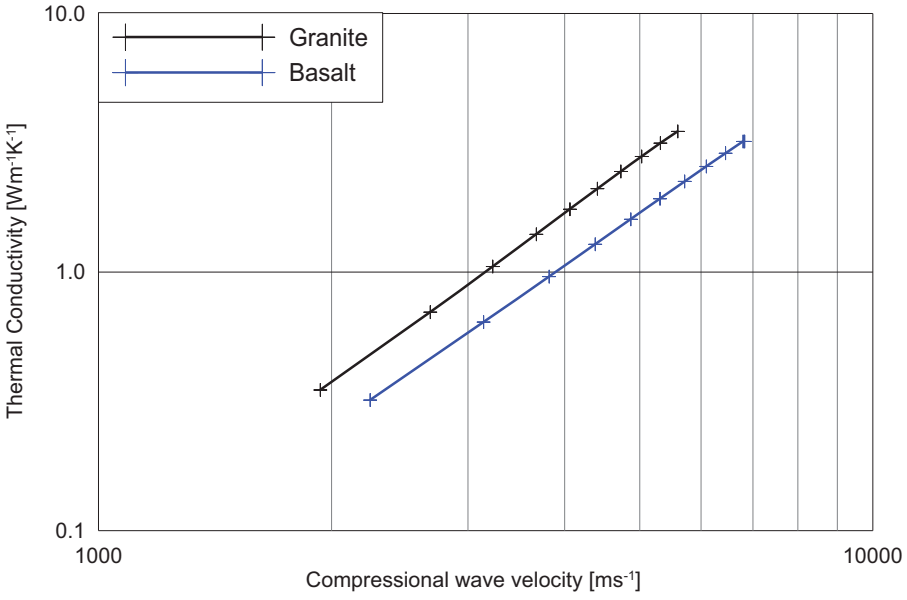

Figure 5-9: Defect model calculations for an acid (granite, λ_{solid}= 3.51 $Wm^{-1}K^{-1}$, $v_{p,solid}$=5688 ms^{-1}, A_{solid}=1.09E-7 $Ws^2m^{-3}K^{-1}$) and a basic (basalt, λ_{solid}= 3.21 $Wm^{-1}K^{-1}$, $v_{p,solid}$=6779 ms^{-1}) rock type in logarithmic scale

5.4.3. Inclusion model – water saturated rock

All models before have been calculated for dry conditions, because most of the samples have been measured in the laboratory under dry conditions. To demonstrate the effect of water saturation (saturated samples) the inclusion model was modified.

The calculation of the thermal conductivity with the equation of Clausius-Mossotti is simple and direct, because only the value of the thermal conductivity of air (λ_{air}=0.025 $Wm^{-1}K^{-1}$) to the one of water (λ_{water}=0.55 $Wm^{-1}K^{-1}$) must be changed.

For the elastic properties a fluid substitution from dry to water-saturated conditions is necessary. Gassmann (1951) developed a theory to predict the velocities of a porous rock saturated with fluid 2 (e.g. water) knowing the velocities saturated with a fluid 1 (e.g. gas).

Gassmann (1951) assumes for his theory:

- the rock is macroscopically homogenous and isotropic
- there is no fluid flow and fluid pressure
- the fluid is non-viscous
- the rock-fluid system is closed
- the pore fluid does not interact with the matrix

The shear modulus is independent of fluids, therefore it stays the same: $\mu_{dry}=\mu_{sat}=\mu$.

The compressional modulus, which is sensitive with respect to pore or fracture fluid, can be calculated as shown in the following flow chart (Schoen, 2011)

Step 1: Compile the material properties of the components:

Moduli: k_s (solid mineral component), $k_{fl,1}$ (fluid 1), $k_{fl,2}$ (fluid 2),

Step 2: Read from measurements the velocities at saturation with fluid 1 (here: air)

Then calculate the effective bulk moduli $k_{sat,1}, \mu_{satl,1}$.

Step 3: Calculate k_{dry}:

$$k_{dry} = \frac{k_{sat,1} \cdot (1-\phi) + k_{sat,1} \cdot \frac{k_S}{k_{fl,1}} \cdot \phi - k_s}{\frac{k_{sat,1}}{k_s} + \frac{k_s}{k_{fl,1}} \cdot \phi - (1+\phi)}$$

Step 4: Calculate effective bulk modulus for the replaced fluid saturation 2:

$$k_{sat,2} = k_{dry} + \frac{\left(1 - \frac{k_{dry}}{k_s}\right)^2}{\frac{\phi}{k_{fl,2}} + \frac{1-\phi}{k_s} - \frac{k_{dry}}{k_s^2}} \qquad \mu_{sat,1} = \mu_{sat,2}$$

Step 6: Calculate velocities for the rock with fluid saturation 2 with the new parameters (Equation 3-3)

5.4.4. Results and discussion of the saturated inclusion models

The result for the calculated saturated model is displayed in Figure 5-10 (additionally with the sandstone data). The measured data for the dry samples are displayed too. So a comparison is easier. Additionally the lines for the dry model calculations are plotted as dashed lines.

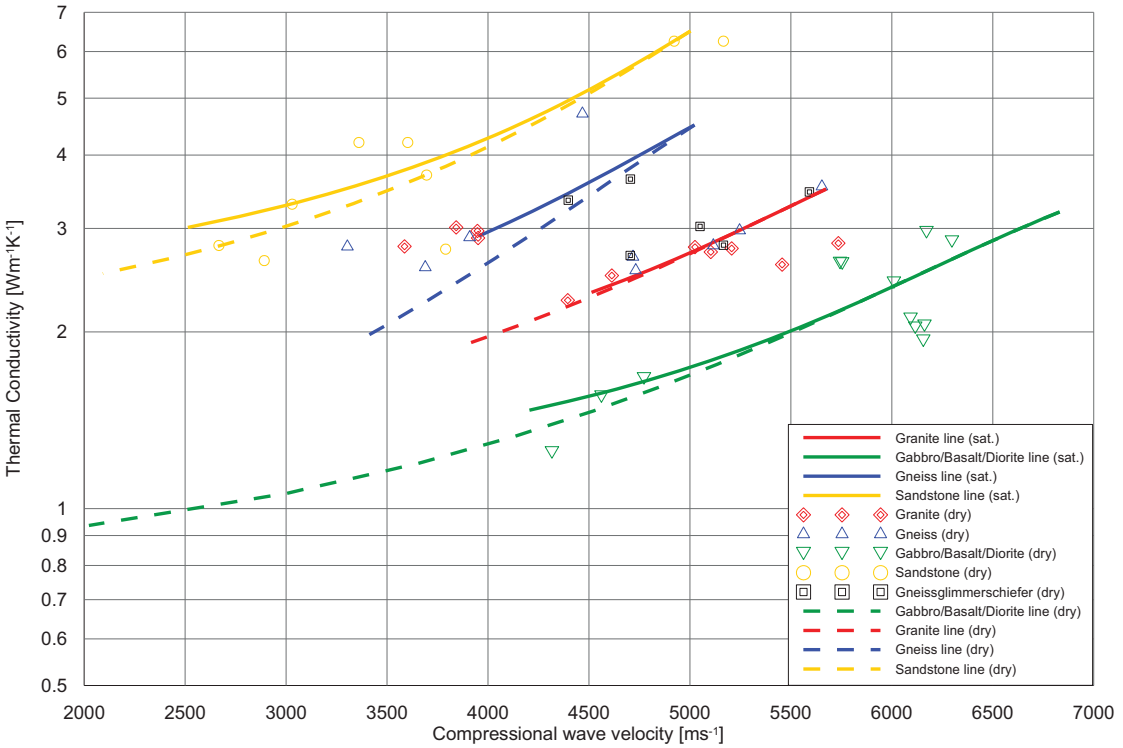

Figure 5-10: Results of the saturated inclusion model compared with the results for the dry inclusion model (dashed lines) for different rock types. Points show measured data

Using different α values (Table 5-3) and the same input data like in Chapter 6 (model calculations for dry sample, Table 6-1), there is hardly any significant difference between the two conditions.

Rocktype	α (dry)	α (saturated)
Granite/Gneiss low quartz content	0.22	0.25
Granite/Gneiss high quartz content	0.20	0.25
Basalt/Diorite/Gabbro	0.27	0.3
Sandstone	0.14	0.22

Table 5-3: Comparison of the Aspect ratios α for the inclusion models (dry and saturated)

The very low difference between the curves for dry and water-saturated rocks result from the generally low porosity and the influence of pore fluid water upon thermal conductivity and compressional wave velocity in the same direction- both properties increase.

Figure 5-10 shows that the model calculations can be used for dry and saturated rocks.

6. Application of model calculations on igneous rocks

6.1. Thermal conductivity versus compressional wave velocity

In the following sections the forward-calculated relationships between thermal conductivity and compressional wave velocity are compared with experimental data.

Based on the model calculations a fit between calculated and measured data can be realized

- for the inclusion model by variation of host properties related to the rock type (petrographic code) and the aspect ratio (fracture geometry)
- for the simple defect model only by variation of host properties related to the rock type (petrographic code) because fracture geometry is given with the model.

6.1.1. Inclusion model

The results from the inclusion model for the relationship between thermal conductivity and compressional wave velocity are displayed in Figure 6-1. The three curves fitting the different rock types are calculated for different input values for the host material and different aspect ratios characterizing the inclusion shape (Table 6-1).

Mean input values from Voigt-Reuss- and Hill- equations for the calculations are given in Table 5-1.

With the second step the implementation of the inclusion is realized. For the inclusions model (Figure 5-4) the curve parameter is the aspect ratio. Table 6-1 gives the aspect ratio for optimal approximation. Table 6-2 gives the corresponding parameter R_{mi}.

Rocktype	Density	k_{solid}	μ_{solid}	$V_{p.\ solid}$	λsolid	α	Curve
	kgm^{-3}	GPa	GPa	ms^{-1}	$Wm^{-1}K^{-1}$		
Granite/Gneiss-lower quartz content	2650	44	31	5600	3.5	0.20	A
Granite/Gneiss-higher quartz content	2650	38	22	5000	4.0	0.20	B
Basalt/Diorite/Gabbro	3000	80	46	6800	3.0	0.25	C

Table 6-1: Mean input values for the inclusion model (*k*...compressional modulus, μ...shear modulus, v_p...compressional wave velocity, λ...thermal conductivity and α...aspect ratio)

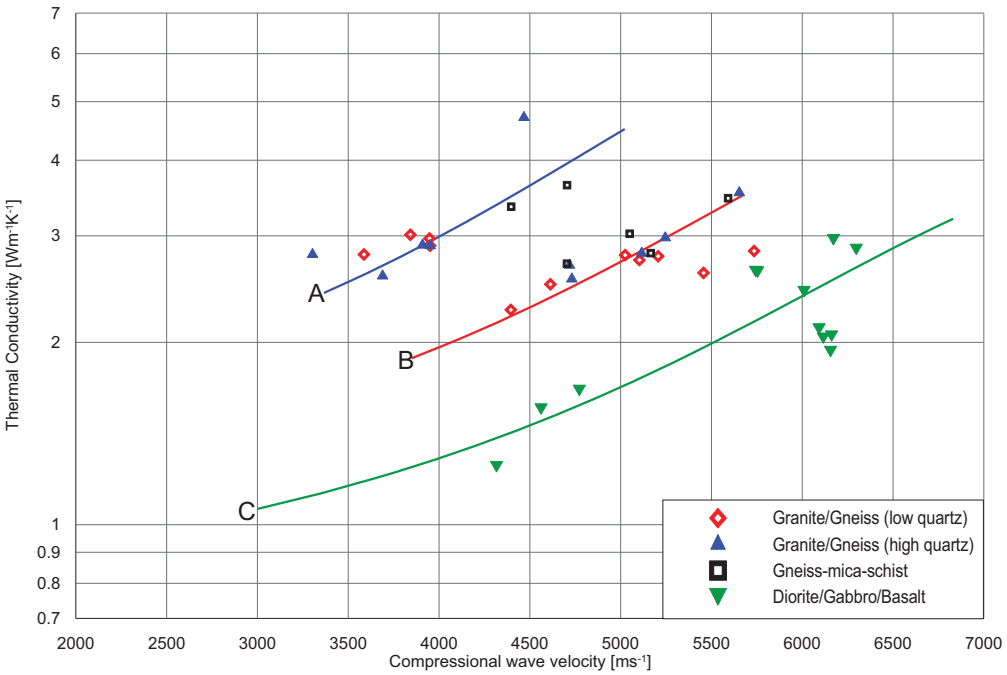

Figure 6-1: Results of the inclusion model for the three rock types: granite/gneiss with high and low value of quartz and basalt/diorite/gabbro. Points show measured data. Curves A, B, C are calculated with input data from Table 6-1.

Aspect ratio for best fit is 0.20 for granites and gneiss respectively granite and gneiss with higher content of quartz. This represents fractures and pores with an axis ratio of about 1:5. Basalt/diorite/gabbro obviously does not show such a flat shape with aspect ratio of 0.25 and axis ratio of 1:4.

Rocktype	α	R^{mi}
Granite/Gneiss-lower quartz content	0.20	0.175
Granite/Gneiss-higher quartz content	0.20	0.175
Basalt/Diorite/Gabbro	0.25	0.174

Table 6-2: Aspect ratios α and R^{mi} values for the inclusion model

In Chapter 12 the derived relationships will be applied on (sonic/acoustic) logs. Therefore the curves are transformed into a more comfortable description by one equation for each rock type. The regression equations for the individual curves were determined. An exponential law gives the best approximation. The results are shown in Table 6-3. These equations give a quicker possibility for thermal conductivity calculation from compressional wave velocity.

Rocktype	Regression equations	R^2
Granite/Gneiss-lower quartz content	$\lambda=9E\text{-}07*v_p^{1.756}$	0.996
Granite/Gneiss-higher quartz content	$\lambda=5E\text{-}08*v_p^{2.14}$	0.994
Basalt/Diorite/Gabbro	$\lambda=6E\text{-}07*v_p^{1.747}$	0.981

Table 6-3: Regressions and coefficient of determination from the model curves of the inclusion model, λ in $Wm^{-1}K^{-1}$, v_p in ms^{-1}

6.1.2. Defect model

For application of the defect model, the data are subdivided in the same three types of rocks: basalt/diorite/gabbro, granite and gneiss respectively granite and gneiss with a higher content of quartz. Mean values from the literature (Table 5-1) and the consideration for granite/gneiss and basalt/diorite/gabbro are defined as matrix solid values for each rock type.

Rocktype	$V_{p,solid}$	λ_{solid}	A_{solid}	Curve
	ms^{-1}	$Wm^{-1}K^{-1}$	$Ws^2m^{-3}K^{-1}$	
Granite/Gneiss-lower quartz content	5600	3.5	1.12E-07	A
Granite/Gneiss-higher quartz content	4900	4.5	1.87E-07	B
Diorite/Gabbro/Basalt	6800	3.2	6.92E-08	C

Table 6-4: Mean input values for the defect model

The defect model is plotted with a logarithmic scale. Figure 6-2 presents the results. The three curves fitting the different rock types are calculated for different input values (Table 6-4): The curve parameter is the value A_{solid}, which is defined as: $\lambda_{\mathrm{solid}}/v_{\mathrm{p,solid}}{}^2$.

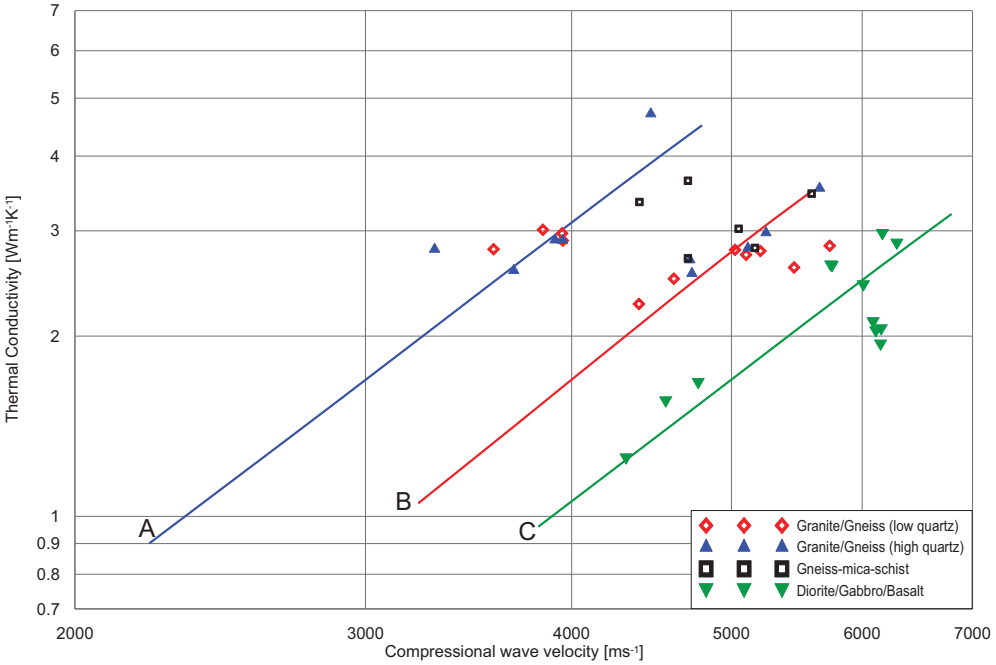

Figure 6-2: Results of the defect model for granite and gneiss with higher and lower content of quartz and basalt/diorite/gabbro. Points show measured data. Curve parameter is the A_{solid} value and the rock type (A,B,C-see Table 6-4).

6.1.3. Discussion and comparison of the two models

Both model approaches predict a correlation between thermal conductivity and compressional wave velocity which is controlled by:

- the influence of mineral composition (solid components) and
- the influence of fractures and cracks.

They confirm the power of the proposed concept of petrographic-coded thermal parameter estimation.

There is a correlation of the experimental data and the calculated curves. All correlations are controlled by the mineral composition and the fractures/pores. The inclusions model, which can demonstrate these two influences, has as controlling factor the host material properties and the aspect ratio in order to model fracture geometry.

The mineral composition for the defect model is expressed by the parameter A_{solid} and the fracture influence by the defect *D*. Thus, the defect model is simple, but can also describe the two important factors: mineral composition and the fractures/pores. Measured values fit to the model lines really well and the outliers can be explained easily.

The inclusions and the defect model show the same outliers:

One sample of the granites, which is described as a granodiorite, lies between the granite and the basalt/diorite/gabbro line.

One gneiss sample has a higher thermal conductivity which can be explained by a higher content of quartz (also anisotropy may be of influence, (Gegenhuber & Schoen, 2010), Chapter 10).

Both models work particularly for the magmatic rocks really well. These correlations form the basis of further calculations, especially the step towards the correlations with logs.

Table 6-5 gives an overview of the used equations for both models for the calculation of the thermal conductivity from acoustic logs.

Rocktype	Inclusion model	Defect Model
Granite/Gneiss-lower quartz content	$\lambda=9E\text{-}07*v_p^{1.756}$	$\lambda=v_p^2*1.12E\text{-}07$
Granite/Gneiss-higher quartz content	$\lambda=5E\text{-}08*v_p^{2.14}$	$\lambda=v_p^2*1.95E\text{-}07$
Basalt/Diorite/Gabbro	$\lambda=6E\text{-}07*v_p^{1.747}$	$\lambda=v_p^2*6.29E\text{-}08$

Table 6-5: Summarized equations for the defect and the inclusion model for the calculation of thermal conductivity from the sonic log (v_p on the equations here); λ in $Wm^{-1}K^{-1}$, v_p in ms^{-1}

6.2. Thermal conductivity versus density

Correlation between thermal conductivity (or compressional wave velocity) and density in fractured rocks meets the problem, that with respect to pore or fracture parameters thermal conductivity is strongly influenced by inclusion or fracture shape, but density is only dependent on porosity as a volume fraction. Therefore a modification of model assumptions is necessary.

Sundberg et al (2009) described in their paper the correlation between thermal conductivity and density. As a result they centralised that for granites with a decrease of thermal conductivity the density increases and for diorite and gabbro with an increase of thermal conductivity the density increases. This effect is not confirmed with our data - probably the investigated samples are characterized by a relative uniform fracture shape (i.e. no variation of aspect ratio).

6.2.1. Inclusion model

For forward calculation the same input parameters as in Chapter 6.1. are used as start assumption. For better approximation the granite/gneiss requires some empirically-defined higher density input for the correlations. Thermal conductivity values stay the same as for the correlation between thermal conductivity and compressional wave velocity for all rock types.

Rocktype	Density	$V_{p.\ solid}$	λ_{solid}	α
	kgm^{-3}	ms^{-1}	$Wm^{-1}K^{-1}$	
Granite/Gneiss	2850	5500	3.5	0.07
Basalt/Diorite/Gabbro	3300	6500	3.0	0.10

Table 6-6: Input parameters for the inclusion model (v_p...compressional wave velocity, λ...thermal conductivity and α...aspect ratio)

With the modified input parameters (Table 6-6) the correlations worked well. It may be noted, that also the aspect ratio for this correlation are modified (compare Table 6-1).

As mentioned before, the same tendency can be observed also for carbonates (Chapter 8.): with increasing density the thermal conductivity increases (Figure 6-3).

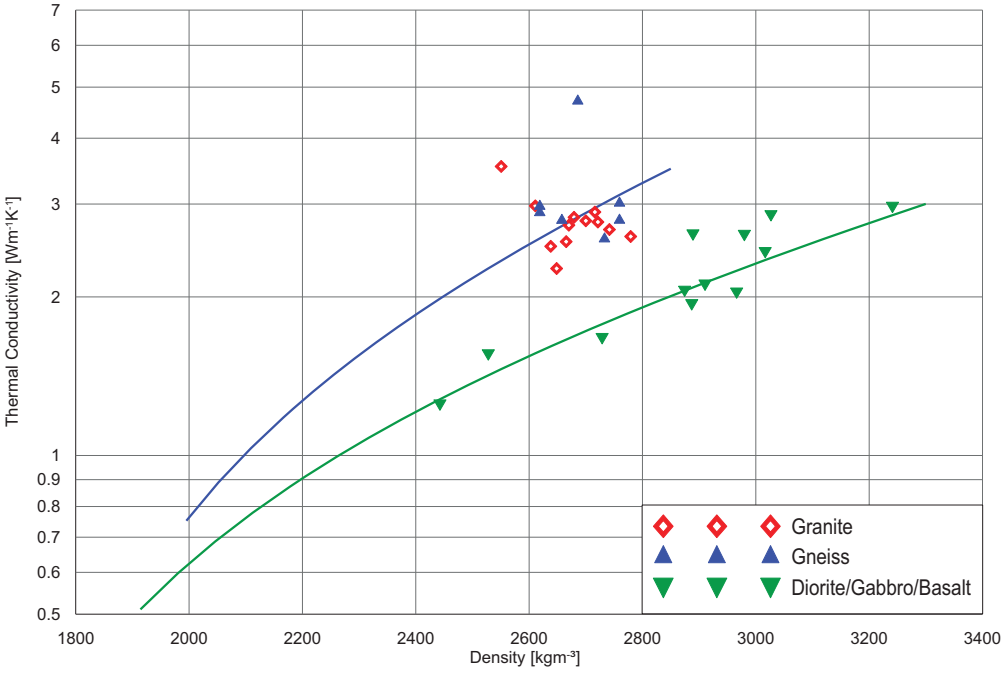

Figure 6-3: Density versus thermal conductivity with the inclusion model for different rock types

The same samples as in Chapter 6.1. are used here. There is no need to separate the granite/gneiss with lower quartz content from granite/gneiss with higher content of quartz. All data fit well to the "granite/gneiss line". Table 6-7 shows the results for the regression equations of the model calculations. For basalt/diorite/gabbro a polynomial regression gives the best approximation.

Rock type	Regression equation	R^2	β
Granite/Gneiss	$\lambda=0.0265e^{0.0017d}$	0.985	0.2
Basalt/Diorite/Gabbro	$\lambda=4E\text{-}07d^2\text{-}9E\text{-}05d\text{-}0.6445$	0.999	0.4

Table 6-7: Regression equations and coefficient of determination for the inclusion model, [*d*...density in kgm^{-3}] and additionally β for the defect model calculations

6.2.2. Defect model

The defect model needs a modification of the defect parameter *D*. The density cannot only be described by the defect parameter; additionally *D* needs a certain thickness. Therefore a parameter *β=d/D* (Table 6-7) is introduced, where *d* is the thickness and *D* the length of the defect (Figure 6-4). This results in the new equation for the density: $d = d_s * (1 - D^2 * \beta)$, where d_s is the density of the solid matrix.

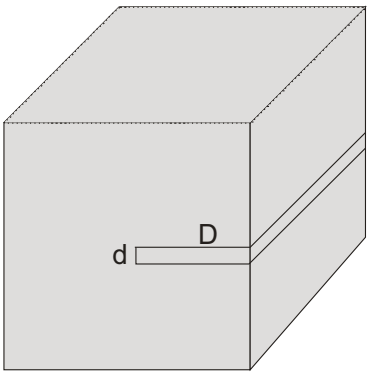

Figure 6-4: Illustration of the modified defect model

With this modification the same input values like in Chapter 6.1. can be used and the results are displayed in Figure 6-5. Again there is no need to separate the granite/gneiss with low quartz content from the granite/gneiss with high quartz content. The effect of increasing density with increasing thermal conductivity can be described again well with this model type.

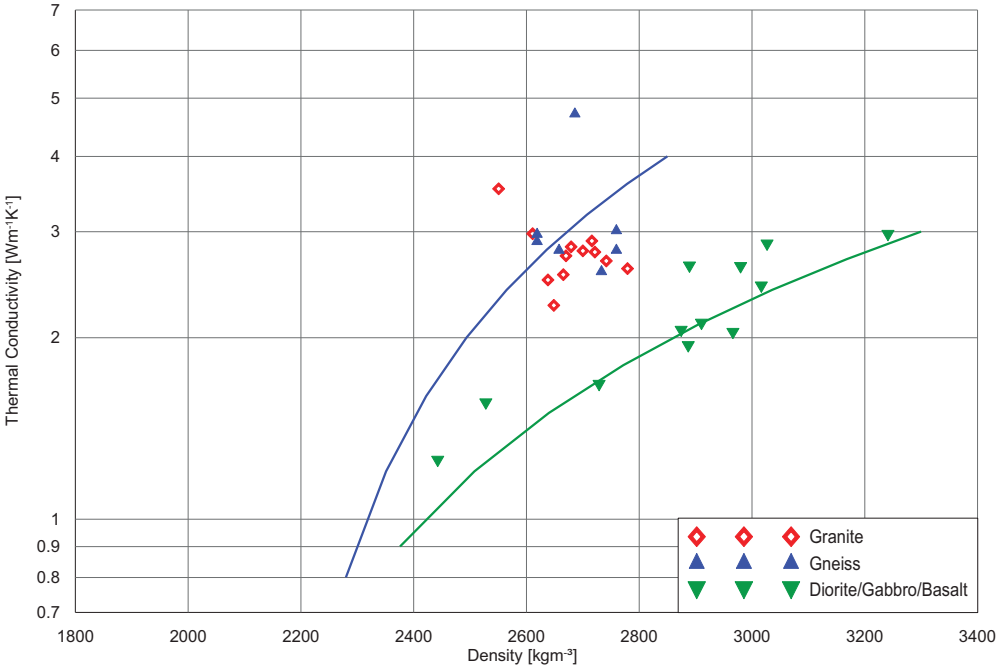

Figure 6-5: Density versus thermal conductivity with the defect model for different rock type

7. Application of model calculations on sandstones

7.1. Thermal conductivity versus compressional wave velocity

Compared with the petrographic type of Chapter 6 (igneous rocks) sandstone has:

- a mineral influence on thermal conductivity dominated by quartz
- a distinctive higher porosity
- a different type of pore shapes

For the analysis of experimental data the same algorithms as explained in Chapter 5, are used. Figure 7-1 shows the thermal conductivity versus compressional wave velocity with the inclusion model. Input data and results for the inclusion and the defect model are presented in Table 7-1. For the thermal conductivity a high starting point for the calculations was needed because quartz has a high thermal conductivity between 5 and 10 $Wm^{-1}K^{-1}$.

Parameter		**Input**
Density	kgm^{-3}	2650
K	GPa	25
M	GPa	14.3
Vp	ms^{-1}	5000
λ	$Wm^{-1}K^{-1}$	6.5
A		0.2
		Output
Defect model		$\lambda=vp^2*2.60E-07$
Inclusion model		$\lambda=1.123e^{0.0003*vp}$

Table 7-1: Input data and results of the model calculations for the sandstone

Best fit gives an unexpectedly low aspect ratio of alpha=0.2. Probably this value covers two effects

- pore shape and
- grain-grain contact.

It may be noted, that the inclusion model is not optimal for sandstone type, because the fundamental assumption of the inclusion model is a homogeneous and continuous solid host material. In case of clastic sediments the grain-grain contact represents a strong distortion of such a “continuous homogeneous” material.

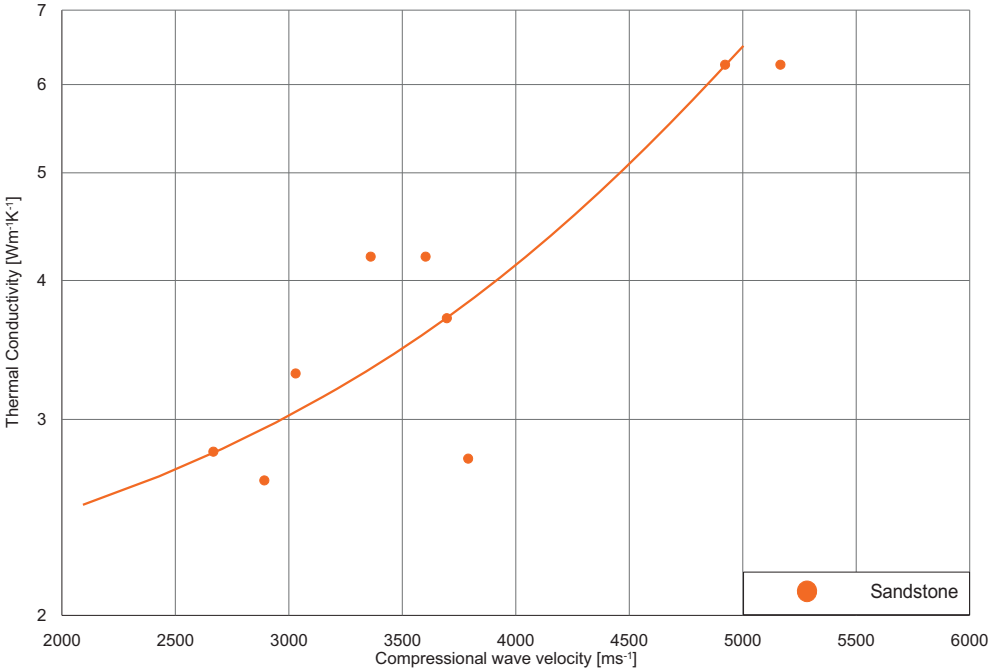

Figure 7-1: Thermal conductivity versus compressional wave velocity for sandstone with the inclusion model

Both models work well and there is a good correlation of experimental data and calculated model curves. The inclusion model fits the date a little bit better than the defect model.

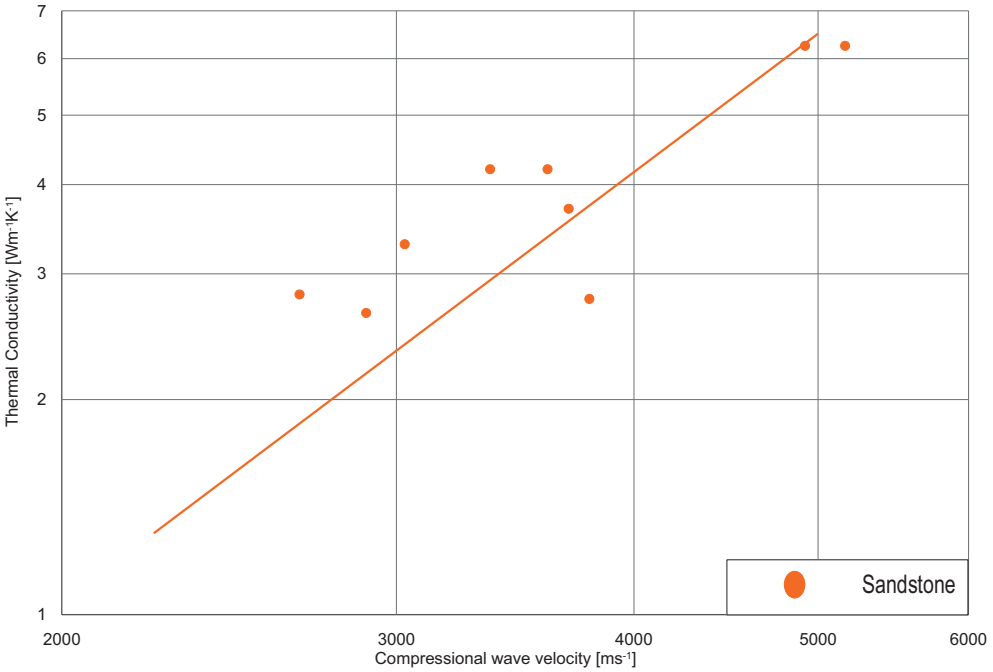

Figure 7-2: Thermal conductivity versus compressional wave velocity for sandstone with the defect model

Only one sandstone sample is an outlier and would fit to the gneiss line of the other model calculations (Chapter 6). An explanation is maybe that this sample has a different mineral content than the other sandstones. Using high thermal conductivities all sandstone can be covered. A high thermal conductivity for sandstone can be explained with the high thermal conductivity of crystalline quartz.

A correlation between thermal conductivity and density could not be derived because of the data scatter. This is the result of different controlling influences on the two parameters:

- thermal conductivity is controlled by solid mineral properties, porosity, contact properties at grain-grain contact, pore shape
- density is controlled by solid mineral properties and porosity only.

8. Application of model calculations on carbonates

Carbonates always present a challenging case for modelling in petrophysics. They have special textural properties and a different way of developing cracks and fractures.

Carbonates represent an important and specific group of rocks also with respect to reservoir properties. Compared with most other rock types carbonates are characterized by

- a relative simple mineral composition
- a complicated pore system.

They are formed by two main minerals calcite and dolomite.

The two corresponding main rock types are:

a.) Limestone is composed of more than 50% carbonates, of which more than half is calcite.
b.) Dolomite is composed of more than 50% carbonates, of which more than half is dolomite. Dolomite frequently forms larger crystals than the calcite it replaces (Al-Awadi, 2009) and forms good reservoir properties.

Carbonates are modified by various post-depositional processes such as dissolution, cementation, recrystallization, dolomitization, and replacement by other minerals. Dolomitization is connected with an increase of porosity. The interaction with meteoric pore fluids can result in a leaching of grains and influence reservoir quality in both directions (new pore space, cementation). As result of these processes carbonate have a complicated pore system ranging from interconnected, intercrystalline pores to fractures and vugs which may be connected or disconnected.

This specific nature is the motivation for a separate discussion of carbonates and the implementation of electrical properties in the data set for correlations. The general concept for the carbonates is an investigation of

- thermal conductivity versus compressional wave velocity
- thermal conductivity versus density
- thermal conductivity versus specific electrical resistivity.

Different dolomite and limestone samples are collected from all over Austria (Vienna Basin, Northern Calcareous Alps, Greywacke Zone) and used for laboratory measurements. Additionally data from Switzerland, determined by Gong (2005) are used too.

8.1. *Thermal conductivity versus compressional wave velocity*

Displaying thermal conductivity versus compressional wave velocity for dolomite and limestone (Figure 8-1) a trend for each group gets recognizable: With increasing thermal conductivity compressional wave velocity increases. The same trend was presented in Chapter 6 and 7 for other rock types (igneous rocks and sandstone).

The two dominant minerals calcite and dolomite have significantly different properties (see Table 8-1). This causes the different position of the starting points for the two sets of curves in Figure 8-1. Table 8-1 gives all input data and the mean aspect ratio for the two families of curves.

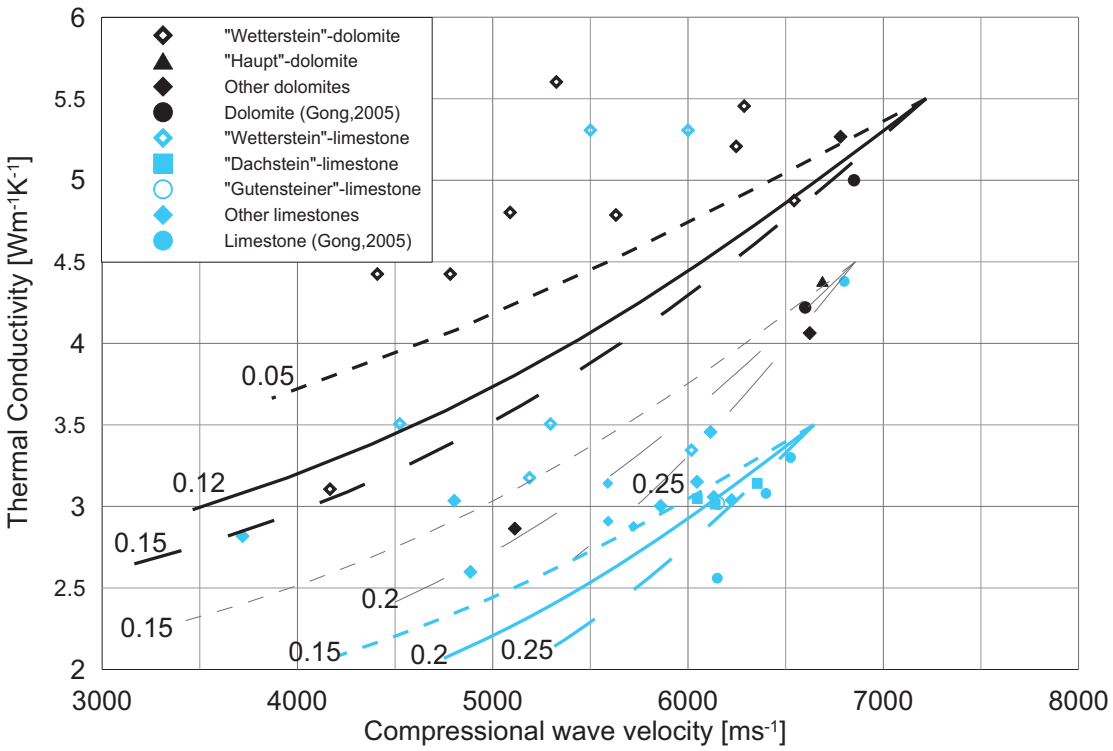

Figure 8-1: Thermal conductivity versus compressional wave velocity with the inclusion model for carbonates (dry) (lines show different aspect ratios), blue lines: limestone, black lines: dolomite and grey lines: mixture

A part of the data points lie between these two families of pure dolomite and pure limestone. Probably they represent a mixture of dolomite and calcite. A third set of curves is calculated using the solid host parameters for the mixture (Hills mean) and explains these data points.

The data points above the pure dolomite line could result from a very compact rock structure and/or some quartz content of the carbonate (quartz increases thermal conductivity but decreases compressional wave velocity).

Thus data distribute but the general trend can be reproduced with the inclusion model. The inclusion model is able to show the correlation of these properties (Figure 8-1) for carbonates. Table 8-1 shows the input data for the model calculations. Equations and calculations are described in detail in chapter 5.

	λ	**k**	**μ**	**V_p**	**Density**
	$Wm^{-1}K^{-1}$	GPa	GPa	ms^{-1}	kgm^{-3}
Limestone	3.5	68	39	6645	2710
Dolomite	5.5	85	49	7220	2870
Mixture	4.5	74	42	6900	2770

Table 8-1: Input data for the inclusion model for carbonates (λ...thermal conductivity; k...compressional modulus; μ...shear modulus; v_p...compressional wave velocity)

The defect model does not work for carbonates. Probably the pore structures are too complex that one defect is not sufficient to explain the combination of pore-(volume) effect and fracture geometry.

Rock type	**α=0.2 (lime.)/α=0.12(dol.)**	**R^2**	**α=0.15(limest.)/α=0.05(dolomite)**	**R^2**
Dolomite	$y=1.94e^{0.0004*x}$	0.97	$y=0.423e^{0.0004*X}$	0.99
Limestone	$y=6E-06*x^{1.5}$	0.99	$y=4E-07*x^{1.8}$	0.99

Table 8-2: Regression equations for the developed inclusion models for carbonates (for two different α)

8.2. *Thermal conductivity versus density*

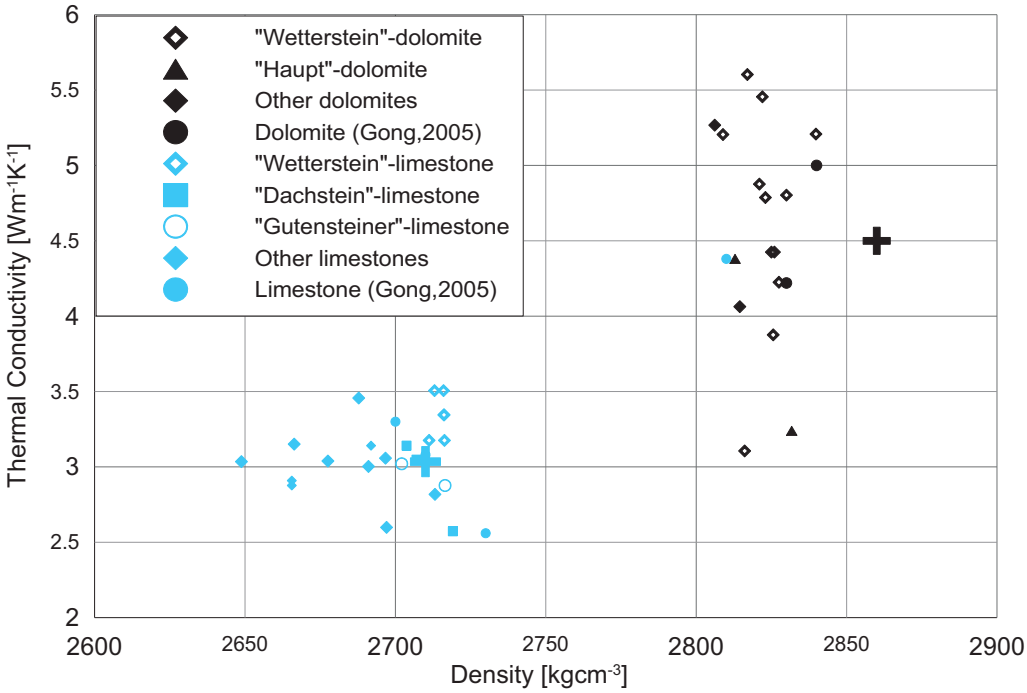

Figure 8-2: Thermal conductivity versus density for different limestone and dolomite samples and the matrix parameters (crosses, blue: limestone; black: dolomite)

The correlation of thermal conductivity and density is displayed in Figure 8-2.

Observable is:

- with increasing density the thermal conductivity increases.
- a separation between dolomite and limestone can be recognized clearly. This is caused by higher density and higher thermal conductivity for dolomite in comparison with limestone.

Different limestone and dolomite samples are displayed. Except one limestone sample from the thesis of Gong (2005) both can be separated clearly. Dolomite has a higher matrix density and thermal conductivity than limestone. This is also shown by plotting the matrix values (plotted as crosses in Figure 8-2).

Within the two groups no tendency can be observed. Dolomite has various thermal conductivities with nearly the same density. This is probably caused by a variation of the rock composition, a variation of the crystallisation type and the heat transfer at crystal boundaries. So the correlation shows that for carbonates the mineral composition is important and porosity has a second order effect and contributes to data scatter.

The data distribution confirms the interpretation of Figure 8-1 some samples represent a mixture of dolomite and calcite.

8.3. *Thermal conductivity versus porosity*

For the carbonate rocks porosity was determined and plotted against thermal conductivity (Figure 8-3). As a general trend, thermal conductivity decreases with increasing porosity. This is the result of the low thermal conductivity of the pore fluid air. The two rock types show a clear separation in the plot. Dolomite samples show higher levels compared with the limestone samples.

In this case

- mineral composition (rock type) controls the level of thermal conductivity
- porosity acts as a second order effect with a decrease within the rock type.

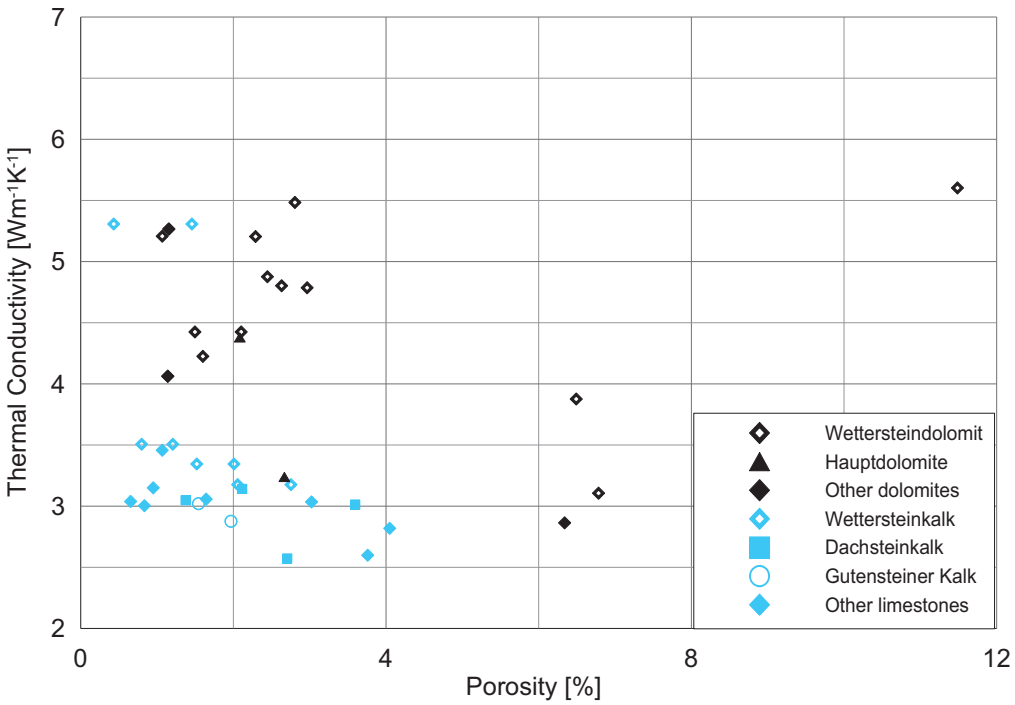

Figure 8-3: Thermal conductivity versus porosity for carbonates

8.4. *Thermal conductivity versus specific electrical resistivity*

The comparison of thermal conductivity and specific electrical resistivity combines two properties with completely different dominant physical dependence:

- thermal conductivity is dominated by solid material properties
- electrical conductivity is dominated by pore space properties.

Therefore no strong correlation can be expected.

Figure 8-4 shows the correlation between thermal conductivity and specific electrical resistivity. The resistivity is plotted in logarithmic scale. Generally a trend of increasing thermal conductivity with increasing resistivity is identifiable. This is the porosity effect as already discussed in the previous section. In this case also the dolomite shows a higher level than the limestone – but this solid material property has an influence only on thermal conductivity. For electrical resistivity calcite as well as dolomite are insulators.

For a comparison of the two properties the inverse of the electrical conductivity – the specific electrical resistivity - is used, because it is the most common applied parameter in geoelectrics.

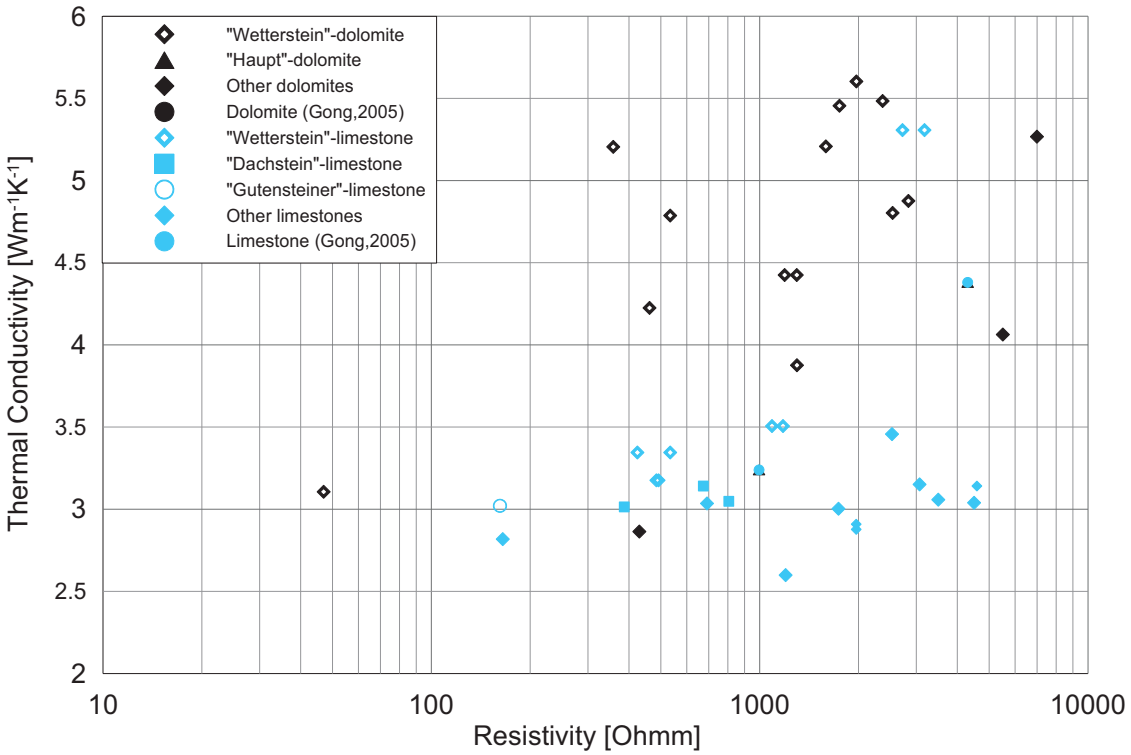

Figure 8-4: Thermal conductivity versus specific electrical resistivity for carbonates

Archie's law (Archie, 1942) gives a direct link between specific rock resistivity, pore water resistivity and porosity via formation factor F:

$$\frac{1}{R} = \frac{\phi^m}{Rw} \qquad R_0 = R_W * F = R_W * \frac{1}{\Phi^m} \qquad (8\text{-}1)$$

where R is the electrical resistivity of the water saturated sample, R_w is the resistivity of the water, ϕ is porosity and m is a rock type specific constant. (R_0 and R_W correspond to the notation as applied in well-logging.

R_w, the resistivity of the water, is measured directly and has a value of 2.5 Ohmm. With the measured resistivity for the sample and the resistivity of the water the formation factor *(R/Rw)* can be calculated for all samples. Data are plotted in Figure 8-5.

As result of the complexity and diversity of pore structures the exponent *m* in carbonates cannot be as clearly determined as in clastic rocks. Systematic studies of these pore types have been published, for example, by Focke & Munn (1987) and Fleury (2002) and show a broad spectrum of exponents.

Figure 8-5 shows a plot of formation factor as a function of porosity in the typical bi-logarithmic presentation Three curves are plotted for different exponents *m* between m=1 (this is an extremly low value; low values are typical of fractured materials), m=1.5, and m=2 (the general accepted "mean value" for Archie's exponent (typical for sandstone or carbonate with interparticle porosity).

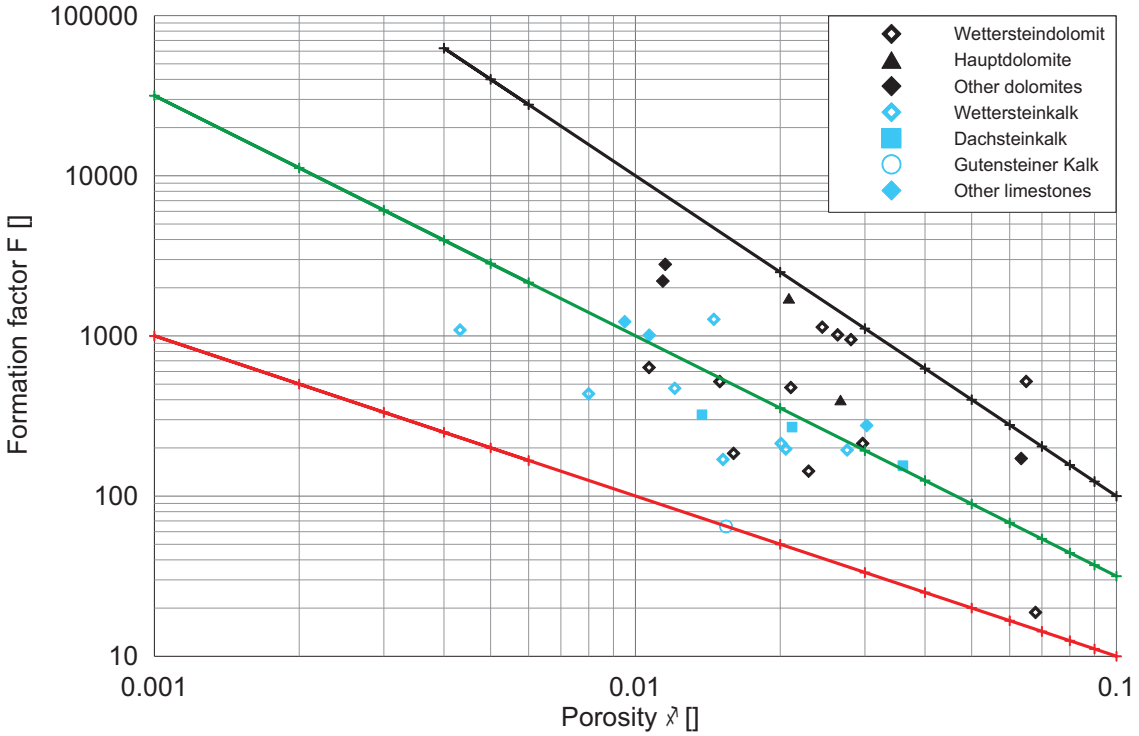

Figure 8-5: Porosity versus formation factor with different values for *m*, red line: m=1; green line: m=1.5 and black line: m=2

A comparison of measured data and the three lines confirm the variability of the exponent for the carbonate samples as result of the pore space diversity. As tendency can be concluded that:

- samples with m≈2.0 are dominated by interparticle porosity
- samples with m≈1.5 have interparticle and fracture porosity.

As a next step a forward calculation of a relationship between formation factor and thermal conductivity was tested. The connecting parameter for this relationship is the porosity. The two properties are calculated with different algorithms:

- formation factor is calculated with Archie's equation; the diversity of pore geometry is implemented by different exponents
- thermal conductivity is calculated with the inclusion model; the diversity of pore geometry is implemented by different aspect ratios.

Because thermal conductivity is controlled mainly by the different mineral properties, a separate calculation is necessary for limestone (calcite) and dolomite; concerning formation factor, the two minerals acting as insulators have the same effect.

Parameter		**Input limestone**	**Input dolomite**
λ	$Wm^{-1}K^{-1}$	3.50	5.50
α		0.10; 0.30	0.10; 0.30
$\mathbf{R^{mi}}$		0.26; 0,28	0.17; 0.18
m		1.3; 1.7; 2.1	1.3; 1.7; 2.1

Table 8-3: Input data for the inclusion model and Archie's equation for the correlation of thermal conductivity and formation factor

Next step was to display formation factor versus thermal conductivity (Figure 8-6). Lines show the results for different *m* values for the Archie equation. Distribution within a rock type can be explained with different *m* value. Aspect ratio has only a minor influence, but lines fit well to the data. Figure 8-6 shows both lines (aspect ratio=0.1 and 0.3). Especially for the limestone no differentiation between these two lines can be seen. Input data are displayed in Table 8-3.

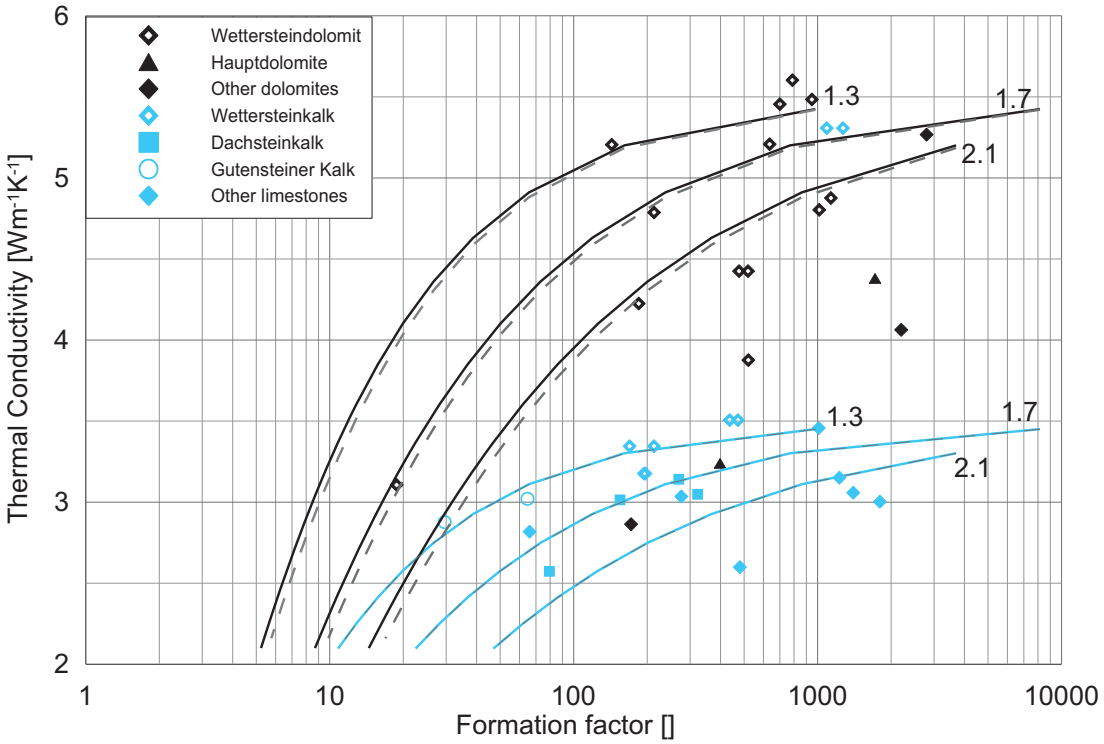

Figure 8-6: Thermal conductivity versus formation factor and calculated lines with the inclusion model (blue: limestone, black: dolomite; with different *m* values; dashed lines: α=0.3, others: α=0.1)

The data position in the plot allows as tendency the following interpretation:

- samples with low exponent (m<1.7) have interparticle and fracture or vug-porosity (vugs, fractures are interconnected)
- samples with intermediate exponent (m≈1.7-2.1) have interparticle porosity
- samples with high exponent (m>2.1) have interparticle and vug porosity (vugs are connected and without influence upon F)

9. Heat capacity versus density correlation

Both heat capacity and density are scalar properties. Therefore a calculation of the volume weighted mean can be performed which results in:

$$c_{\mathrm{p}} = \sum c_{\mathrm{pi}} * V_{\mathrm{i}} \qquad (9\text{-}1)$$

$$d = \sum d_{\mathrm{i}} * V_{\mathrm{i}} \qquad (9\text{-}2)$$

where c_{pi} is the heat capacity of a certain mineral and V_{i} its volume and d_{i} its density. Properties of each component and its volume fraction completely control the two parameters and their relationship.

Figure 9-1 shows some rock-forming minerals with their densities and heat capacities. Additionally the value of water at 20° and the change of limestone and dolomite (as example) with increasing porosity is displayed. Water has a high heat capacity and is the most prominent influencing factor in comparison to the values of the minerals. Minerals themselves almost all have similar values ranging from 650 to 900 $Jkg^{-1}K^{-1}$.

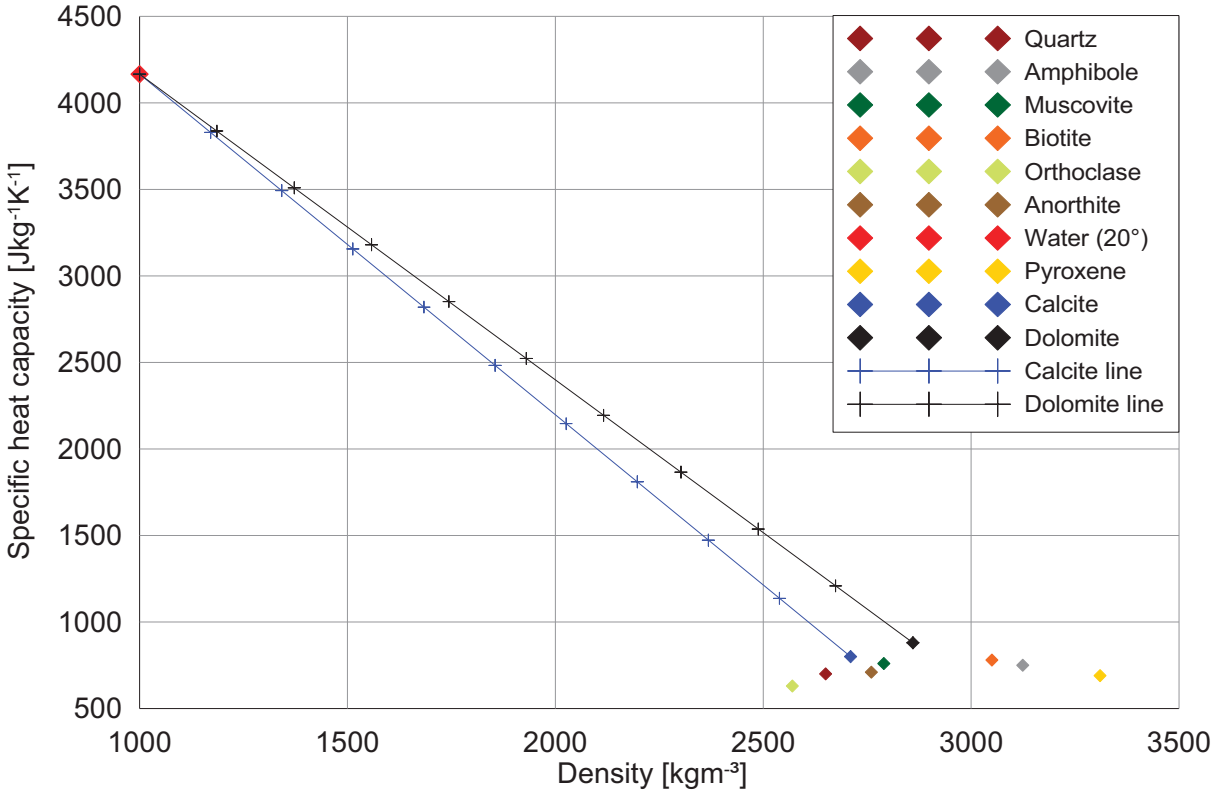

Figure 9-1: heat capacity versus density for rock forming minerals. Additionally calcite and dolomite with increasing water content or porosity are displayed (Schoen,2011)

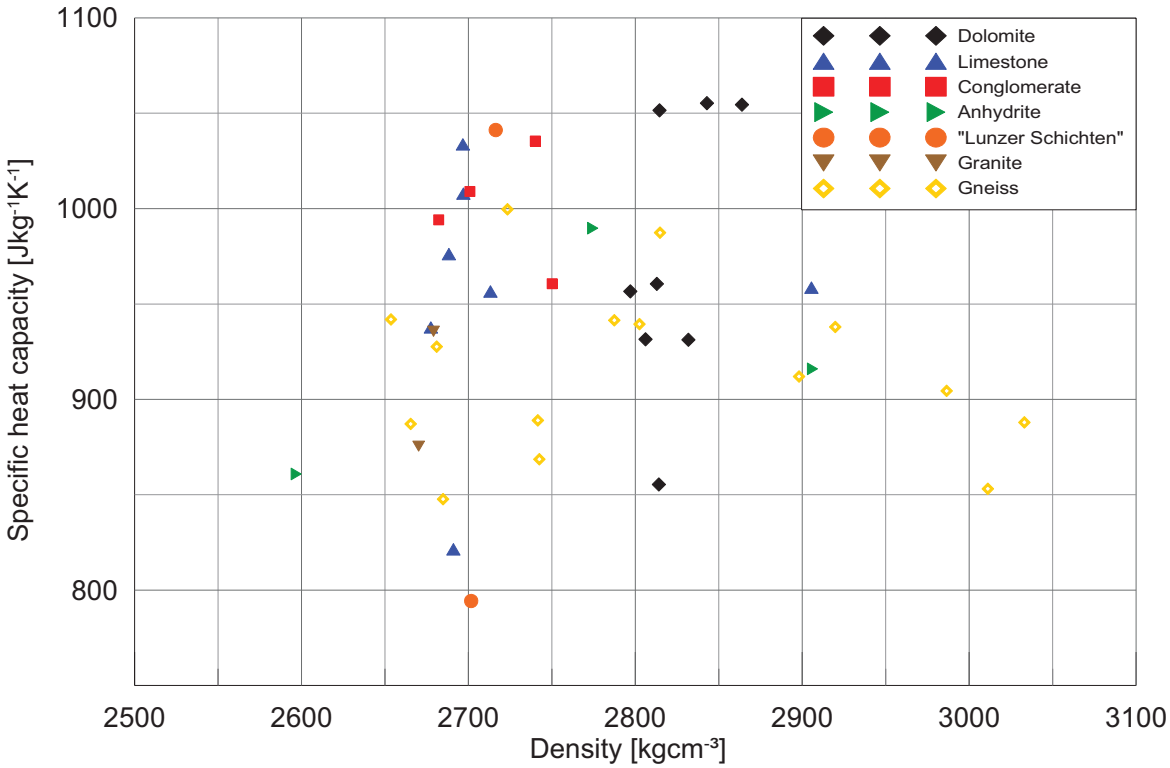

Figure 9-2: Heat capacity versus density for different types of rock

Because for the minerals no correlation exists between density and heat capacity, also a scatter of rocks must be expected as shown in Figure 9-2.

Plotting the density of different rock types against heat capacity, it becomes clear that at the first sight there is no linear correlation. So I subdivided the data into different rock types: dolomite, limestone, conglomerate, granite/gneiss and anhydrite. Also with this subdivision no trend can be observed. Having a look for example at the dolomite values (black dots), it becomes visible that for nearly the same densities, different heat capacities are plotted.

Also the influence of porosity cannot be negligible. More porosity means more water, which results in a higher heat capacity but lower density.

10. Anisotropy of thermal conductivity

10.1. Introduction

In anisotropic rocks, thermal conductivity and elastic wave velocity – both properties are tensors - depend on the direction of heat flow and wave propagation, respectively. Scalar properties (e.g. density, specific heat capacity) are uninfluenced by any direction.

The origins of anisotropy in sediments are aligned grains and lamination (laminated shaly sands), in igneous and metamorphic rocks aligned crystals, aligned fractures and cracks, and stress create an anisotropy.

Obvious and visible anisotropy exists:

- in metamorphic rocks with schistosity and oriented fracturing (typical gneiss), and
- in sedimentary rocks with layering or bedding (e.g. laminated shaly sand), but also if fractures are present.

In this chapter I will describe the effects of an anisotropic material (the "Stainzer Plattengneis") on thermal conductivity and compressional wave velocity by experimental investigations and model calculations.

10.2. Experimental investigations

10.2.1. "Stainzer Plattengneis" – petrographic characterisation

The selected rock sample is an anisotropic gneiss ("Stainzer Plattengneis") from the Koralpe, Austria. It consists of about 45-50 per cent of quartz, 40 per cent of feldspar and 5 percent of mica, garnet, tourmaline and disthene. The mean density of the gneiss sample is 2.80 gcm^{-3}.

This gneiss was selected, because it shows clear schistosity (Figure 10-1) and therefore a strong anisotropy could be expected. Important for the thermal conductivity are the brighter layers which consist mainly out of quartz and are highly thermal conductive.

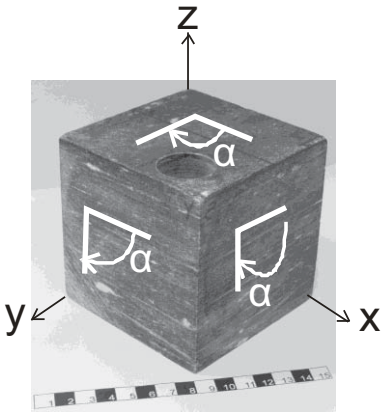

Figure 10-1: "Stainzer Plattengneis" with main axes for anisotropy description and model calculation

For experimental investigations a sample is cut in form of a cube of 10cm x 10cm x 10cm. The cube edges are parallel and perpendicular to the visible schistosity. Before measuring, the planes have to be polished because even small roughness causes errors in the thermal conductivity measurements.

10.2.2.Determination of the anisotropy of the thermal conductivity

Figure 10-2 shows the results of the measurements at the three planes in different directions of the "Stainzer Plattengneis". On the x-axis the angle of the heat flow direction and on the y-axis the measured thermal conductivity in [W $m^{-1}K^{-1}$] is plotted.

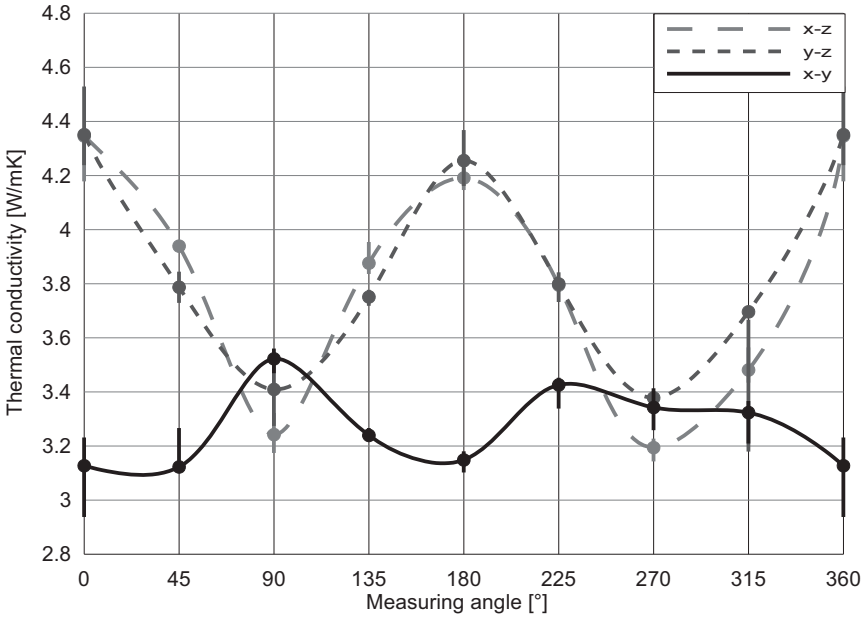

Figure 10-2: Results of the measurements of thermal conductivity in three directions (x-axes: angle of measured heat flow direction)

Two curves (grey dashed lines) show strong anisotropy on two planes (x-z and y-z plane). The black one (x-y plane) is normal to the schistosity and shows only minor anisotropy and low amplitude. The low amplitude results from the position of this plane with a “dark layer” of the gneiss with low quartz content.

The measurements indicate a strong anisotropy as result of schistosity. A second order anisotropy within the x-y-plane is visible. The curves do not follow an ideal sinus. This results from the inhomogeneity. For any model calculation a 3-axial anisotropy must be considered. As reference these measurements form the basis of the models.

The „Stainzer Plattengneis“ shows

- a dominant “first order anisotropy” when comparing parallel and perpendicular schistosity, originated by the strong influence of the aligned quartz components,
- a “second order anisotropy” within the plane of schistosity, probably as result of unequal shape of quartz components in x- and y –direction
- thermal conductivities λ_x=3.4 $Wm^{-1}K^{-1}$, λ_y=4.3 $Wm^{-1}K^{-1}$ and λ_z=3.2 $Wm^{-1}K^{-1}$ for the main axes, determined from the minimum and maximum values of the measurements.

Details of measuring and device are described in chapter 3.1.

10.2.3.Determination of compressional wave velocity in the three main axes

In addition to the thermal conductivity the compressional wave velocity is determined with the ultrasonic device in the three main axes. The measuring principle of the ultrasonic device is described in detail in chapter 3.4.

The velocities in the main axes are:

$V_{p,x}$ = 5312 ms^{-1} $V_{p,y}$ = 5749 ms^{-1} and $V_{p,z}$ = 4562 ms^{-1}.

Compressional wave velocity also shows no simple transverse isotropy, but different velocities in the three main axes. Thus, both anisotropies are controlled by the internal rock texture.

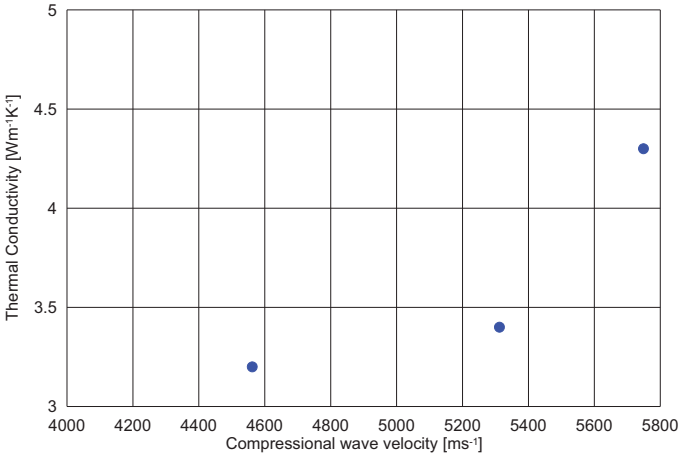

Figure 10-3: Measured thermal conductivity versus compressional wave velocity in the main axes

Figure 10-3 shows the measured thermal conductivity versus compressional wave velocity for the three main axes directions.

10.3. Model development and calculations

10.3.1. Introduction

The tensorial parameters thermal conductivity and compressional wave velocity show a first and a second order anisotropy effect. Models have been developed and calculated in two steps

Step 1: Consideration of first order effect using a simple sheet or layer model

Step 2: Consideration of first and second order effects using two model concepts:

- a modified sheet or layer model
- an inclusion model with aligned ellipsoids.

These considerations are focussed mainly on thermal conductivity in order to explain the detailed result of experiments.

A look on the mean values for dominant rock-forming minerals (Appendix A1) confirms the general simplification of a two-component material as a first approximation. Material 1 with high thermal conductivity is represented by quartz with values in the order of 6.5 to 10 $Wm^{-1}K^{-1}$(Schoen, 1996).

For my calculations I used values from 6.8 to 7.4 $Wm^{-1}K^{-1}$ to study the effect of the input value. The host material is composed of the other minerals (feldspar, mica) with thermal conductivities in the order of 2 to 3 $Wm^{-1}K^{-1}$ (this will result from the calculations).

10.3.2. Modelling of first order effects

These types of models are based on the fundamental studies of Voigt (1910) and Reuss (1929) as described in Chapter 5.3. The rock is modelled as a number of sheets or layers. Each sheet represents one mineral component with a certain set of properties (thermal conductivity, density, elastic properties). The volume fraction of each component gives the relative thickness of each sheet. The results are one "parallel" and one "series" model (Figure 5-3).

The relations for the general case of *n* components for thermal conductivity are:

parallel model (heat flow along schistosity) $$\lambda_{\parallel} = \sum V_i * \lambda_i \qquad (10\text{-}1)$$

series model (heat flow perpendicular schistosity) $$\lambda_{\perp} = \left[\sum V_i * \lambda_i^{-1}\right]^{-1} \qquad (10\text{-}2)$$

where V_i is the volume fraction and λ_i the thermal conductivity of the component *i*.

The two equations represent the upper ($\lambda_{\parallel}$) and the lower ($\lambda_{\perp}$) bound of the thermal conductivity for a rock of a given composition. These are shown in Figure 10-4.

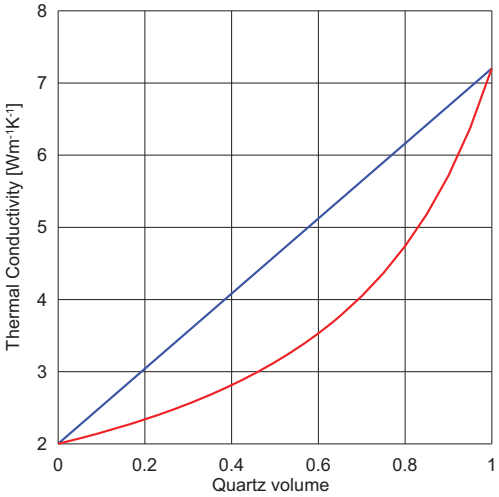

Figure 10-4: Results of the Voigt and Reuss model calculations for thermal conductivity; Input data: λ_1=2.0 $Wm^{-1}K^{-1}$ and λ_2=7.2 $Wm^{-1}K^{-1}$

As input values for the calculations and comparison with experimental results are used:

$\lambda_{1,quartz}$=7.2 and $\lambda_{2,host}$=2.0 $Wm^{-1}K^{-1}$ and for the volume $V_{1,quartz}$=0.45.

Equations (10-1) and (10-2) result in the following thermal conductivities in the main directions $\lambda_x=\lambda_y$= 4.3 $Wm^{-1}K^{-1}$ and λ_z=2.96 $Wm^{-1}K^{-1}$.

To calculate the anisotropy from the sheet models in different directions the following equations were used:

$$\lambda_{x\text{-}y}(\alpha) = \lambda_x * cos^2\alpha + \lambda_y * sin^2\alpha \qquad (10\text{-}3)$$

$$\lambda_{x\text{-}z}(\alpha) = \lambda_x * cos^2\alpha + \lambda_z * sin^2\alpha \qquad (10\text{-}4)$$

$$\lambda_{y\text{-}z}(\alpha) = \lambda_y * cos^2\alpha + \lambda_z * sin^2\alpha \qquad (10\text{-}5)$$

for $\lambda_x=\lambda_y$ results $\lambda_{x\text{-}z}(\alpha)=\lambda_{y\text{-}z}(\alpha)$

where λ_x, λ_y, λ_z are the calculated values from the sheet models and α (0-360°) the angle of the heat flow on the sample (Figure 10-1).

The two sheet models give good results for the main influence, the mineral composition, as upper and lower bounds for the measurements (Figure 10-4). However the two models cannot give the complex second order anisotropy (Figure 10-5). Thus I had to modify the simple sheet models.

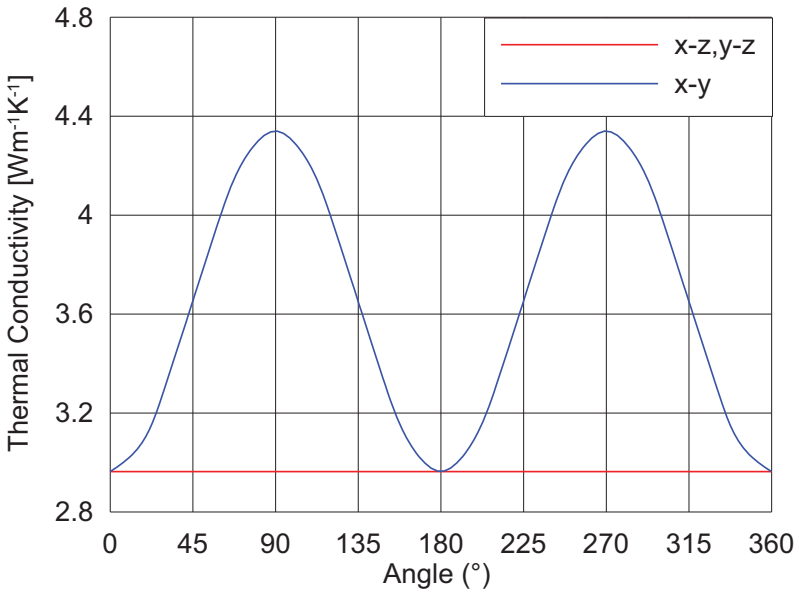

Figure 10-5: Calculated anisotropy in three directions with the sheet models of Voigt and Reuss

10.3.3.Sheet model with modification

As general concept the two components are no longer modelled as a layered material, but as a host material with an embedded rectangular block (Figure 10-6) in order to implement a non-uniform shape of the quartz within the layering.

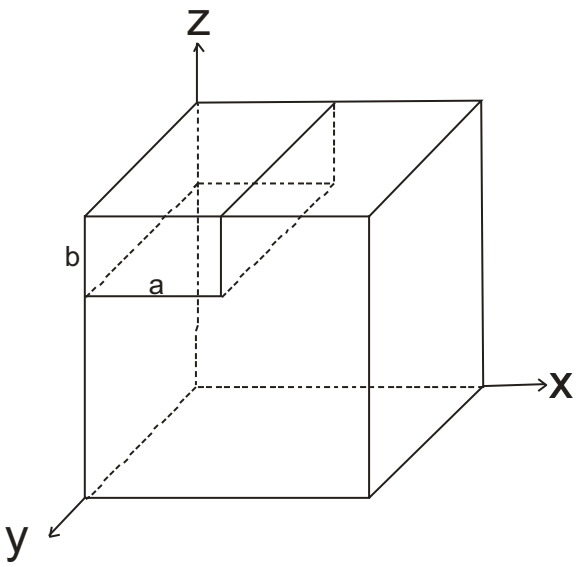

Figure 10-6: Sheet model with modification (embedded quartz block)

The layer with material 1 (here: quartz) is a rectangular block with preferred direction along the y-axis. In the x-direction only the part *a*b* is filled with this material. Parameter *b* can be expressed with $b=V_1/a$, where V_1 is the volume fraction of quartz.

Two different methods for the calculation are presented. The first one will be used in this thesis but both types are additionally shown in Figure 10-7.

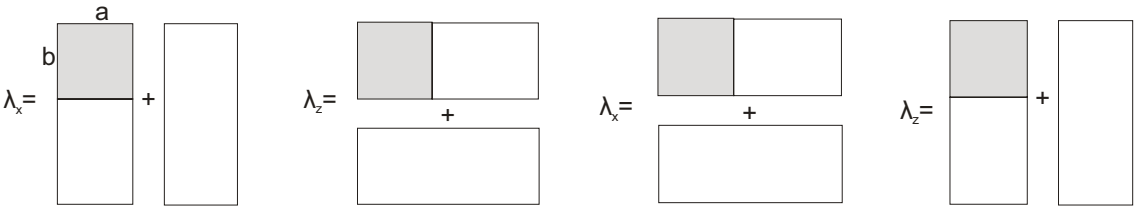

Figure 10-7: a) Variant 1 (left) b) Variant 2 (right)

With the equations a forward modelling of thermal conductivity in the main axes is possible; the directional dependence results in a vectorial addition of the corresponding main axes conductivities using the angle α (0-360°) as defined in Figure 10-1.

Variant 1 (Figure 10-7/a):

Consideration of only linear terms results in the equations:

$$\lambda_y = (1 - V_1) * \lambda_2 + V_1 * \lambda_1 \quad (10\text{-}6)$$

$$\lambda_x = \left[\frac{1-a}{\lambda_2} + \frac{a}{\lambda_2 * \left(1-\frac{V_1}{a}\right) + \lambda_1 * \left(\frac{V_1}{a}\right)}\right]^{-1} \quad (10\text{-}7)$$

$$\lambda z = \left[\frac{1-\frac{V1}{a}}{\lambda 2} + \frac{\frac{V1}{a}}{a*\lambda 1 + (1-a)*\lambda 2}\right]^{-1} \quad (10\text{-}8)$$

Variant 2 (Figure 10-7/b):

Equation for λ_y stays the same.

$$\lambda_x = \left[\left(1 - \frac{V1}{a}\right) * \lambda_{2,\text{host}} + \frac{V1}{a} * \left(\frac{a}{\lambda 1,quartz} + \frac{(1-a)}{\lambda 2,host}\right)\right]^{-1} \quad (10\text{-}9)$$

$$\lambda_z = \left[(1 - a) * \lambda_2 + a * \frac{V_1}{a*\lambda_1} + \frac{(1-\frac{V_1}{a})}{\lambda_2}\right]^{-1} \quad (10\text{-}10)$$

Both variants are mathematically equivalent and represent only linear terms; for this application I use variant 1:

For the model calculation the thermal conductivities of the two components $\lambda_{1,\text{quartz}}$, $\lambda_{2,\text{host}}$ and the geometrical model parameters $V_{1,quartz}$, a are necessary as input.

An inversion algorithm based on equations (10-6), (10-7) and (10-8) allows the determination of these parameters. As input the (measured) three main axis conductivities λ_x, λ_y, λ_z and an assumption regarding one of the material conductivities are necessary. Here we used the value for quartz $\lambda_{1,\text{quartz}}$= 7.2 W $m^{-1}K^{-1}$. To give an overview how the value of quartz influences $\lambda_{2,\text{host}}$ I additionally tried a range from 6.8 to 7.4 W $m^{-1}K^{-1}$ for $\lambda_{1,\text{quartz}}$ (see Table 10-1).

λ_1 [$Wm^{-1}K^{-1}$]	λ_2 [$Wm^{-1}K^{-1}$]	V_1	a
6.8	1.68	0.51	0.75
7.0	1.73	0.49	0.73
7.2	1.78	0.47	0.72
7.4	1.82	0.44	0.70

Table 10-1: Results for λ_2, $V_{1,quartz}$ and *a* with variable $\lambda_{1,quartz}$

With $\lambda_{1,quartz}$ = 7.2 W $m^{-1}K^{-1}$ and the measured conductivities λ_x = 3.4 W $m^{-1}K^{-1}$, λ_y = 4.3 W $m^{-1}K^{-1}$ and λ_z = 3.2 W $m^{-1}K^{-1}$ inversion results in:

$\lambda_{2,host}$ = 1.78 W $m^{-1}K^{-1}$, the volume fraction of quartz $V_{1,quartz}$= 0.47 and the geometric parameter *a* = 0.72.

A modification of λ_1 between 6.6 and 7.4 $Wm^{-1}K^{-1}$ results in some different values for λ_2, V_1 and *a* (see Table 10-1).

10.3.4.Inclusion model – non-spherical inclusion

There are many different approaches for inclusion models (compare Chapter 5.4.). Most of them are based on an ellipsoidal inclusion which requires the implementation of a depolarisation factor *L* related to the axes of the ellipsoid. Sen et al. (1981) described a model with aligned ellipsoids in a host material and applied the differential effective medium algorithm (DEM) for calculation:

$$\left(\frac{\lambda_1-\lambda_{\mathrm{DEM}}}{\lambda_1-\lambda_2}\right) * \left(\frac{\lambda_2}{\lambda_{\mathrm{DEM}}}\right)^{L} = V_1 \qquad (10\text{-}11)$$

where λ_{DEM} is the rock conductivity, λ_1 the inclusion material conductivity, λ_2 the host material conductivity and V_1 is the volume fraction of the inclusion. *L* is the depolarisation factor of the dispersed particles. The depolarization factor refers to the direction of the main axes of the ellipsoid. The equations for aligned ellipsoids are:

x-direction: $$\left(\frac{\lambda_1-\lambda_{\mathrm{x}}}{\lambda_1-\lambda_2}\right) * \left(\frac{\lambda_2}{\lambda_{\mathrm{x}}}\right)^{L_{\mathrm{x}}} = V_1 \qquad (10\text{-}12)$$

y-direction: $$\left(\frac{\lambda_1-\lambda_{\mathrm{y}}}{\lambda_1-\lambda_2}\right) * \left(\frac{\lambda_2}{\lambda_{\mathrm{y}}}\right)^{L_{\mathrm{y}}} = V_1 \qquad (10\text{-}13)$$

z-direction $$\left(\frac{\lambda_1-\lambda_{\mathrm{z}}}{\lambda_1-\lambda_2}\right) * \left(\frac{\lambda_2}{\lambda_{\mathrm{z}}}\right)^{L_{\mathrm{z}}} = V_1 \qquad (10\text{-}14)$$

The directional dependence is controlled by the three depolarisation factors. The sum of these is: $L_{\mathrm{x}} + L_{\mathrm{y}} + L_{\mathrm{z}} = 1$

Sen (1981) recommends the following approximation for plate-like objects

$(a = b \gg c)$

$$L_c = 1 - \frac{\pi}{2} * \frac{c}{a} = 1 - \frac{\pi}{2} * \alpha \qquad (10\text{-}15)$$

where $\alpha = \frac{c}{a}$ is the aspect ratio.

For the gneiss I assume an oblate ellipsoid in x-direction (Figure 10-8). This resembles a layer of quartz from the gneiss with the cross section of an ellipse on the x-z faces.

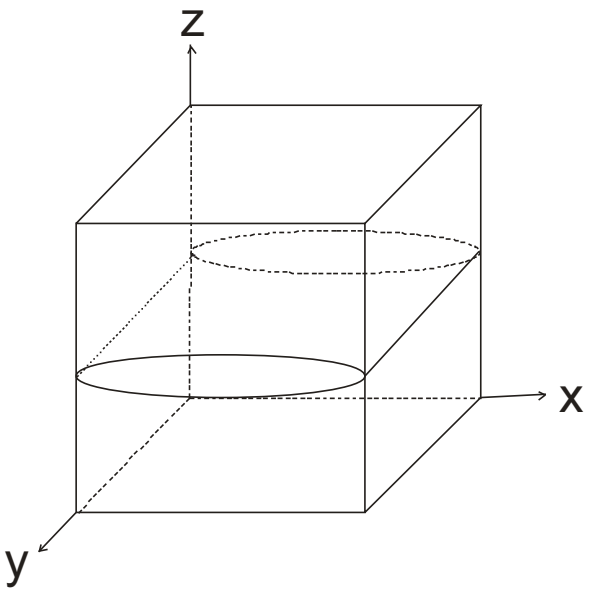

Figure 10-8: Inclusion model with ellipsoid inclusion

Therefore the factor L_y is extremely small. For calculation a value L_y = 0.0 is used. Therefore only one variable factor results

$$L_x = 1 - L_z \qquad (10\text{-}16)$$

For the model calculation the thermal conductivities of the two components $\lambda_{1,\,quartz}$, $\lambda_{2,\,host}$ and the geometrical model parameters $V_{1,quartz}$, a and α are necessary as input.

An iterative inversion algorithm – based on equations (10-12), (10-13), (10-14) and (10-16) allows the determination of the parameters $\lambda_{2,host}$, L_x, L_z and $V_{1,quartz}$. Again the (measured) three main axes conductivities λ_x, λ_y, λ_z and an assumption regarding one of the material conductivities are used as input. The value for quartz is the same as in the sheet model with the geometrical modification applied (Chapter 10.3.3.). So the comparison of the two $\lambda_{2,host}$ values out of the calculations of both models is easier.

Calculation results in the following model parameters:

- conductivity of host material: $\lambda_{2,host}$ = 1.82 $Wm^{-1}K^{-1}$
- volume fraction of quartz: $V_{1,quartz}$ = 0.37
- polarization factors L_x = 0.43, L_y = 0.0, L_z = 0.57.

Comparison with the result derived from the modified sheet model shows

- the conductivity of host material is in the same order (1.78 and 1.82 $Wm^{-1}K^{-1}$)
- the inclusion model delivers a lower volume fraction of quartz (37%) compared to the sheet model (47%); this confirms that ellipsoidal inclusions show a stronger effect as the simple sheet model with linear approximation
- both models demonstrate an unequal distribution of the quartz. The sheet model gives a value a = 0.72; with V_1 = 0.47 for the other dimension results b = 0.65; thus the ratio is b/a = 0.9. In case of the inclusion model this geometry effect is expressed by the different depolarization factors (L_x = 0.43, L_y = 0.57) which indicates a comparable situation of a stronger elongation of the quartz in x-direction compared to the z-direction.

Additionally the Hudson model for the compressional wave velocity was used.

10.3.5.Hudson model for the anisotropy of the compressional wave velocity

Hudson (1980) delivered with his equations a method for modelling elastic properties of fractured rocks with aligned penny-shaped ellipsoidal inclusions. Hudson (1980) uses for the host material the background moduli (c^0_{ij}) and implements inclusion effects as first order correction (c^1_{ij}) which results in the stiffness parameters for the fractured rock: $c^{eff}_{ij} = c^0_{ij} + c^1_{ij}$.

Because of the oriented fractures Hudson's model describes anisotropy. The symmetry of the model results in a transverse isotropy with the corresponding stiffness tensor. This transverse isotropy can therefore model only the observed first order effect.

For the correction term equations are presented in Table 10-2. Hudson used the Lamé constants λ and μ for description of elastic properties.

The crack normals are aligned along the 3-axis (*z*-axis); **horizontal cracks, VTI medium**	**The crack normals are aligned along the 1,2-axis (*x*-,*y*-axis);** **vertical cracks, HTI medium**
$c_{11}^1 = -\frac{\lambda_h^2}{\mu_h} \cdot \varepsilon \cdot U_3$ $c_{13}^1 = -\frac{\lambda_h \cdot (\lambda_h + 2\mu_h)}{\mu_h} \cdot \varepsilon \cdot U_3$ $c_{33}^1 = -\frac{(\lambda_h + 2\mu_h)^2}{\mu_h} \cdot \varepsilon \cdot U_3$ $c_{44}^1 = -\mu_h \cdot \varepsilon \cdot U_1$ $c_{66}^1 = 0$	$c_{11}^1 = -\frac{(\lambda_h + 2\mu_h)^2}{\mu_h} \cdot \varepsilon \cdot U_3$ $c_{13}^1 = -\frac{\lambda_h \cdot (\lambda_h + 2\mu_h)}{\mu_h} \cdot \varepsilon \cdot U_3$ $c_{33}^1 = -\frac{\lambda_h^2}{\mu_h} \cdot \varepsilon \cdot U_3$ $c_{44}^1 = 0$ $c_{66}^1 = -\mu_h \cdot \varepsilon \cdot U_1$

Table 10-2: Correction terms, λ_h and μ_h are the Lamé constants for solid material (host material)

The crack density ε is described as $\varepsilon = \frac{3*\phi}{4*\pi*\alpha}$ where ϕ is the crack porosity and α is the aspect ratio. Additionally U1 and U3 are expressed with the following equations:

$$U_1 = \frac{16*(\lambda_h+2*\mu_h)}{3*(3*\lambda_h+4*\mu_h)} * \frac{1}{1+M} \quad (10\text{-}17) \qquad U_3 = \frac{4*(\lambda_h+2*\mu_h)}{3+(\lambda_h+\mu_h)} * \frac{1}{1+K} \quad (10\text{-}18)$$

K and M are described through:

$$M = \frac{1}{\pi*\alpha} * \frac{\mu_i}{\mu_h} * \left(\frac{4*(\lambda_h+2*\mu_h)}{3*\lambda_h+4*\mu_h}\right) \quad (10\text{-}19) \qquad K = \frac{\left(ki+\frac{4}{3}*\mu i\right)*(\lambda h+2*\mu h)}{\pi*\alpha*\mu h*(\lambda h+\mu h)} \quad (10\text{-}20)$$

where k_i and μ_i are the bulk and shear modulus of the inclusion material (Schoen, 2011). As inclusion material I used quartz with k_i=38 GPa and μ_i=43 GPa. For the host material I assumed k_h=45 GPa and μ_h=22 GPa is assumed. Using this input values and additionally d_{host}=2710 kgcm^{-3} as well as d_{quartz}=2650 kgcm^{-3} I receive a compressional wave velocity of the host material with 5730 ms^{-1}.

Next step was the calculation of v_p in different directions with Hudson's equations (Table 10-2) described before. This was accomplished for different aspect ratios and porosities. With an aspect ratio of 0.35 and the volume of the quartz of 0.4 (like determined with the models for the thermal conductivity) the result is for $v_{p,x}$=5470 ms^{-1} and for $v_{p,y}$ = 4536 ms^{-1}. They fit to the measured data very well. Table 10-2 shows the comparison of measured data and calculated data.

	Measured	**Calculated**	**Deviation**
	ms^{-1}	**ms^{-1}**	**%**
$V_{p,x}$	5748	5540	3.6
$V_{p,y}$	4562	4564	0.02
V_p (c_{33}=c_{11})	5311	5470	3.0

Table 10-3: Comparison of measured and calculated values for the compressional wave velocity with the Hudson model

To sum it up, the Hudson model can express the anisotropy in different directions for the compressional wave velocity.

10.4. Discussion and comparison of the two models for the thermal conductivity

Two different approaches were used for modelling the anisotropy of thermal conductivity of the "Stainzer Plattengneis". Both models can explain the experimentally measured 3-axial anisotropy mainly as result of the internal rock texture, particularly the shape and orientation of the quartz. As input values for modelling and inversion the measured conductivities λ_x, λ_y, λ_z in the main axes direction were used.

In detail, the start was a sheet model with two components, but it was too simple to express the complex 3-axis anisotropy. The next step was a modification of the sheet with the highest thermal conductivity. With this it is possible to show the anisotropy in three directions. The model is a linear approximation. The resulting thermal conductivity of the host material is 1.78 $Wm^{-1}K^{-1}$. This value is less than would have been expected. Probably it is a result of the micro fractures, which decrease thermal conductivity. The calculated volume of the quartz is nearly the same as the estimated value from the thin section.

The second approach was the inclusion model. Calculations with an iterative method were realized. The value for the host material is of about the same magnitude and the volume of the higher conductive material (quartz) is a bit smaller than from the sheet model. Also in this case the host material conductivity is influenced by micro fracturing. The calculated volume of the quartz is less than the estimated value from the thin section.

The two models can give an explanation of the influence of the mineral composition and “internal mineral geometry” (particularly of the quartz fraction) as origin of the anisotropy. The shape of the quartz component in both models explain the maximum conductivity in y-direction, an intermediate value in x-direction and the lowest conductivity for z-direction.

Results for the host material conductivity additionally give an idea of the influence of micro fractures. When the expected value for the host material is significantly less than the calculated value, there are probably a lot of micro fractures and other “defects” present.

11. Estimation of heat production from GR-logs

Radiogenic heat production is an important property, especially for modelling the temperature distribution and thermal evolution of a sedimentary basin or interpretation of the heat flow density. The radiogenic heat production has a high effect on the whole heat flow of the Earth. The mean heat flow at the Earth's surface is about 65 mWm^{-2} and the heat flow from the mantle in continental areas approximately 20 mWm^{-2}. The difference is due to radioactive heat generation in the crustal rocks (Rybach & Cermak, 1982).

Usually the radiogenic heat production is calculated from the Potassium (K), Uranium (U) and Thorium (Th) content and the rock density by using the formula by Rybach (1976).

The K, U and Th content and the density can be taken from

- laboratory measurements at samples,
- borehole measurements from the Natural Gamma Spectrometry log and a Density log.

In many cases only a (integral) gamma log is available. Buecker & Rybach (1996) published a simple method to determine heat production from such an integral gamma-ray log. This method is based on a linear relationship between the gamma ray intensity GR and heat production *A*. Authors note that the equation is valid for a wide variety of lithologies extending from granite through gneiss, carbonate and amphibolites to basaltic rocks.

For the case of only a (integral) gamma log in API units being available, a petrographic-coded approximate method for heat generation estimate is developed. It implements mean values for the ratios *U/K* and *Th/K* which are controlled by rock type.

11.1. Rybach & Buecker's equation (1996)

Rybach (1976) documented the radioactive heat production and its relationship to other petrophysical properties. For the calculation of the heat production, when the concentrations of Uranium [ppm], Thorium [ppm] and Potassium [%] are known, he used the equation:

$$A = 0.317 * d * (0.718 * c_{\mathrm{U}} + 0.193 * c_{\mathrm{Th}} + 0.262 * c_{\mathrm{K}}) \qquad (11\text{-}1)$$

where *A* is the heat production [HGU=10^{-13} cal cm^{-3}], *d* is the density [gcm^{-3}]and c_U, c_{Th} and c_K are the concentrations of Uranium, Thorium and Potassium.

Usually the radiogenic heat production rate is calculated from the Potassium, Uranium, and Thorium content and the rock density using the formula of Rybach (1976) and Rybach & Cermak (1982):

$$A = \frac{d}{100} * (9.52 * U + 2.56 * Th + 3.48 * K) \quad (11\text{-}2)$$

where

A is the heat generation in μW m^{-3}

d is rock density in g cm^{-3}

U,Th are the concentrations of Uranium and Thorium in ppm

K is the concentration of Potassium in %.

The conversion between SI-unit and HGU (Heat Generation Unit) is:

1 μW m^{-3} = 2.39 HGU = 2.39·10^{-13} cal s^{-1}cm^{-3}

1 HGU = 0.418·10^{-6} Wm^{-3} = 10^{-13} cal s^{-1}cm^{-3}.

Gamma ray spectrometry is the easiest way to get the concentrations. The values for the density and the concentrations can also be taken from a density log and spectral natural gamma spectrometry logs (Rybach, 1976). Another method would be a determination through chemical analysis.

The problem is that in many cases the standard gamma log is just an integral one and not a spectral one. Buecker and Rybach (1996) developed a simple method to determine heat production from gamma-ray logs:

$$A = 0.0158 * (GR - 0.8) \quad (11\text{-}3)$$

where *A* is the heat generation [µWm^{-3}] and GR is the gamma intensity [API]. This equation is valid for most lithologies and shows an error under 10% in the range of 0-350 API and 0.0-7 µWm^{-3}.

11.2. A modified petrographic coded equation

The following derivation uses two basic equations. The first one is the combination of the integral gamma ray intensity (GR in API) with the concentrations of Uranium, Thorium and Potassium:

$$GR(API) = y_1 * K + y_2 * U + y_3 * Th \quad (11\text{-}4)$$

y_1,y_2 and y_3 are calibration constants for the gamma measurement.

Ellis and Singer (2007) give y_1=16, y_2=8 and y_3=4 as typical values. The calibration constants for the gamma measurement derived from data in Schlumberger, 1982 are y1=15.38, y2=8.10 and y3=3.83.

The second one is Rybach's (1986) relationship between heat generation *A* (μWm^{-3}), density *d* (kgm^{-3}) and the concentrations of U, Th (ppm) and K (%) as shown in equation (11-2). In a more general formulation the equation is:

$$A = d * (x_1 * K + x_2 * U + x_3 * Th) * 10^{-5} \quad (11\text{-}5)$$

where for Rybach's equation are x_1=9.52, x_2=2.56 and x_3=3.48. Density *d* is in kgm^{-3}.

Combination of these two equations (11-4) and (11-5), results in:

$$A = GR * d * \frac{x_1 + x_2 * \frac{U}{K} + x_3 * \frac{Th}{K}}{y_1 + y_2 * \frac{U}{K} + y_3 * \frac{Th}{K}} * 10^{-5} \quad (11\text{-}6)$$

This equation combines (integral) gamma intensity GR and the rock properties density and the ratios U/K and Th/K.

To simplify the equation I introduce a parameter *l*, implementing the ratios for the considered rock type and the sensitivity factors of the integral measurement (in equation(11-4):

$$l = \frac{x_1 + x_2 * \frac{U}{K} + x_3 * \frac{Th}{K}}{y_1 + y_2 * \frac{U}{K} + y_3 * \frac{Th}{K}} * 10^{-5} \quad (11\text{-}7)$$

The ratios of U/K and Th/K are influenced by the mineral composition of the rock. To give an overview of some values from the literature, Table 11-1 shows value for this parameter for some rock types.

Then the new equation is

$$A = GR * d * l = k * GR \quad (11\text{-}8)$$

where *GR* is the integral gamma intensity

d is the bulk density

l is the new parameter implementing the petrographic code (rock type)

11.3. Comparison of the new equation with data from the literature

Using data from the literature and calculate the I value, I get the following equations for the main rock types:

Rock type		U/K	Th/K	I	Ref.
Sedimentary rocks	Limestone	6.67	5.00	8.9 E-06	R
	Dolomite	1.43	1.14	6.3 E-06	R
	Anhydrite	0.25	0.75	3.7 E-06	R
	Shale	3.00	6.00	7.4 E-06	BA
	Sandstone	0.45	1.55	4.6 E-06	BA
Igneous rocks	Peridotite	0.05	0.25	2.6 E-06	BA, Sch
	Gabbro	1.67	5.35	6.5 E-06	Sch
	Diorite	1.82	7.73	6.6 E-06	BA, Sch
	Granitic rocks	1.06	3.70	5.9 E-06	Sch
	Plateau basalt	0.87	3.21	5.6 E-06	BA, Sch

Table 11-1: Lithology-controlled parameters for compiled rock types; References R - Rybach (1986); BA – Baker Atlas (1985) ; Sch – Schlumberger (2000)

In Buecker & Rybach's equation the two properties *d* and *I* combined (k≈0.0158 μWm^{-3} /API).

Additionally to compare the improved equation with the equation of Buecker & Rybach, the heat generation normalized by GR was calculated (Table 11-2) and plotted (Figure 11-1). Density values were taken from the literature (Schoen, 1996). To give an idea of the influence of the density a range was considered for the calculations.

Rock type	L	Density (min)	Density (max)	k (min)	k (max)	A (Buecker)
Limestone	8.90E-06	2300	2900	2.05E-02	2.58E-02	1.57E-02
Dolomite	6.30E-06	2500	2900	1.58E-02	1.83E-02	1.57E-02
Anhydrite	3.70E-06	2800	2950	1.04E-02	1.09E-02	1.57E-02
Shale	7.40E-06	2300	2800	1.70E-02	2.07E-02	1.57E-02
Sandstone	4.60E-06	2000	2800	9.20E-03	1.29E-02	1.57E-02
Peridotite	2.60E-06	2800	3300	7.28E-03	8.58E-03	1.57E-02
Gabbro	6.50E-06	2900	3100	1.89E-02	2.02E-02	1.57E-02
Diorite	6.60E-06	2600	2900	1.72E-02	1.91E-02	1.57E-02
Granitic rocks	5.90E-06	2500	2700	1.48E-02	1.59E-02	1.57E-02
Plateau basalt	5.60E-06	2300	3200	1.29E-02	1.79E-02	1.57E-02

Table 11-2: *l* from Table 11-1, with density values (Schoen, 1996) and calculated *k (d*l)* and *A*

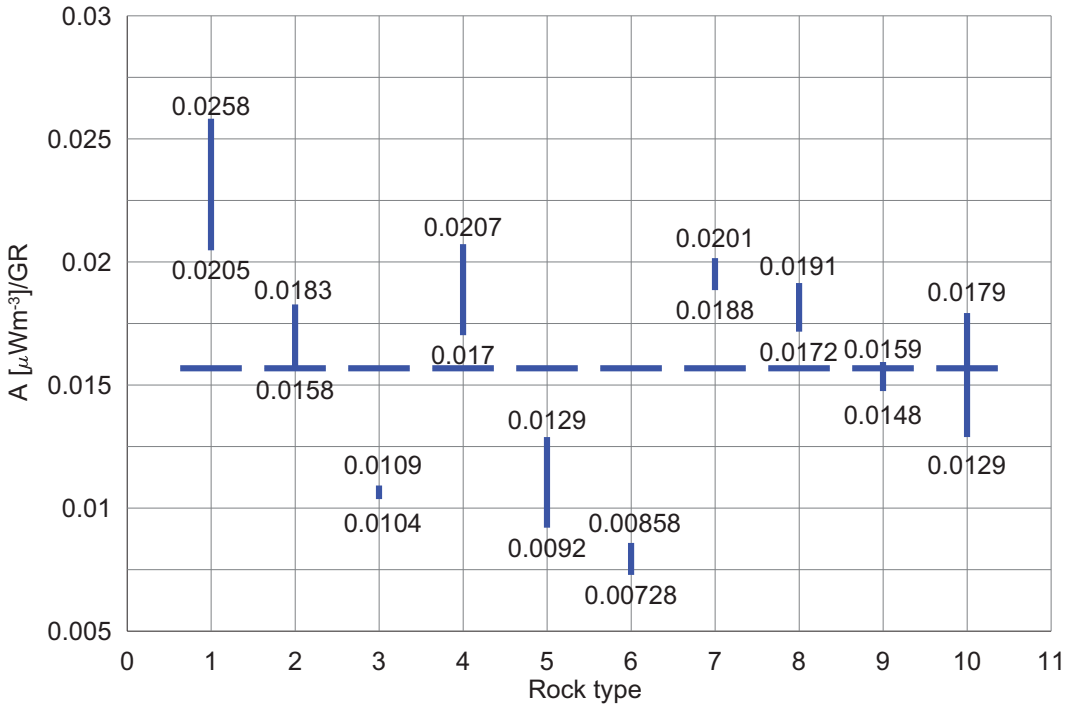

Figure 11-1: Normalized heat generation for different rock types, blue dashed line (at 1.57E-2) give the heat generation from the equation by Buecker & Rybach.(Rock type: 1=limestone, 2=dolomite, 3=anhydrite, 4=shale, 5=sandstone, 6=peridotite, 7=gabbro, 8=diorite, 9=granitic rocks, 10=plateau basalt)

Figure 11-1 shows the value of Buecker & Rybach (blue dashed line) which stays the same for all rock types because the equation is only influenced by the GR in API. The values give the upper or lower value of the results of the improved equation.

So an additionally input *of the ratios U/Th and Th/K and* the density as rock properties makes the result more precise. This also explains the deviation of the calculated values for boreholes in the following chapters.

With the new equation the following methods for heat generation calculation are offered:

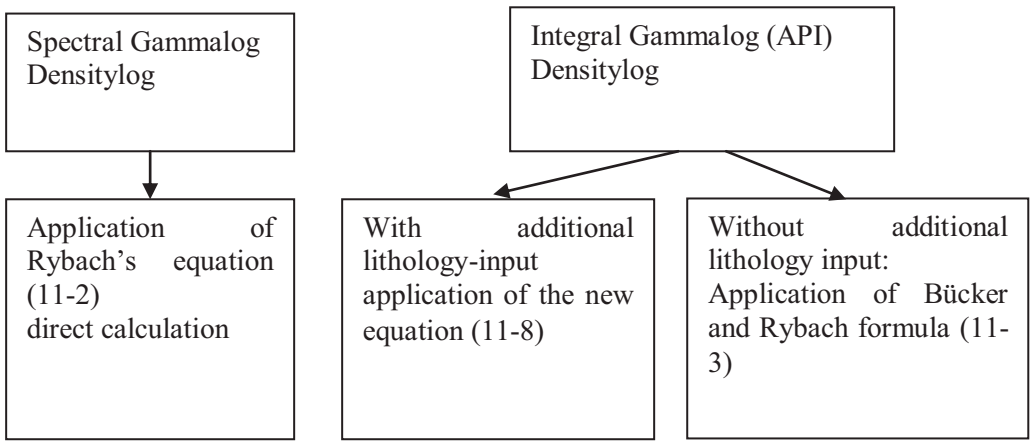

11.4. Comparison and application

The new equation was tested and compared for three wells representing different situations:

- Well with a known metamorphic rock profile; input are gamma log and density log
- Well with a carbonate profile; input are density-, Pe-, and gamma log
- Well with a metamorphic profile; input are spectral gamma log and density log.

As first example for comparison of the calculated logs, a borehole in the central part of the Alps is selected. The rocks are gneiss-mica-schist with a main mineral composition of: quartz, feldspar, biotite and muscovite.

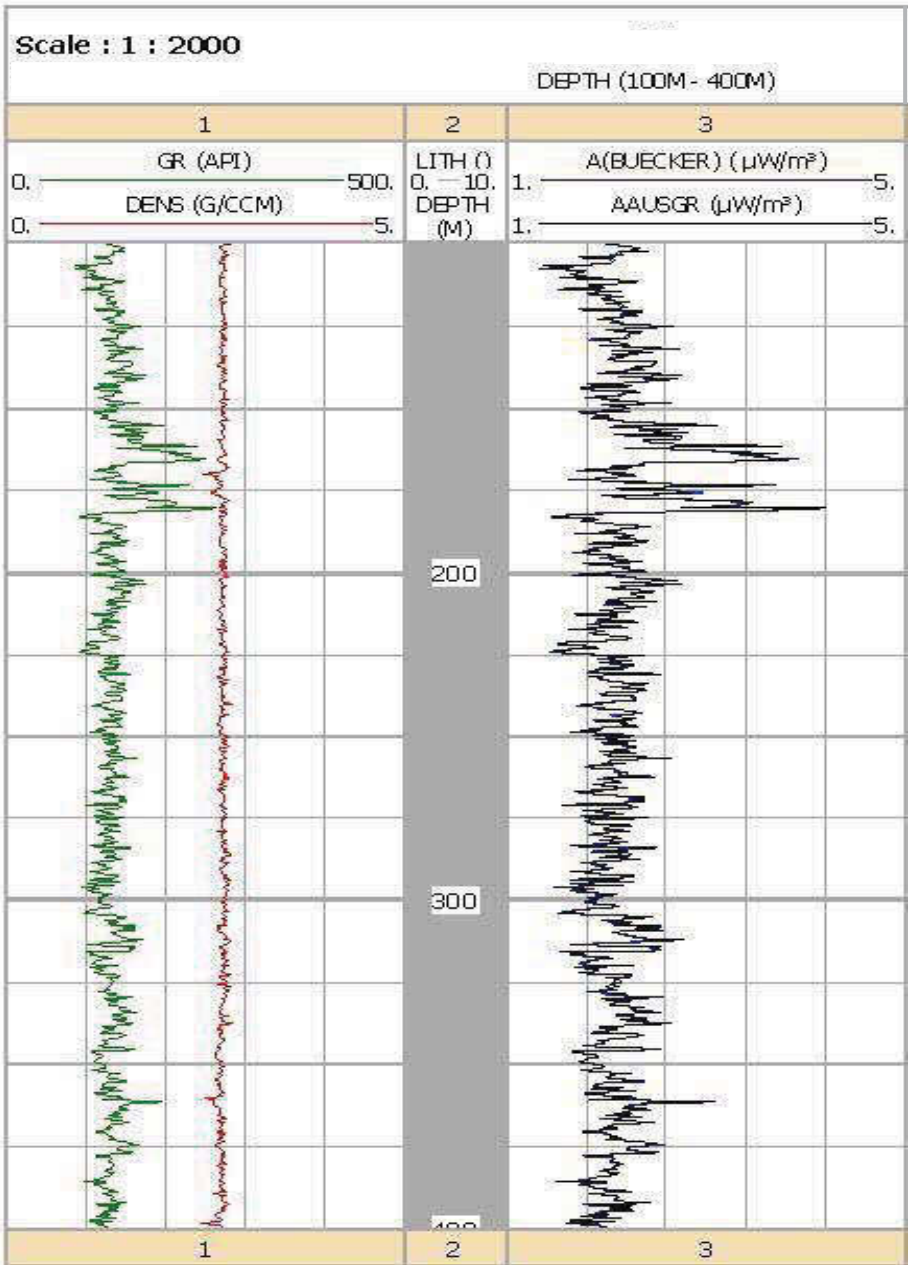

Figure 11-2: Comparison of the equation of Buecker & Rybach (1996) (blue line) and the new equation (black line) for a selected section of a borehole of the central part of the Alps (100-400m) with gneiss-mica schist

The information about the lithology is used for the calculations of the heat production *A*. A density and gamma ray log are here available and for the parameter *l* I used the value for granite (l=5.86 *10^-6), because it has a comparable mineral composition. Figure 11-2 displays the results for a part of the well, the gamma ray (green line), the density (red line) and the calculated heat production with the equation of Buecker & Rybach (1996) (blue line) and with the new equation (black line). There is practically no difference between the two calculated heat production curves in this section.

This fit can also be explained by consideration of Figure 11-1. The value of normalized heat production is closed to the dotted line representing the Buecker & Rybach equation (1996).

A second borehole from the Vienna Basin was selected. The lithology of the carbonate section has to be derived from a PE-log because no further lithology information is available. Between 2980 and 2990m limestone with PE=5.1 is present. Then the lithology changes to a dolomite with PE=3.1.

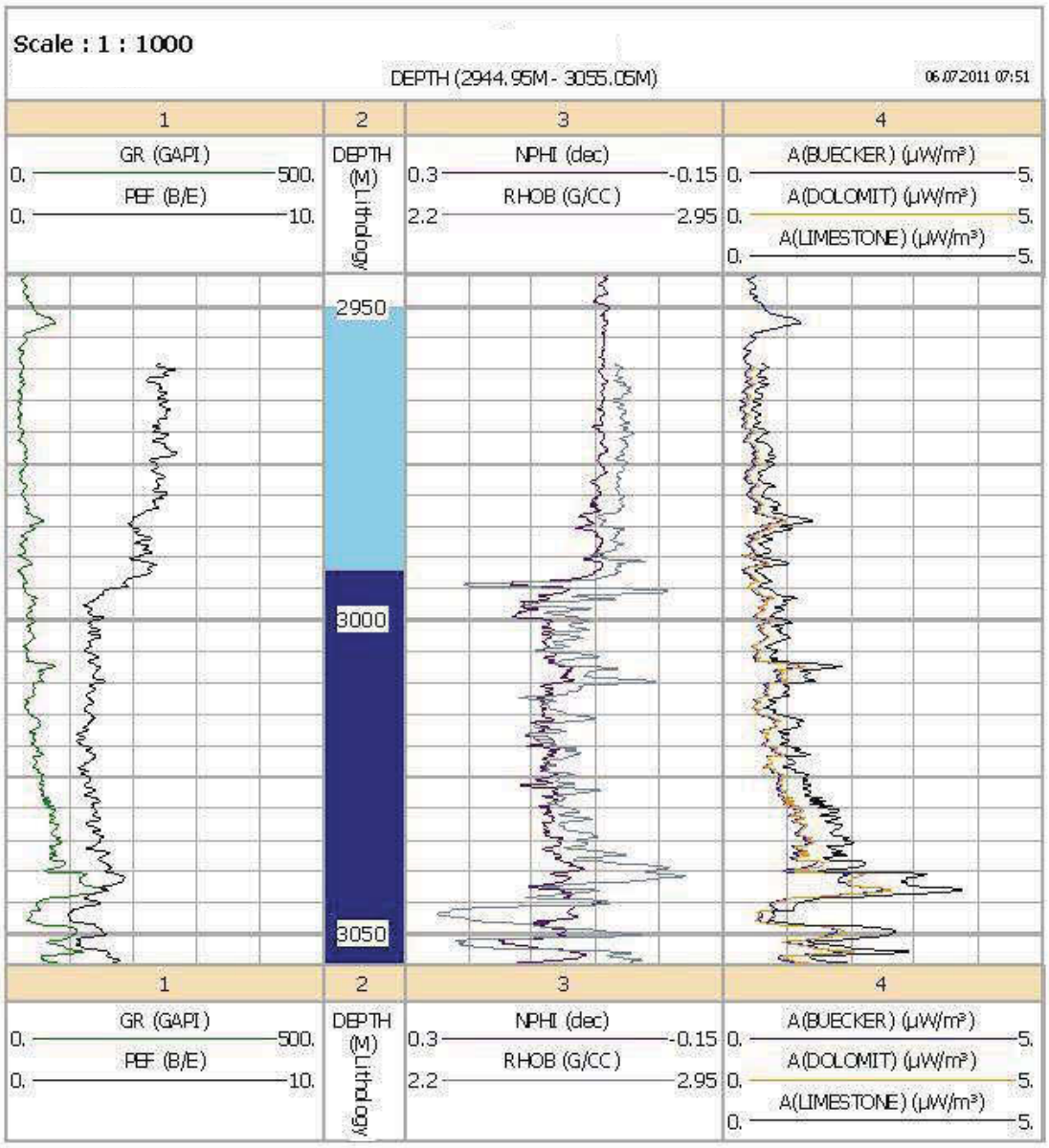

Figure 11-3: Comparison of the equation of Buecker & Rybach (1996) and the new equation for a selected section of a borehole in the Vienna Basin (2945-3055m); Trace 1: PE (black) and gamma ray (green); Trace 3: density (grey), NPHI (violet); Trace 4: Heat generation with equation from Buecker & Rybach (1996) (blue) and new equation for with dolomite (orange) and limestone (black)

Figure 11-3 shows the GR, Nphi, density and PE log and additionally the calculated heat generation with the equation of Buecker & Rybach (blue line) and with the new equation on the one hand with l=8.93 for the limestone (black line) and on the other hand l= 6.25 for the dolomite (orange line). The equation for limestone gives higher heat generation values than the equation for dolomite. The equation of Buecker & Rybach (1996) gives the lowest values.

The third selected borehole consists of dolomite and limestone. Only low heat generation is expected. Figure 11-4 and Figure 11-5 displays the results of the calculations, where the blue line again is the result of the equation of Buecker & Rybach (1996).

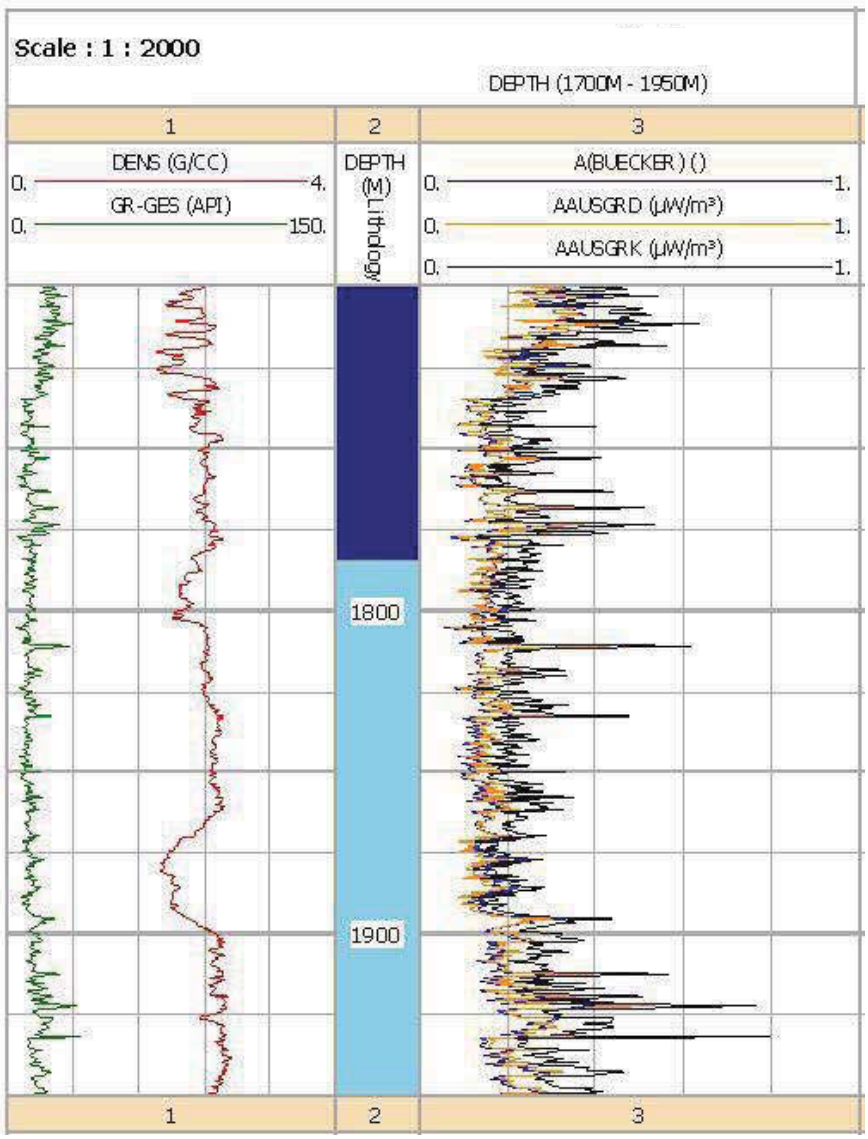

Figure 11-4: Comparison of the equations of Buecker & Rybach and new equation for limestone and dolomite (1700-1950m); Trace 1: density (red) and gamma ray (green); Trace 2: dark blue: limestone, light blue: dolomite; Trace 3: Heat generation with equation from Buecker & Rybach (1996) (blue) and with new equation for dolomite (orange) and limestone (black)

The orange line presents for dolomite and the black one limestone. The equation of Buecker & Rybach (1996) again shows the lowest values for the heat generation and limestone the highest values. Here the influence of the lithology information becomes visible. Depending on which equation is used, the heat generation shows higher or lower values.

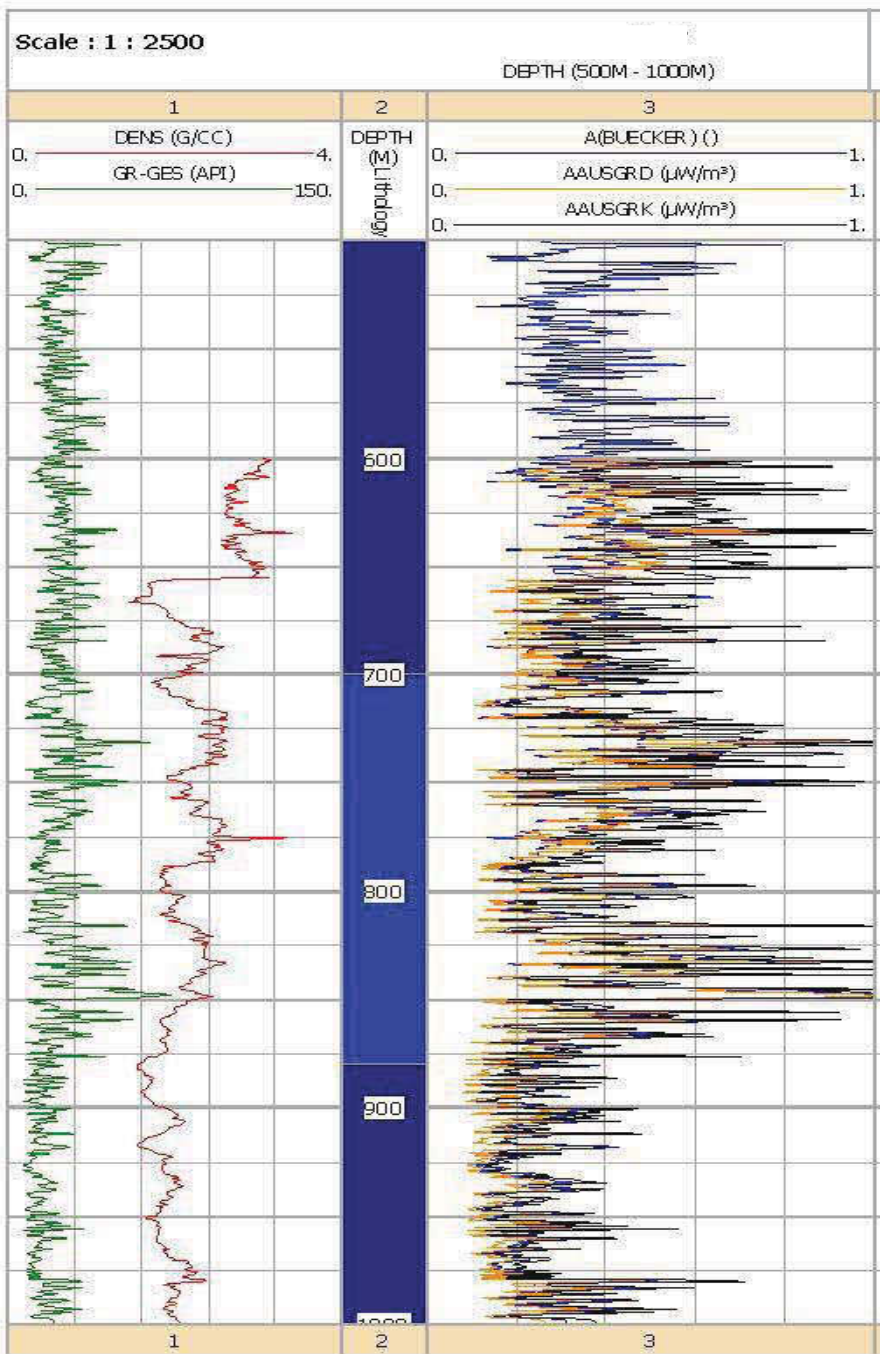

Figure 11-5: Comparison of the equations of Buecker & Rybach and the new one for limestone and dolomite (500-1000m); Trace 1: density (red) and gamma ray (green); Trace 2: dark blue: limestone, blue: mixture dolomite/limestone; Trace 3: Heat generation with equation from Buecker & Rybach (1996) (blue) and after new equation for dolomite (orange) and limestone (black)

The fourth borehole is the one from the continental drilling project in Germany. Here metabasite and gneiss alternate. Figure 11-6 displays the results of the calculations for the equation by Buecker & Rybach (blue line) and the new equation for granite (I value for granite and basalt are nearly the same; black line). Both show nearly the same values, only in some parts the new equation delivers a little bit higher values. Heat generation is here really low. Additionally spectral gamma logs are available here. Using both the basic equation of Rybach (1976) and the improved equation was possible. Rybach's equation shows the highest values. The new equation with the spectral logs provides a little bit lower values. Lowest values are calculated from the equation of Buecker & Rybach (1996).

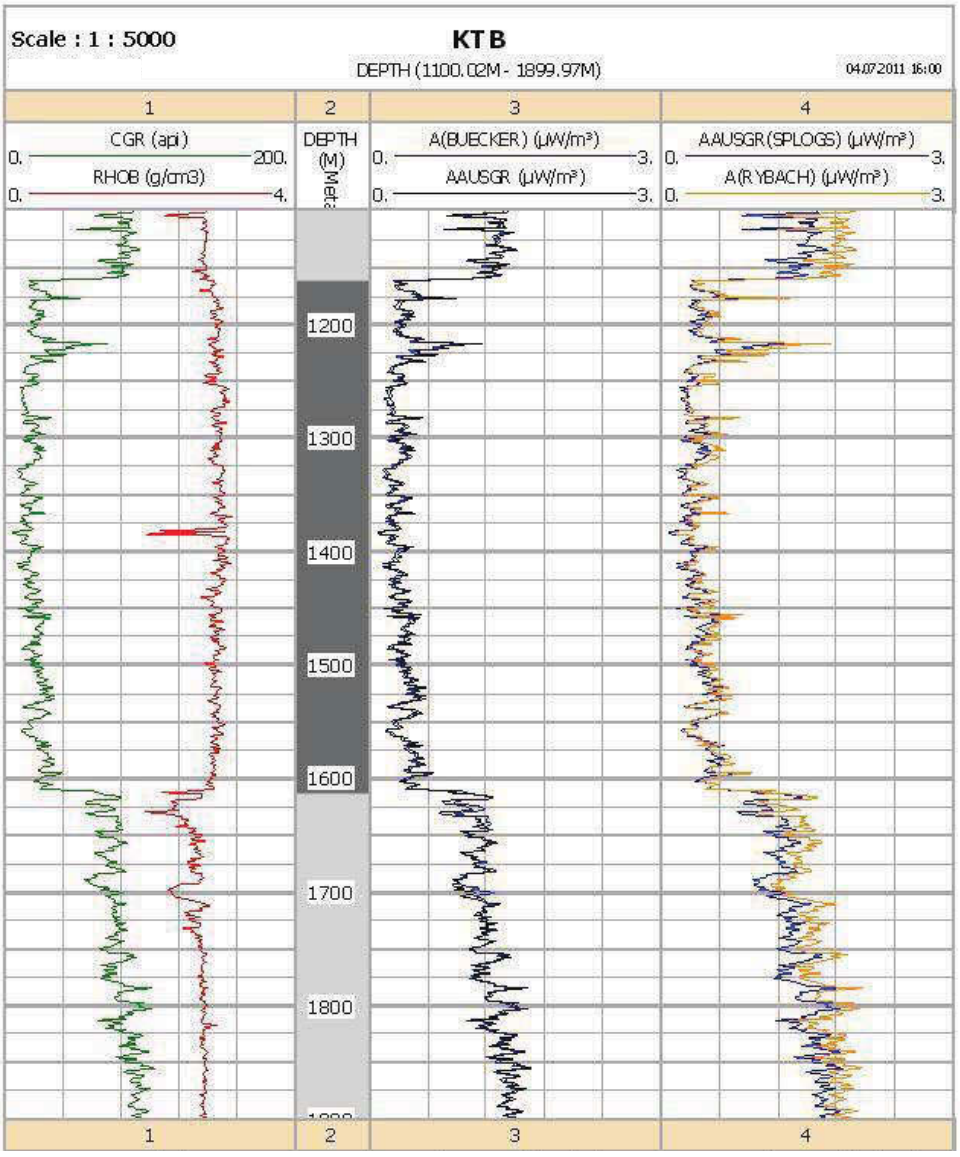

Figure 11-6: Comparison of the equations for the KTB additionally with spectral gamma ray logs (1100-1900m); lithology: grey=gneiss; dark grey=metabasite; Trace 1: gamma ray (green) and density (red); Trace 3: Heat generation with the equation of Buecker & Rybach (1996) (blue) and the new equation (black); Trace 4: Heat generation of the spectral gamma ray with the equation of Rybach (1976) (blue) and the new one (orange)

11.5. Discussion

In comparison to the equation of Buecker & Rybach (1996), I considered additionally the density as input and as an input for the rock type the value *I*. This makes the equation more exactly but supplementary a density log must be available. For magmatic rocks both equations give nearly the same values. This is demonstrated with the borehole containing the gneiss-mica schist.

Carbonates have only low heat generation in the majority of the cases. The new improved equations for dolomite and limestone deliver a little bit higher values than the one of Buecker & Rybach (1996). Limestone has the highest values for the heat generation.

Next step would be an improvement of the ratios of Uranium, Thorium and Potassium with laboratory measurements on cores from a borehole.

12. Estimation of thermal conductivity from logs

One motivation of this study is the development of methods for an estimation of thermal conductivity from conventional logs.

Figure 12-1 demonstrates the individual steps for the correlations and calculations on the way from the laboratory to the field. In the following chapters the results for different boreholes and different sections are discussed. The logs for the whole borehole are summarized in the appendix.

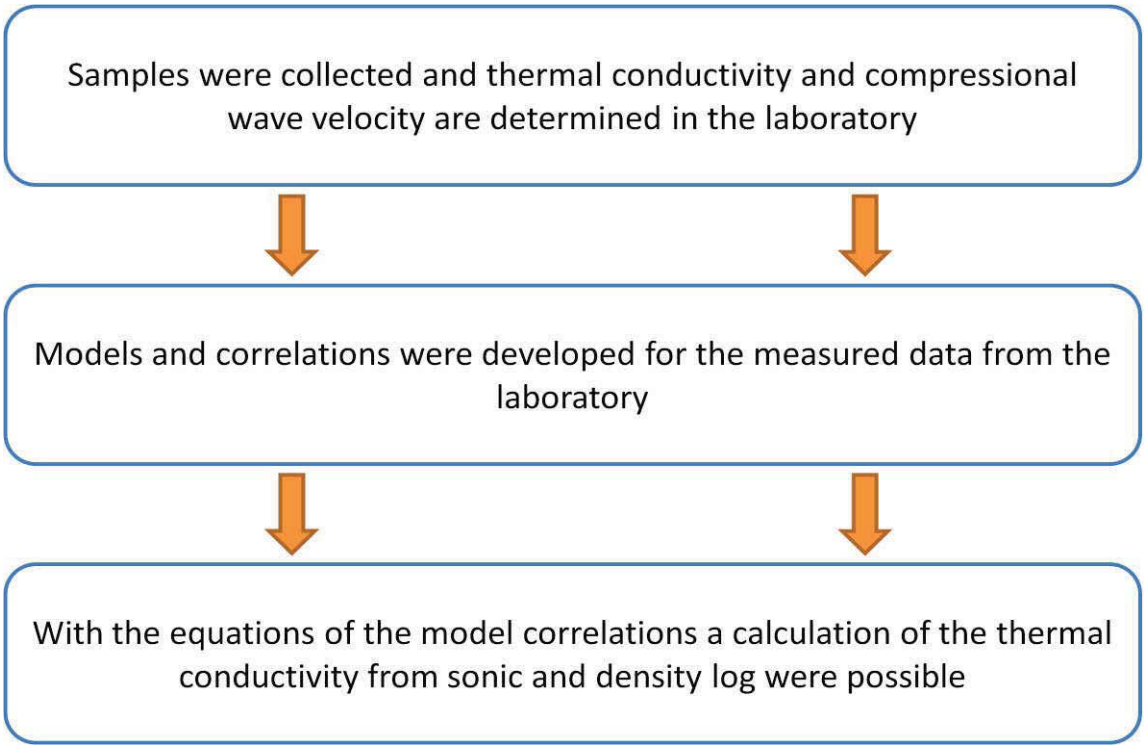

Figure 12-1: Summarized flowchart of the working plan

12.1. Overview and equations

For a derivation of thermal conductivity from log data the sonic and the density log can be used; preferred for the calculation is the sonic or acoustic log, because it shows the stronger correlation to thermal conductivity. As input the knowledge or assumption of the rock type is necessary.

The acoustic probe of a sonic log can is composed of one or more ultrasonic transmitters and one or more receivers. Three different types of waves occur: a direct wave through the borehole fluid, compressional and shear waves as head waves in the formation along the borehole wall and Stoneley- and Pseudo-Rayleigh-waves as interface waves. Best way to measure, is an open hole.

The velocity is indicated as [ms^{-1}] and the slowness as [μsm^{-1}] (Fricke & Schoen, 1999). The sonic log is one of the most common logs that get measured in a borehole.

Model calculations (Chapter 5.) can be applied in order to derive a "thermal conductivity log". Using the two models (the defect and the inclusion model), next step was to calculate the thermal conductivity with the velocities from the sonic log. Depending on the lithologies (granites/gneiss with higher or lower content of quartz, basalt/diorite/gabbro, sandstone and carbonates) different equations are applied. Table 12-1 gives an overview of the developed equations. For the inclusion model approximations have been calculated to make it easier to use them.

Figure 12-2 shows the relationships from Table 12-1 in a graphic presentation; curves for the inclusion and the defect model are plotted for the different rock types.

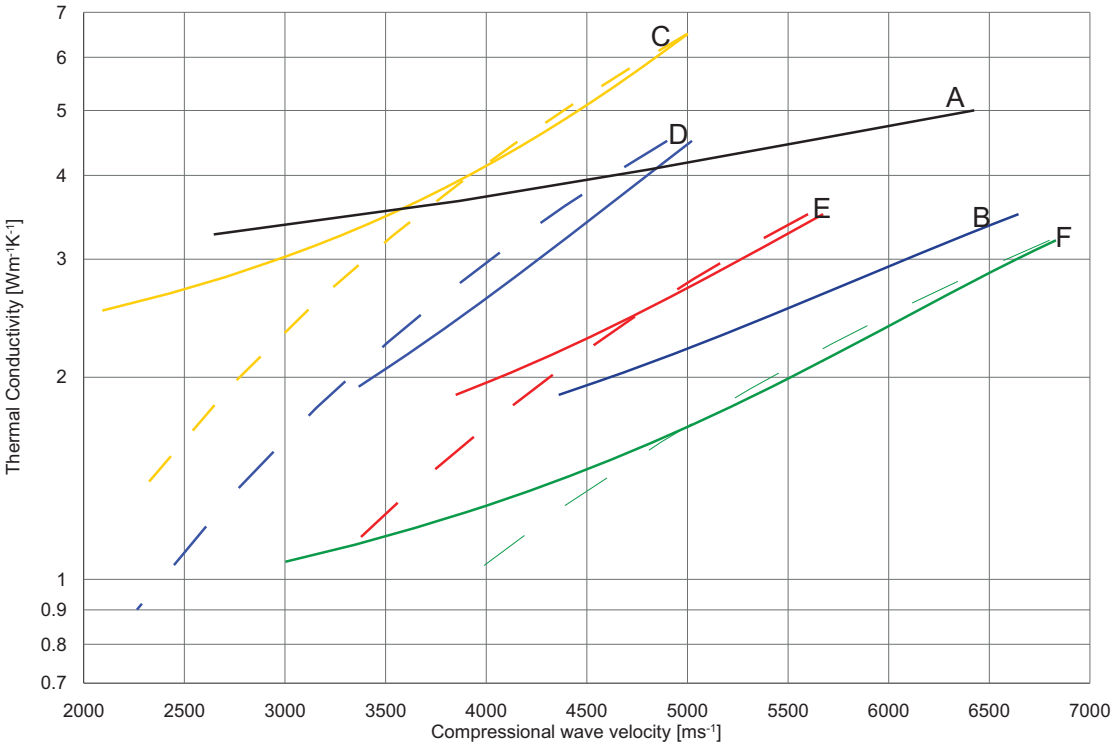

Figure 12-2: Calculated curves from the inclusion and defect model for different rock types; dashed lines = defect model; (A=dolomite, B=limestone, C=sandstone, D=granite/gneiss with high quartz content, E=granite/gneiss with low quartz content, F=basalt/diorite/gabbro)

In some cases additionally the density log was used. The density is measured with a gamma-gamma-method. Gamma rays from a source are emitted into the formation and the interaction with it is detected with a gamma detector. Detectors are placed in different spacing in order to correct calliper or mud cake effects. (Fricke & Schoen, 1999)

For the calculations of the thermal conductivity from density logs the same models (with a modification) as for the correlation between thermal conductivity and compressional wave velocity are used (Chapter 5.). As shown in the previous sections, the thermal conductivity versus density correlation only for magmatic and metamorphic rocks shows a reasonable scatter of data.

Rocktype	Inclusion model	Defect model
Granite/gneiss (less quartz)	$y=9E\text{-}07x^{1.76}$	$y=x^2*1.12E\text{-}07$
Gneiss/granite (more quartz)	$y=5E\text{-}08x^{2.14}$	$y=x^2*1.87E\text{-}07$
Diorite/Gabbro/basalt	$y=6E\text{-}07x^{1.75}$	$y=x^2*6.29E\text{-}08$
Sandstone	$y=1.212e^{0.0003*x}$	$y=x^2*2.60E\text{-}07$
Limestone	$y=1.945e^{0.0001*x}$	
Dolomite	$y=6E\text{-}06x^{1.50}$	

Table 12-1: Overview of the equations from the model calculations (y...thermal conductivity in $Wm^{-1}K^{-1}$, x...compressional wave velocity in ms^{-1}, in this chapter: velocity (x) determined from the sonic log)

Rock type	Inclusion model	Defect model
Granite/Gneiss	$y= 0.1186e^{0.0011x}$	y=181.25x+2175
Basalt/Gabbro/Diorite	$y=4E\text{-}07x^2\text{-}9E\text{-}05x\text{-}0.6645$	y=440x+1980

Table 12-2: Equations for the calculations of the thermal conductivity (y) from the density log (x)

These equations are then used with the program “Interactive Petrophysics” from Senergy to calculate the thermal conductivity from the sonic log and the density log. Depending on the rock type the suitable equation is chosen.

The results for different boreholes with different rock types are presented in the following chapters.

12.2. Example 1

The rocks in this borehole are gneiss-mica schist with a main mineral composition of: quartz, feldspar, biotite and muscovite (Gasser, 2000). The well has a depth of 1000m.

For the defect model the parameters for granite are used. $\lambda_{solid} \cdot v_{p,solid}^{-2} = 1.12E-7$ characterizes the non-fractured mineral composition which results in: $\lambda_{rock} = (1.12E-7) \cdot v_{p,rock}^2$ for the thermal conductivity.

For the inclusion model the “granite line” was approximated for low porosity by the exponential equation (see Table 12-1). For x (v_p) the velocity from the sonic log is used.

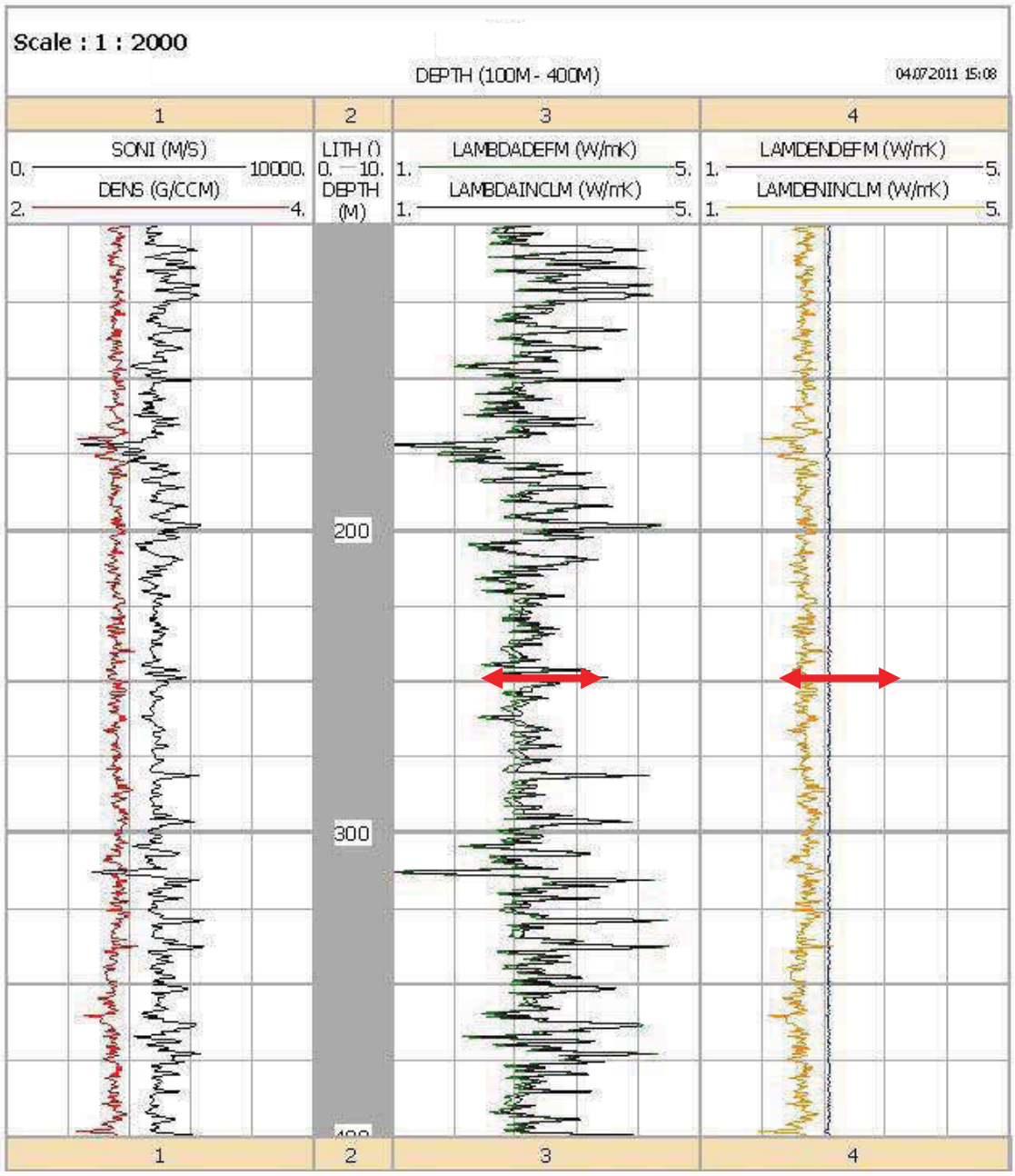

Figure 12-3: Well Example 1 (100-400m): Trace 1: Sonic and density log; Trace 2: lithology: gneiss-mica schist, Trace 3: "thermal conductivity log calculated from the sonic log" (green: Defect model; black: Inclusion model) ; Trace 4: "Thermal conductivity log" calculated from the density log (orange: Inclusion model; blue: defect model) Range from sample measurements 2.5-3.60 $Wm^{-1}K^{-1}$ is given as line at 250 m

Figure 12-3 shows the results of the calculated thermal conductivity of the sonic and the density log with the inclusion and the defect model. Measured values of the thermal conductivity on cores in the laboratory lie between 2.5 and 3.60 $Wm^{-1}K^{-1}$ and fit to the calculated thermal conductivity from the sonic log. The values from the defect model are a little bit higher (green line) than the ones from the inclusion model (black line).

The calculations of the thermal conductivity from the density log are also displayed in Figure 12-3. The defect model shows nearly a constant thermal conductivity for the whole borehole whereas the inclusion model shows more influence from the density log. Thermal conductivity values derived from the defect model are a little bit higher than from the inclusion model, probably because the defect model is not able to model the porosity effect correctly (which controls density). In general, the calculated thermal conductivity is below the mean value from the laboratory data.

12.3. Example 2 (KTB)

The continental deep drilling project is situated in Germany and was carried out from 1986 till 1992. All possible methods (logs and core analysis) have been measured. All data are still available on the internet[1]. So this borehole was a good choice for the calculations because all logs which are needed are present and additionally thermal conductivity data from cores have been measured.

[1] www.icdp-online.org/sites/ktb/welcome.html

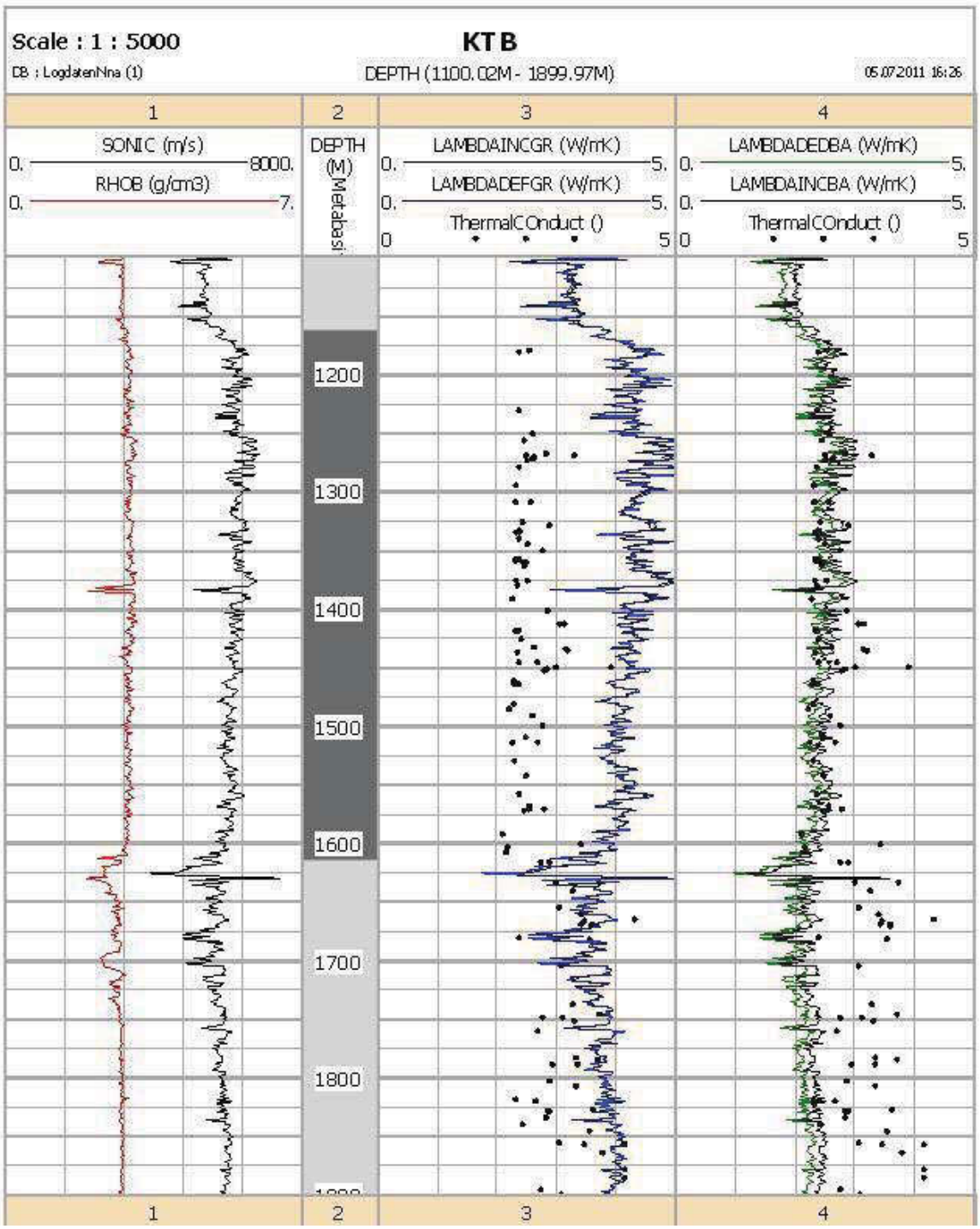

Figure 12-4: Well KTB (1100-1900m): Trace 1: Sonic and density log; Trace 2: lithology grey=gneiss, dark grey=metabasite; Trace 3: "thermal conductivity log calculated from the sonic log for the granite" (blue: Defect model; black: Inclusion model); Trace 4: "thermal conductivity log calculated from the sonic log for the basalt"(green: Defect model; black: Inclusion model); Additionally: dots show core data

The rocks are metabasite and gneiss (alternately). So I had to use two equations (granite and basalt/diorite/gabbro equations) for the different sections. Figure 12-4 shows the results for the defect and the inclusion model from the sonic log, once with the equation for basalt/diorite/gabbro and once with the equation for granite always for the whole borehole, to give an idea what would be the result when the “wrong” equations for a lithology are used. Using the correct equation for the different sections gives good results. Values are in the same range as the measured thermal conductivity from the cores. First I used the gneiss equation but this would lead to too high thermal conductivity values, so I am of the opinion that the gneiss from the KTB has lower quartz content.

If only one equation for the whole borehole is used, too high or too low values for the thermal conductivity, depending on the rock type, are the result. So the differentiation of the lithologies is important. The metabasite sections show lower thermal conductivity than the granites. Both models deliver the same values for the metabasite in comparison to the gneiss where the results lie a little bit apart.

Figure 12-5 shows a calculated “thermal conductivity log” for the same section like in Figure 12-4.

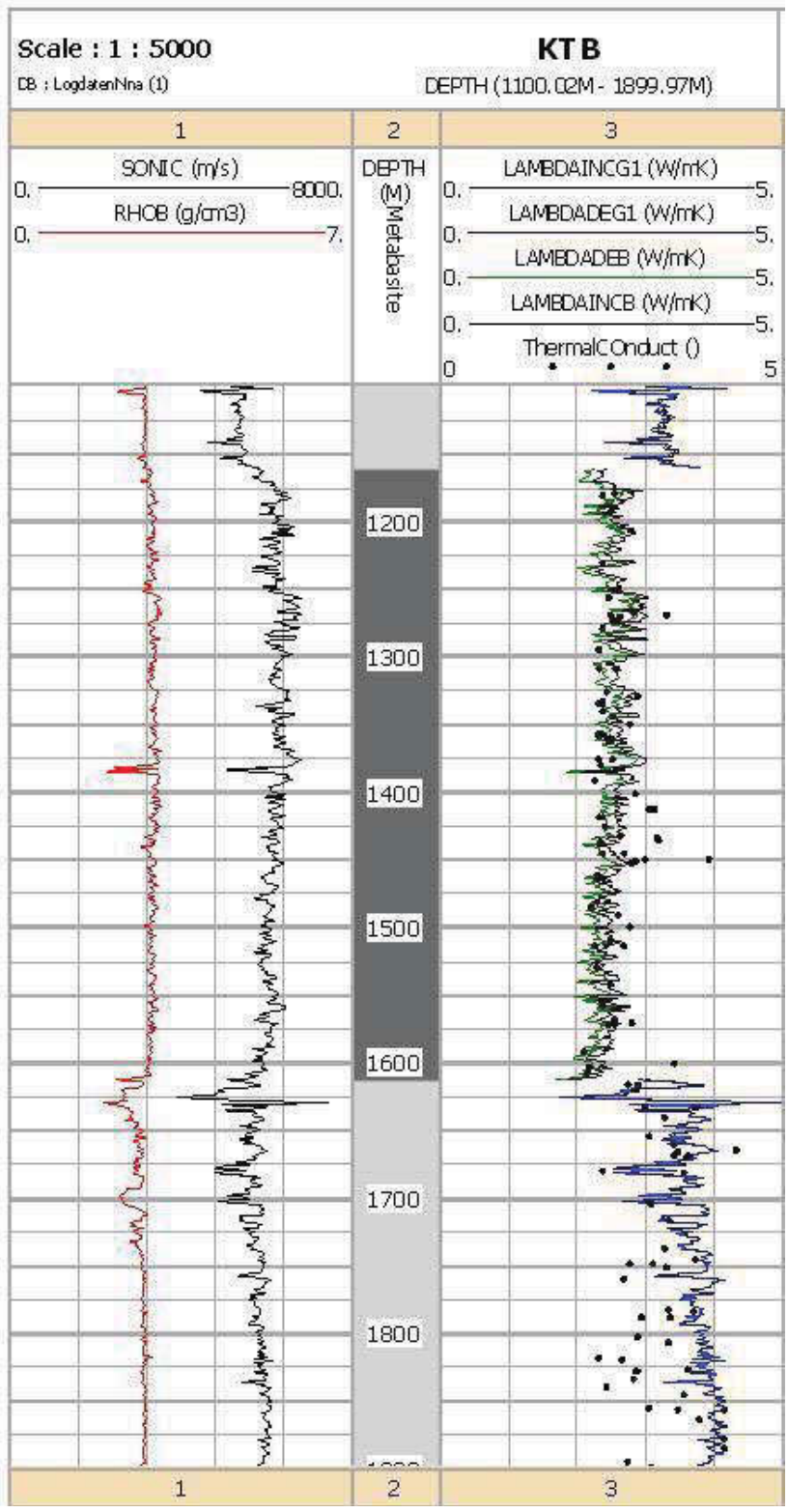

Figure 12-5: Trace 1: Sonic and density log; Trace 2: Lithology: dark grey: metabasite, grey: gneiss; Trace 3: Calculated thermal conductivity log from the sonic log (blue (defect model) and black (inclusion model)=gneiss, green (defect model) and black (inclusion model)=metabasite ; Dots: Thermal conductivity values from cores

12.4. Example 3

This borehole is subdivided into limestone in the upper part (100-1880 m) and dolomite in the lower part (1880-2410m). For the calculations I used the inclusion model again depending on the depth once with the solid parameters for dolomite and once for limestone.

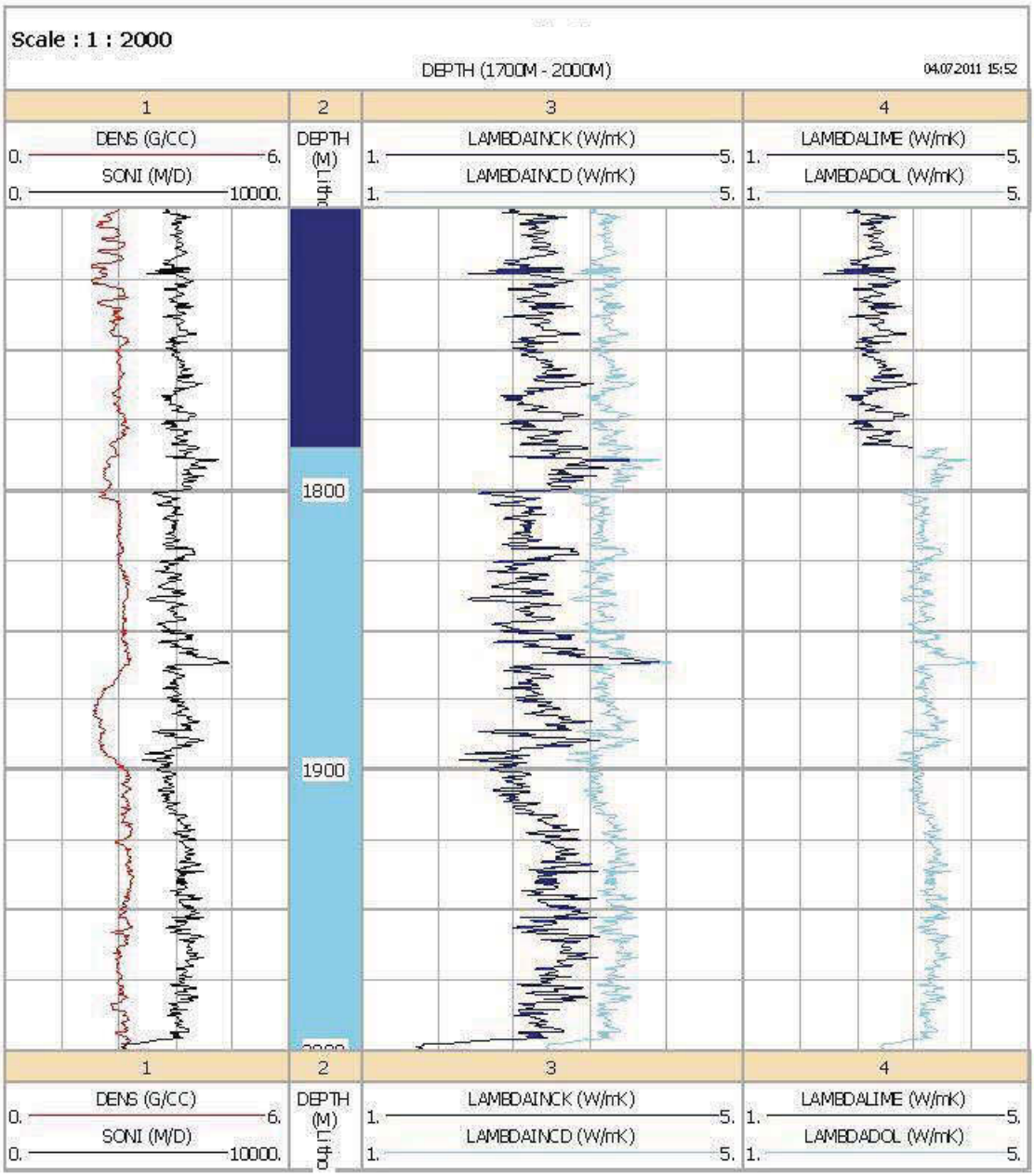

Figure 10-4: Well (1700-2000m): Trace 1: Sonic and density log; Trace 2: lithology (dark blue=limestone, light blue=dolomite), Trace 3: "thermal conductivity log calculated from the sonic log for limestone" (light blue: Inclusion model for dolomite; dark blue: Inclusion model for limestone) ; Trace 4: "Thermal conductivity log" calculated from the sonic log

The calculations worked really well again. Using the equations for limestone for the whole borehole causes low thermal conductivities in the dolomite area. Next step was to calculate thermal conductivity for the dolomite. This leads to too high values for the limestone in the upper part.

Unfortunately no cores have been available here. But data fit to values for dolomite and limestone from the literature. Again the important fact, that the lithology needs to be integrated in the calculations, becomes clear.

12.5. Comparison

All four model calculations (defect and inclusion model from the sonic and the density log) show nearly the same results for the first example. Values are between 1.5 and 3.5 $Wm^{-1}K^{-1}$ with some outliers where the logs show maxima or minima. The mean value is around 2.5 $Wm^{-1}K^{-1}$. Measured data from core samples are between 2.5 and 3.64 $Wm^{-1}K^{-1}$ and fit therefore to the model calculations.

Example 2 (KTB) shows for the metabasite sections, that the thermal conductivity from density logs with the defect model, delivers the highest values. The other three models deliver nearly the same values. For the granite section the thermal conductivities from the sonic log provide the highest values.

13. Discussion and outlook

Thermal conductivity is one of the key properties of geothermal and other geological and geophysical applications. Due to difficulties in thermal conductivity measurements in boreholes, for an indirect method - using correlations between thermal conductivity and other petrophysical properties (compressional wave velocity, density, electrical resistivity), which are measurable in a well – a new concept of a petrographic-coded estimation was developed.

In detail the comparison of measured and calculated data show:

- Correlations are controlled by mineral composition and fractures/pores.
- Inclusion and defect models are one possibility to derive model-based relationships. They demonstrate both properties (mineral composition and fractures).
- A mathematical simplification of the derived curves from the inclusion model by a regression is possible.

In order to implement these influences, a modular concept of model architecture was developed. It has two main steps:

Step 1: Modeling of mineral composition – this controls the petrographic code or rock type

Step 2: Modeling or implementation of fractures, pores etc. with two model types (inclusion model, defect model).

For step 1 “mixing rules” or averaging equations give a possibility of forward calculation; as a result of the variation of rock composition within one rock type in some cases a pure empirical assumption of the “solid parameters is a more practical way and comparable to the practice of “matrix properties” in log interpretation.

For step 2 the inclusion model is a powerful basis for correlation between thermal conductivity and compressional wave velocity. The application on experimental data shows

- the inclusion model delivers the general correlation very well
- correlation is strongly influenced by the aspect ratio, particularly for fractured rocks.

The correlation between thermal conductivity and density seems relatively simple, but has a principal problem: Thermal conductivity is strongly controlled by pore and fracture shape, and by porosity – but, density is controlled only by porosity. Thus, density cannot cover the influence of internal rock geometry. This causes – also within one rock type – some unexpected scatter.

Additionally, the model calculations for the anisotropy of thermal conductivity have been developed as well as an improved method to calculate the heat production from gamma ray logs.

The general concept of the modular construction with a petrographic-coded start (host material) could be confirmed by the results. For a continuation of this concept the following next steps are possible

- development of a more detailed petrographic coding system based on a statistical analysis of measured physical parameters (for example natural gamma activity, density, velocity) and geologic input information.
- implementation of a set of input parameters of different sensitivity with respect to the

    - mineral composition or rock type
    - pore- or fracture volume fraction (porosity)
    - pore- or fracture geometry

  Such parameters are velocities, density, resistivity, nuclear cross sections (PE).
  An implementation results in multiparameter regressions.

- development of more complex pore models. Two directions seem necessary
    - bimodal pore systems (particularly for carbonates)
    - models for granular rock types (clastic sediments) with consideration of the contact properties and specific pore shape.
- further development of models for an analysis of anisotropic rock behavior.

Figure captions

Figure 10-4: Results of the Voigt and Reuss model calculations for thermal conductivity; Input data: λ_1=2.0 $Wm^{-1}K^{-1}$ and λ_2=7.2 $Wm^{-1}K^{-1}$
Figure 10-5: Calculated anisotropy in three directions with the sheet models of Voigt and Reuss
Figure 10-6: Sheet model with modification (embedded quartz block)
Figure 10-7: a) Variant 1 (left) b) Variant 2 (right)
Figure 10-8: Inclusion model with ellipsoid inclusion

Figure 11-1: Normalized heat generation for different rock types, blue dashed line (at 1.57E-2) give the heat generation from the equation by Buecker & Rybach.(Rock type: 1=limestone, 2=dolomite, 3=anhydrite, 4=shale, 5=sandstone, 6=peridotite, 7=gabbro, 8=diorite, 9=granitic rocks, 10=plateau basalt)
Figure 11-2: Comparison of the equation of Buecker & Rybach (1996) (blue line) and the new equation (black line) for a selected section of a borehole of the central part of the Alps (100-400m) with gneiss-mica schist
Figure 11-3: Comparison of the equation of Buecker & Rybach (1996) and the new equation for a selected section of a borehole in the Vienna Basin (2945-3055m) Trace 1: PE (black) and gamma ray (green); Trace 3: density (grey), NPHI (violet) Trace 4: Heat generation with equation from Buecker & Rybach (1996) (blue) and new equation for with dolomite (orange) and limestone (black)
Figure 11-4: Comparison of the equations of Buecker & Rybach and new equation for limestone and dolomite (1700-1950m); Trace 1: density (red) and gamma ray (green); Trace 2: dark blue: limestone, light blue: dolomite; Trace 3: Heat generation with equation from Buecker & Rybach (1996) (blue) and with new equation for dolomite (orange) and limestone (black)
Figure 11-5: Comparison of the equations of Buecker & Rybach and the new one for limestone and dolomite (500-1000 m); Trace 1: density (red) and gamma ray (green); Trace 2: dark blue: limestone, blue: mixture dolomite/limestone; Trace 3: Heat generation with equation from Buecker & Rybach(1996) (blue) and after new equation for dolomite (orange) and limestone (black)
Figure 11-6: Comparison of the equations for the KTB additionally with spectral gamma ray logs (1100-1900 m); lithology: grey=gneiss; dark grey=metabasite; Trace 1: gamma ray (green) and density (red); Trace 3: Heat generation with the equation of Buecker & Rybach (1996) (blue) and the new equation (black); Trace 4: Heat generation of the spectral gamma ray with the equation of Rybach (1976) (blue) and the new one (orange)

Figure 12-1: Summarized flowchart of the working plan
Figure 12-2: Calculated curves from the inclusion and defect model for different rock types; dashed lines = defect model; (A=dolomite, B=limestone, C=sandstone, D=granite/gneiss with high quartz content, E=granite/gneiss with low quartz content, F=basalt/diorite/gabbro)
Figure 12-3: Well Example 1 (100-400m): Trace 1: Sonic and density log; Trace 2: lithology: gneiss-mica schist; Trace 3: “thermal conductivity log calculated from the sonic log” (green: Defect model; black: Inclusion model) ; Trace 4: “Thermal conductivity log” calculated from the density log (orange: Inclusion model; blue: defect model) Range from sample measurements 2.5-3.60 $Wm^{-1}K^{-1}$ is given as line at 250 m
Figure 12-4: Well KTB (1100-1900m): Trace 1: Sonic and density log; Trace 2: lithology grey=gneiss, dark grey=metabasite; Trace 3: “thermal conductivity log calculated from the sonic log for the granite” (blue: Defect model; black: Inclusion model); Trace 4: “thermal conductivity log calculated from the sonic log for the basalt”(green: Defect model; black: Inclusion model); Additionally: dots show core data

Figure 12-5: Trace 1: Sonic and density log; Trace 2: Lithology: dark grey: metabasite, grey: gneiss; Trace 3: Calculated thermal conductivity log from the sonic log (blue (defect model) and black (inclusion model)=gneiss, green (defect model) and black (inclusion model)=metabasite ; Dots: Thermal conductivity values from cores

Table captions

Table 12-1: Overview of the equations from the model calculations (y...thermal conductivity in $Wm^{-1}K^{-1}$, x...compressional wave velocity in ms^{-1}, in this chapter: velocity (x) determined from the sonic log)

Table 12-2: Equations for the calculations of the thermal conductivity (y) from the density log (x)

Reference list

ABBADY, A.G.E., EL-ARABI, A.M., ABBADY, A. [2006] Heat production rate from radioactive elements in igneous and metamorphic rocks in Eastern Desert, Egypt, Applied Radiation and Isotopes, 64, 131-137, Elsevier Science B.V.

ABDULAGATOV, I.M., EMIROV, S., ABDULAGATOVA, Z., ASKEROV, S.Y. [2006] Effect of pressure and temperature on the thermal conductivity of rocks, Journal of Chemical and Engineering Data, Vol. 51, Issue 1, 22-33

ABDULAGATOVA, Z., ABDULAGATOV, I.M., EMIROV, V.N. [2009] Effect of temperature and pressure on the thermal conductivity of sandstones, International Journal of Rock Mechanics and Mining Science, 46, 1055-1071

AL-AWADI, M., CLARK, W.J., HERRON, M., ZANG, T., ZHAO, W., HURLEY,N., KHE, D., MONTARON,B., SADONI, F. [2009] Dolomite: Perspectives on a Perplexing Mineral, Oilfield Review/Schlumberger, Autumn 2009, 32-45

ARCHIE, G.E. [1942] The electrical resistivity log as an aid in determining some reservoir characteristics, Trans. Americ. Inst. Mineral. Met., 146, 54-62

BAKER ATLAS [1985] Introduction to Wireline Log Analysis

BERRYMAN, J. [1995] Mixture theories for rock properties; In: A Handbook of Physical Constants (American Geophysical Union, Ed.), 205 – 228

BIOT, M. A. [1956] Theory of propagation of elastic waves in a fluid-saturated porous solid (I. Low frequency range): J. Acoust. Soc. Am., 28, 168-178

BIOT, M. A. [1956] Theory of propagation of elastic waves in a fluid-saturated porous solid (II. Higher frequency range): J. Acoust. Soc. Am., 28, 179-191

BIRCH, F. UND CLARK, H. [1940] The thermal conductivity of rocks and its dependence upon temperature and composition, Part I, American Journal of Science, Vol. 238, No. 8, 529-558

BIRCH, F. UND CLARK, H. [1940] The thermal conductivity of rocks and its dependence upon temperature and composition, Part II, American Journal of Science, Vol. 238 , No. 9, 613-635

BOERNER, F. [2006] Complex conductivity measurements, In: Kirsch, R.: Groundwater Geophysics, Springer Berlin

BUDIANSKY, B. AND O'CONNELL R.J. [1976] Elastic moduli of a cracked solid, Int. Journ. Solids Struct., 12, 81-97

BUECKER, CH. & RYBACH, L. [1996] A simple method to determine heat production from gamma-ray logs, Marine and Petroleum Geology, Vol. 13, N. 4, 373-375, Elsevier Science Ltd.

BUNTEBARTH, G. [1980] Geothermie, Springer Verlag

CHIOZZI, P., PASQUALE, V., VERDOYA, M. [2002] Heat from radioactive elements in young volcanics by γ - ray spectrometry, Journal of volcanology and geothermal research, 119, 205-214, Elsevier Science B.V.

DAVIS, M.G., CHAPMAN, D., VAN WAGONER, TH., ARMSTRONG, P. [2007] Thermal conductivity anisotropy of metasedimentary and igneous rocks, Journal of Geophysical Research, Vol. 112, B05216

ERBAS, K. [2001] Eine universelle Methode zur Bestimmung der Wärmeleitfähigkeit aus Aufheizkurven konstant geheizter Zylinderquellen, Dissertation, Berlin

ESHELBY, J.D. [1957] The determination of the elastic field of an ellipsoidal inclusion and related problems, Proc. Roy.Soc., Ser.A, 221, 376-396

FLEURY, M. [2002] Resistivity in carbonates: new insights, SPE Annual Technical Conference and Exhibition, San Antonio, Texas, 29 Sept.-2 Oct., paper SPE 77719.

FOCKE, J.W. & MUNN, D. [1987] Cementation exponents in Middle Eastern carbonate reservoirs, SPE Formation Evaluation, June, 155-167, paper SPE 13735.

FRICKE, S. & SCHOEN, J.H. [1999] Praktische Bohrlochgeophysik, Enke Verlag

GASSER, K. [2000] Lithologie, Petrophysik und geologischer Rahmen der Tiefbohrung Soelden Te1, Diploma-thesis, Leoben

GASSMANN, F. [1951] Elastic waves through a packing of spheres, Geophysics, Vol. 16., 673-685

GEERTSMA, I. & D. C. SMITH [1961] Some aspects of elastic wave propagation in fluid saturated porous solids: Geophysics, 26, 169-181

GEGENHUBER, N.M. & SCHÖN, J.H. [2010] Anisotropy of thermal conductivity of a gneiss-experiments and models, *EGU general assembly, 2010,* EGU2010-1535, Vienna

GONG, G. [2005] Physical Properties of Alpine Rocks: A laboratory investigation, PhD thesis, Geneva

GRIFFITHS, C.M., BRERETON, N.R., BEAUSILLON, R., CASTILLO, D. [1992] Thermal conductivity prediction from petrophysical data: a case study, Geological applications of wireline logs II, 299-315

GUNN, D., JONES, L., RAINES, M., ENTWISLE, D., HOBBS, P. [2005] Laboratory measurement and correction of thermal properties for application to the rock mass, Geotechnical and Geological Engineering, 23, 773-791

HARA, G. [1935] Theorie der akustischen Schwingungsausbreitung in gekoernten Substanzen und experimentelle Untersuchungen an Kohlepulver, Elektr. Nachrichtentechnik, 12, 7, 191-200

HARTMANN, A., RATH, V., CLAUSER, C. [2005] Thermal conductivity from core and well log data, International Journal of Rock Mechanics and Mining Science, 42, 1042-1055

HASHIN, Z. & SHTRIKMAN, S. [1963]A variational approach to the theory of the elastic behaviour of multiphase materials, J. Mech. Phys. Solids, 11, 127-40

HUDSON, J. A. [1980] Overall properties of a cracked solid, Journ. Math. Proc. Cambridge Philos. Soc. 88:371-384

KRISCHER, O. & ESDORN H. [1956] Die Wärmeübertragung in feuchten porigen Stoffen verschiedener Struktur, Forsch.a.d. Gebiet der Ingenierwesens, 2, 1, 1-8

MAVKO, G., MUKERJI, T., DVORKIN, J. [1998] The Rock Physics Handbook, Cambridge University Press

MOTTAGHY, D. & VOSTEEN, H.-D. [2008] Temperature dependence of the relationship of thermal diffusivity versus thermal conductivity for crystalline rocks, International Journal of Earth Science, 97, 435-442, Springer Verlag

NORDEN, B. & FOERSTER, A. [2006] Thermal conductivity and radiogenic heat production of sedimentary and magmatic rocks in the Northeast German Basin, AAPG Bulletin, V. 90, No. 6, 939-962

O'CONNELL R.J. & BUDIANSKY, B. [1974] Seismic velocities in dry and saturated cracked solids, Journal of Geophysical Research, 79, 5412-5426

POPOV, Y., PRIBNOW, D., SASS, J., WILLIAMS, C., BURKHARDT, H. [1999] Characterization of rock thermal conductivity by high-resolution optical scanning, Geothermics, 28, 253-276

REUSS, A. [1929] Berechnung der Fließgrenze von Mischkristallen auf Grund der Plastizitätsbedingungen für Einkristalle, Zeitschrift für Angewandte Mathematik und Mechanik, Band 9, 49-58

RYBACH, L. [1976] Radioactive heat production in rocks and its relation to other petrophysical parameters, Pageoph, Vol 114, Birkhäuser Verlag, Basel

RYBACH, L. & CERMAK, V. [1982] Radioactive heat generation in rocks, In: Haack, U. [1982] Radioactivity in rocks, In: Landolt –Boernstein Numerical data and functional relationships in science an technology, New series, Group V, Geophysics and space research, Vol 1, Physical properties of rocks, subvol b, 433-481

RYBACH L. [1986] Amount and significance of radioactive heat sources in sediments, In: Thermal Modelling in Sedimentary Basins, Collections Colloques et Seminaires (Ed J.Burus) 44

SCHLUMBERGER [2000] Log interpretation Charts, Schlumberger Ed.Serv.

SCHOEN, J. H. [1996] Physical properties of rocks: Fundamentals and Principles of Petrophysics (Handbook of Geophysical Exploration Series) - Pergamon Press London, Amsterdam

SCHOEN, J.H. [2011] Physical properties of rocks – a workbook (Handbook of Petroleum Exploration and Production Vol. 8), Elsevier

SEIPOLD, U. [1990] Pressure and temperature dependence of thermal transport properties of granites, High Temperatures-High Pressure, Vol.22, 541-548

SEIPOLD, U., MUELLER, H.-J., TUISKU, P. [1998] Principle differences in the pressure dependence of thermal and elastic properties of crystalline rocks, Physical Chemistry of Earth, Vol 23, No.3, 357-360, Elsevier Science Ltd

SEN, P.N. [1981] Relation of certain geometrical features to the dielectric anomaly of rocks, Geophysics, 46, 1714-1720

SIEGESMUND, S., VOLLBRECHT, A., CHLUPAC, A., NOVER, G., DÜRRAST, H., MÜLLER, J., WEBER, K. [1993] Fabric-controlled anisotropy of petrophysical properties observed in KTB core samples, Scientific Drilling 4, 31-54

SUNDBERG, J., BACK, P.-E., ERICSSON, L., WRAFTER, J. [2009] Estimation of thermal conductivity and its spatial variability in igneous rocks from insitu density logging, International Journal of Rock Mechanics and Mining Science, 46, 1023-1028

TIAB, D. & DONALDSON, E. [2004] Petrophysics, Elsevier

TOKSOEZ, M.N., CHENG, C.H., TIMUR, A. [1976] Velocities of seismic waves in porous rocks, Geophysics, 41, 4, 621-645

VOIGT, W. [1910] Lehrbuch der Kristallphysik: Teubner-Verlag, Leipzig.

VOSTEEN, H.-D. UND SCHELLSCHMIDT, R. [2003] Influence of temperature on thermal conductivity, thermal capacity and thermal diffusivity for different types of rock, Physic and Chemistry of the Earth, 28, 499-509

WHITE, J. E. [1983] Underground Sound: Elsevier Publ. Amsterdam, Oxford, New York.

Appendix A1

Mineral	λ in W m^{-1} K^{-1}	λ in W m^{-1} K^{-1}	c_p in kJ kg^{-1} K^{-1}
	CH		
Silica minerals			
Quartz - α	7.69	7.69 (CR), 7.7 (B)	0.70 (CR), 0.74 (M)
Quartz – amorphous	1.36		
Quartz - mean		6.5 (Ca)	
Ortho- and ring silicates			
Olivine - Forsterite	5.03 ± 0.18	6 (M), 5.06 (CR)	0.68 (M),
Olivine – Fayalite	3.16	3 (M), 3.16 (CR)	0.55 (CR), 0.84 (M)
Garnets – Almandine	3.31	3.3 (M), 3.31 (CR)	
Garnets – Grossularite	5.48 ± 0.21	5.48 (CR)	
Zircon	5.54	5.7(M)	0.61 (CR)
Titanite (sphene)	2.34	2.33 CR)	
Al_2SiO_5 group - Andalusite	7.58	7.57 (CR)	0.77 (CR)
Al_2SiO_5 group - Sillimanite	9.10	9.09 (CR)	0.7 (M), 0.74 (CR)
Al_2SiO_5 group – Kyanite	14.16	14.2(CR)	0.78 (M), 0.70 (CR)
Epidote	2.83 ± 0.21	2.82 (CR)	
Chain silicates			
Pyroxene – Enstatite	4.47 ± 0.30	4.8 (M), 4.34 (CR)	0.7... 0.75 (M), 0.80 (CR)
Pyroxene – Diopside, Augite	4.66 ± 0.31	4.1-5.1(M)	0.67 (M), 0.69 (CR)
Amphibole – Hornblende	2.81 ± 0.27	2.9-3.0 (M), 2.85 (CR)	0.75 (M)
Sheet silicates			
Mica – Muskovite	2.28 ± 0.07	2.32 (CR)	0.76 (M)
Mica – Biotite	2.02 ± 0.32	0.7-1.6 (M), 1.17 (CR)	0.78 (M)
Talc	6.10 ± 0.90	6.10 (CR)	0.87 (CR)
Chlorite	5.15 ± 0.77	4.2 (M), 5.14 (CR)	0.6 (M)
Serpentine	3.53 ± 1.28	1.8 - 2.9 (M)	0.65
Smectite		1.9 (B)	
Illite		1.9 (B)	
kaolinite		2.6 (B)	0.93
Mixed –layers		1.9 (B)	
Clay minerals (mean)		2.9 (Q), 1.7 (Ca)	
Framework silicates – Feldspar			
Feldspar – mean		2.3(H) 2.0(DJ)2.0 (Ca)	
Orthoclase	2.31	2.31 (CR),2.40 (DJ)	0.63-0.75 (M), 0.61 (CR)
Microcline	2.49 ± 0.08	2.9(M), 2.49(CR)	0.67-0.69 (M), 0.68 (CR)
Albite	2.14 ± 0.19	2.31(CR)	0.71 (CR)
Anorthite	1.69	1.68 (CR)	0.71 (CR)
Nepheline		1.73 (CR)	
Oxides			
Magnetite	5.10	4.7-5.3(M), 5.10 (CR)	0.6 (M), 0.60 (CR)
Hematite	11.28	11.2-13.9(M), 11.3	0.62 (M), 0.61 (CR)
Ilmenite	2.38 ± 0.18	(CR)	0.77 (M)
Spinel	9.48	2.2(M)	0.82 (M)
Rutile	5.12	13..8(M), 9.48 (CR)	0.74-0.94 (M)
		7.0-8.1(M)	
Sulfides			
Pyrite	19.21	19.2 (CR)	0.5-0.52 (M), 0.5 (CR)
Pyrrhotite	4.60		0.58-0.60 (M)
Galena	2.28	2.28 (CR)	0.21 (M), 0.207 (CR)
Sulfates			

Baryte	1.31	1.5-1.8(M), 1.33(CR)	0.48-0.6 (M), 0.45 (CR)
Anhydrite	4.76	4.76 (CR), 5.4 (Ca)	0.55-0.62 (M), 0.52 (CR)
Gypsum	1.26	1.0-1.3(M),	1.07 (M)
Carbonates			
Calcite	3.59	3.25–3.9(M), 5.57 (CR)	0.8-0.83 (M), 0.79 (CR)
Dolomite	5.51	5.5(CR), 5.3(B)	0.86-0.88 (M), 0.93 (CR)
Aragonite	2.24	2.23 (CR)	0.78-0.79 (M), 0.78 (CR)
Magnesite	5.84	4.6(M), 5.83 (CR)	0.88 (M), 0.86 (CR)
Siderite	3.01	3.0(M),3.0(B), 3.0 (CR)	0.72-0.76 (M), 0.68 (CR)
Phosphates			
Apatite	1.38 ± 0.01	1.4(M), 1.37 (CR)	0.7 (M)
Halides			
Halite, rocksalt	5.55 ± 0.18	5.3-10(M),5.3-7.2(D)	0.79-0.84 (M)
Sylvite	Xx	6.7-10(M)	0.55-0.63 (M)
Fluorite	9.51	9-10.2(M), 9.5 (CR)	0.9 (M), 0.85 (CR)
Organic materials		0.25(Q), 1.0(B)	

Table A1-1: Thermal properties of rock forming minerals, compiled after data from: (CH) - Clauser and Huenges, 1995, compiled and converted data from Horai, 1971; Ca – Clauser, 2006; Cb – Clauser et. al, 2007; (CR) - Cermak and Rybach, 1982; M – Melnikov et al., 1975; C – Clark, 1966; B - Brigaud et al., 1989, 1992; Q – Quiel, 1975; H – Huenges, 1989; DJ – Drury and Jessop, 1983 (Schoen, 2011)

Mineral	ρ kg m^{-3}	k GPa	μ GPa	V_p m s^{-1}	V_s m s^{-1}	ν	Ref.
Quartz	2650	38.2	43.3	6050	4090	0.08	G
	2650	37.0	44.0	6050	4090	0.08	C
	2650	36.5	45.6	6060	4150	0.06	M
Hornblende	3124	87	43	6810	3720	0.29	G
Olivine	3320	130	80	8540	4910	0.24	C
Forsterite	3224	129.6	81.0	8570	5015	0.24	G
Garnets-almandine	4180	176.3	95.2	8510	4770	0.27	M
Garnets-zircon	4560	19.8	19.7	3180	2080	0.13	M
Epidote	3400	106.5	61.1	7430	4240	0.26	M
Pyroxene-diopside	3310	111.2	63.7	7700	4390	0.26	M
Pyroxene-augite	3260	94.1	57.0	7220	4180	0.25	M
“Average” feldspar	2620	37.5	15.0	4680	2390	0.32	M
Anorthite	2760	84	40	7050	3800	0.29	G
Albite	2630	55	29.5	5940	3290	0.28	G
Oligoclase	2640			6240	3390		A
Orthoclase	2570	46.8	27.3	5690	3260		A
Labradorite	2680			6550	3540		A
Microcline	2560			6000	3260		A
Nepheline	2620	45.5	31.5	5750	3450	0.22	G
Biotite	3050	51	27	5350	3000	0.27	G
	3050	59.7	42.3	6170	3730	0.21	M
Muscovite	2790	52	32	5810	3370	0.25	G
	2790	42.9	22.2	5100	2820	0.28	M
	2790	52.0	30.9	5780	3330	0.25	M
Kaolinite	1580	1.5	1.4	1440	930	0.14	M
Clay	2580	20.9	6.85				H
“Gulf clays”	2550	25	9	3810	1880	0.34	M

	2600	21	7	3410	1640	0.35	M
Chlorite		95.3	11.4				K
Illite		39.4	11.7				K
Kaolinite		37.9	14.8				K
Calcite	2712 2710	73 76.8	32 32.0	6540 6640	3430 3440	0.31 0.32	G M
Dolomite	2860 2870	94 94.9	46 45.0	7370 7340	4000 3960	0.29 0.30	G M
Siderite	3960	123.7	51.0	6960	3590	0.32	M
Aragonite	2930	47	38.5	5790	3630	0.18	G
Anhydrite	2970 2980	55 56.1	30 29.1	5620 5640	3140 3130	0.27 0.28	G M
Barite	4500	54.9	23.7	4350	2250	0.32	G
Gypsum	2350			5800			M
Apatite	3218			6680	3830	0.26	G
Pyrite	5010 4930	143 147.4	128 132.5	7920 8100	5060 5180	0.16 0.15	G M
Halite	2160			4560	2590	0.26	G
Fluorite	3180	86.4	41.8	6680	3620	0.29	M
Sylvite	1990	17.4	9.4	3880	2180	0.27	M
Kerogen	1300	2.9	2.7	2250	1450	0.14	M

Table A1-2: Density, elastic moduli, and wave velocities of some rock-forming minerals. Reference key: G: Gebrande et al. (1982) (k and μ are Hills mean); A: Alexandrov et al. (1966); C: Carmichael (1989); M: data from a compilation by Mavko et al. (1998); H: Helgerud et al. (1999); K: Katahara (1996). (Schoen, 2011)

Appendix A2

Metamorphic/Magmatic Rocks and Sandstone

	Rock type	λ	v_p	d
		$Wm^{-1}K^{-1}$	ms^{-1}	kgm^{-3}
L5	Granit	2.77	5206.25	2721.35
L6	Migmatit. Mischgranit	2.79	5024.87	2700.04
L10	Tonalit (Stangl Granit)	2.60	5456.34	2779.17
L20	Granit	2.49	4613.41	2638.08
L24	Granit (Granodiorit)	2.26	4394.63	2648.40
Tkb15/1	Granit	2.74	5103.00	2670.19
Tkb15/2	Granit	2.83	5735.00	2679.10
gr1_2	Granit	3.01	3842.81	2759.44
gr1_3	Granit	2.80	3586.94	2759.44
gr3_2	Granit	2.97	3947.37	2618.88
gr3_3	Granit	2.89	3951.07	2618.88
hmf2	Gneiss	2.68	4718.00	2741.61
Hmg2	Gneiss	2.55	4731.54	2665.36
L13	Gneiss	2.58	3689.36	2733.02
L17	Granitgneis	2.79	3303.54	2657.82
L29	Granitgneis	4.71	4467.66	2685.89
L25	Gneiss	2.90	3908.91	2715.92
g1	Granit	2.98	5246.22	2610.98
g2	Granit	3.53	5653.50	2550.53
g3	Granit	2.81	5115.74	2550.53
L2	Basalt (shoshonit)	1.67	4772.58	2728.85
L4	Metagabbro	2.96	6171.90	3241.14
L9	Basalt	2.61	5754.25	2979.75
L12	Diorit	2.85	6297.88	3026.54
L19	Gabbro	2.43	6010.33	3016.47
L21	Gabbroider Diorit	2.62	5743.04	2889.03
L22	Basanitlava	1.25	4316.38	2442.69
L30	Traychandesit	1.55	4561.62	2528.06
	Basalt/Klöch	2.05	6161.72	2874.31
	Basalt/Klöch	2.10	6092.27	2910.40
	Basalt/Klöch	2.03	6115.49	2966.16
	Basalt/Klöch	1.93	6156.07	2886.98
L7	Quarzsandstein	2.64	2891.98	2327.76
L11	Quarzsandstein	2.81	2667.33	2123.30
L31	Quarzsandstein	2.77	3790.20	2616.45
SA1	Sandstein	6.25	5165.88	2403.31
SA2	Sandstein	6.25	4922.08	2279.67
SB1	Sandstein	4.20	3602.63	2221.71
SB2	Sandstein	4.20	3360.67	2277.44
EBS	Sandstein	3.70	3696.00	2043.13

ES	Sandstein	3.30	3030.00	1863.16
ug1	gneiss mica schist	3.02	5050.00	
ug2	gneiss mica schist	3.35	4397.16	
ug3	gneiss mica schist	3.46	5592.00	
ug4	gneiss mica schist	3.64	4705.00	
ug5	gneiss mica schist	2.81	5166.00	
ug6	gneiss mica schist	2.70	4704.55	

Carbonates

		Density	Porosity	vp	λ	R	1/R	F
		kgm^{-3}	%	ms^{-1}	$Wm^{-1}K^{-1}$	Ohmm	1/Ohmm	
Limestone	B1	2648.81	3.02	4803.31	3.04	691.00	0.00	276.40
	K2	2687.82	1.07	6115.29	3.46	2528.00	0.00	1011.20
	H1	2666.33	0.95	6045.86	3.15	3070.00	0.00	1228.00
	gba 10	2697.03	3.76	4886.20	2.60	1200.00	0.00	480.00
	gba14	2691.04	0.83	5860.22	3.00	1738.00	0.00	1800.00
	gba 15	2677.54	0.65	6223.62	3.04	4500.00	0.00	978.40
	gba 33	2688.31	1.81			2446.00	0.00	978.40
	gba 40	2713.16	4.05	3719.30	2.82	165.00	0.01	66.00
	e6	2696.69	1.64	6131.60	3.06	3500.00	0.00	1400.00
Wettersteinkalk	K2	2716.00	0.80	5295.45	3.51	1090.00	0.00	436.00
	K3	2713.00	1.21	4523.81	3.51	1178.00	0.00	471.20
	K4	2708.00	0.43	6000.00	5.31	2723.00	0.00	1089.20
	K5	2707.00	1.46	5500.00	5.31	3178.00	0.00	1271.20
	Tat 1-A/1	2716.30	2.75	5188.68	3.18	485.00	0.00	194.00
	Tat 1-A/2	2711.20	2.06		3.18	492.00	0.00	196.80
	Tat 1 B/1	2716.10	1.52		3.35	424.00	0.00	169.60
	Tat 1 B/2	2716.20	2.01	6017.19	3.35	534.00	0.00	213.60
Dachsteinkalk	Baum 5 - A	2719.10	2.71		2.57	199.00	0.01	79.60
	Obw 1	2703.70	2.12	6353.80	3.14	674.00	0.00	269.60
	Lax 2-A		3.60	6138.96	3.01	387.00	0.00	154.80
	Lax 2-C	2707.00	1.37	6047.62	3.05	805.00	0.00	322.00
Gutensteinerkalk	Gän T2-B	2702.10	1.54	6153.25	3.02	161.78	0.01	64.71
	Gän T2-C	2716.50	1.97		2.88	74.00	0.01	29.60
	gr2_2	2665.53		5720.81	2.88	1967.00	0.00	786.80
	gr2_3	2665.53		5591.01	2.91	1967.00	0.00	786.80
	gr4_2	2691.92		5589.13	3.14	4585.00	0.00	1834.00
Gong	Cs55	2710.00	0.50	6399.00	3.08			
	cs69	2700.00	0.34	6525.00	3.30			
	jb19	2810.00	1.50	6800.00	4.38			
	jb33	2730.00	1.04	6150.00	2.56			

Dolomite		Density	Porosity	vp	λ	R	1/R	F
		kgm^{-3}	%	ms^{-1}	$Wm^{-1}K^{-1}$	Ohmm	1/Ohmm	
Wettersteindolomit	Baum 7-A	2816.10	6.78	4166.97	3.11	47.00	0.02	18.80
	Baum 7-C	2808.90	2.29		5.21	358.00	0.00	143.20
	Baum 7 -E	2827.50	1.60		4.22	462.00	0.00	184.80
	Dol3	2825.00	1.50	4782.61	4.42	1297.00	0.00	518.80
	Dol4	2826.00	2.10	4409.09	4.42	1191.00	0.00	476.40
	S1A	2830.00	2.63	5088.91	4.80	2539.58	0.00	1015.83
	S1	2822.00		6287.43	5.46	1749.87	0.00	699.95
	S5	2823.00	2.97	5630.75	4.79	533.68	0.00	213.47
	S6	2821.00	2.45	6543.23	4.88	2836.47	0.00	1134.59
	S7	2817.00	11.49	5325.78	5.60	1969.78	0.00	787.91
	S8	2839.80	1.07	6246.33	5.21	1590.43	0.00	636.17
	S9	3430.40	2.81	2675.59	5.48	2368.76	0.00	947.50
	S10	2825.60	6.49	1908.71	3.88	1299.05	0.00	519.62
other	gba16	2806.13	1.15	6780.49	5.27	6989.00	0.00	2795.60
	E1	2814.51	1.14	6623.11	4.06	5500.00	0.00	2200.00
	gba1	3583.73	6.34	5113.64	2.86	430.00	0.00	172.00
Hauptdolomite	gba11	2812.90	2.08	6688.09	4.38	4300.00	0.00	1720.00
	gba23	2831.75	2.67		3.24	995.00	0.00	398.00
Gong	jb16	2840.00	0.56	6850.00	5.00			
	tm25	2830.00	0.27	6600.00	4.22			